

**The Static and Dynamic Conformational Properties
of Some (1,5)-Naphthalenophanes.**

Thesis by
Brian B. Masek

*In Partial Fulfillment of the Requirements
for the Degree of
Doctor of Philosophy.*

California Institute of Technology
Pasadena, California

1987

(submitted October 16, 1986)

to my family

ACKNOWLEDGEMENTS

First and foremost, thanks must go to my wife, Deb, and kids, Gabi and Joshua, for their love. Secondly, my sincere thanks go to my research advisor, Dennis Dougherty, for his excellent advice and support. Thanks also to the entire Dougherty group. Particularly, to Gary Snyder, my classmate, for numerous sailing expeditions, and to Dave Stauffer for proofreading this thesis.

I would like to acknowledge Dick Marsh, Bill Schafer, and especially Bernie Santarsiero for their help and suggestions related to X-ray diffraction. Thanks go to Doug Meinhart for assistance with the 400-MHz NMR. Also, I would like to acknowledge James Yesinowski, Helmut Eckert, and Paula Watanick for assistance with and discussions about solid state NMR. Thanks to Tim Swager of the Grubbs' group for lending me their rotors.

Solid state NMR was done at the NSF Southern California Regional NMR Facility. Financial support for my graduate work was provided, in part, by the National Science Foundation as a Predoctoral Fellowship.

ABSTRACT

The Molecular Mechanics (MM) method has been applied to several dioxo-(1,5)-naphthalenophanes (**1**: n=14, 15, and 16, referred to as **C14**, **C15**, and **C16** respectively). A systematic search, which considered many low-lying conformations, lead to the conclusion that there is no significant statistical contribution to the large negative activation entropies observed for the enantiomerization reactions of **C14** and **C15**.

Simple rules from the conformational analysis of large-ring alkanes indicated relatively few possible low energy conformations. Evaluation of the structures by MM lead to predictions about the ground state conformations of **C14-C16**. For **C16**, the [9373] conformation is predicted to be the preferred conformation, with the [8383] conformation near in energy. For **C15**, a class of ring expanded or contracted structures, related to higher and lower homologues, are found to be lowest in energy. Two structures, [83163] and [83712], were predicted to be the lowest in energy. For **C14**, the [8363] conformation is predicted to be the ground state.

X-ray diffraction shows the conformation of **C16** in the solid state to be [9363]. Fully refined structures were not obtained for **C14** and **C15** because of disorder. Therefore, a method based on ^{13}C chemical shifts in the solid state was applied. Solid state CP-MAS ^{13}C NMR correctly identifies the conformation of **C16** as [9373]. In addition, the ^{13}C shifts indicate the conformation of **C14** to be [8363], as predicted. For **C15**, only the ring expanded or contracted class of conformations is consistent with the ^{13}C NMR data.

The kinetics for the jump-rope reaction of an N,N,N',N'- tetramethyldiamino-(1,5)-naphthalenophane (**2**) have been obtained by DNMR in D₂O, CD₃CN, and CD₃OD. The solvent has little or no effect on the derived activation parameters. However, large differences between **2** and **C14** were noted. The differences were rationalized as being due to a change in the ground state from the [8363] conformation in **C14** to the [5555] conformation in **2**.

Finally, the kinetics of the jump-rope reaction of a gem-dimethyl substituted dioxo-(1,5)-naphthalenophane (**3**) were investigated. Comparison with **C15** indicates no changes were induced in the activation parameters for the process.

Table of Contents

Chapter 1. Introduction	1
References for Chapter 1.	9
Chapter 2. Molecular Mechanics Studies of Dioxa-(1,5)-Naphthalenophanes.	11
Introduction.	12
The Systematic Approach to Ring Generation.	14
A Rational Approach to the Elucidation of the Low-Lying Conformations of Macrocycles.	24
Conclusion.	36
References for Chapter 2.	37
Chapter 3. The Conformations of C14 , C15 , and C16 as Determined by Solid State CP-MAS ¹³ C NMR and X-ray Diffraction.	41
Introduction.	42
Results and Discussion	
X-ray Diffraction.	42
Solid State CP-MAS ¹³ C NMR.	49
Conclusion.	63

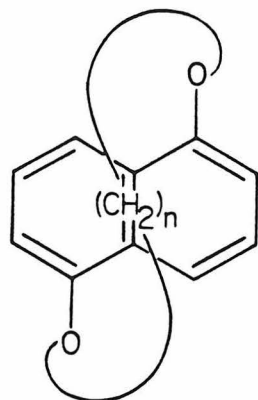
Experimental Section.	66
References for Chapter 3.	69
Chapter 4. The Enantiomerization Kinetics of an	
N,N,N',N'-Tetramethyldiamino-(1,5)-Naphthalenophane.	71
Introduction.	72
Synthesis.	74
DNMR Results.	74
Discussion.	86
Conclusion.	90
Experimental Section.	91
References for Chapter 4.	95
Chapter 5. The Effect of Gem-Dimethyl Substituents on the Jump-Rope	
Reaction of a (1,5)-Naphthalenophane.	97
Introduction.	98
Synthesis.	101
DNMR Results.	101
Discussion.	108
Conclusion.	109

Experimental Section.	110
References for Chapter 5.	113
Appendix A.	115
The Ring Generation Program.	116
Appendix B.	138
Coordinates, Temperature Factors, and Structure Factors for C16 from X-ray Diffraction.	139
Fourier Map for C14.	148
Fourier Map for C15.	162
Appendix C.	176
Complete Solid State CP-MAS ¹³ C NMR Spectra of C14, C15, and C16 and Deconvolutions.	177
Complete Variable Temperature Solution ¹³ C NMR Spectra of C14.	181

Chapter 1
INTRODUCTION

Macrocycles represent an important structural unit in organic chemistry. A large number of naturally occurring compounds, including the general classes of ionophores¹ and macrolide antibiotics,² contain large rings. Additionally, the area of synthetic host-guest chemistry is dominated by macrocycles.³ The specific binding properties of these structures imply they have well defined shapes. In general, however, large rings are known to be very flexible, having a number of low-lying conformations available, all of which may be rapidly interconverting.⁴ Such flexibility is known to be undesirable when designing structures with specific binding properties.⁵ In nature, the ionophores and macrolides contain specific substituent patterns^{1,2} which are thought to diminish their flexibility as well as enforce the shape adopted. In the area of host-guest chemistry, structurally rigid units such as aromatic rings are used to limit flexibility.

Part of the work described herein was initiated with the goal of quantifying the effects of substituents on the dynamic processes of macrocycles. Such information would be valuable in designing new synthetic hosts and in understanding the properties of naturally occurring macrocycles. The [1,5]-naphthalenophanes were chosen as model compounds for such studies. For several reasons, [1,5]-naphthalenophanes are ideal for the study of substituent and solvent effects on the dynamic properties of macrocycles. First, they undergo an unambiguously defined conformational process involving the large ring. Secondly, the rates for this process are amenable to accurate, quantitative evaluation. And finally, the synthesis of these molecules is sufficiently flexible to allow other substituents to be easily incorporated.



n
14
15
16

An initial investigation into the parent system, **1**, with $n = 14, 15,$ and 16 , referred to as **C14**, **C15**, and **C16** respectively, produced intriguing results,^{6,7} which we will briefly summarize here. The process of interest is the enantiomerization reaction of **1**. These molecules are chiral, having at most C_2 symmetry. All methylene groups when n is even and all but the central methylene when n is odd consist of a diastereotopic pair of protons. The enantiomers can interconvert by simply moving the polymethylene chain around to the other face of the naphthalene system, in what Marshall has termed a "jump-rope" reaction.⁸ This process, and only this process, also interconverts the diastereotopic protons of each methylene group, thereby providing a potential dynamic NMR (DNMR) probe of the enantiomerization. Structures such as **1** thus provide an opportunity for the direct observation of an unambiguously defined conformational process in a macrocyclic compound involving a polymethylene chain.

It should be emphasized from the start that such enantiomerization processes are well precedented. The stereochemical phenomenon is identical with that involved in the enantiomerization of trans-cycloalkenes, a process that was probed by DNMR almost 20 years ago.⁹ However, the [1,5]-naphthalenophanes present a unique situation. One can envision that as the polymethylene chain is made shorter, the steric demands on the transition state for the jump-rope reaction, in which the chain must slide past the edge of the naphthalene, become more severe. For certain chain lengths, the chain may be relatively flexible and strain free in the ground state. However, on going to the transition state, severe conformational restrictions will be encountered.

A detailed understanding of the dynamics of unsubstituted chains is necessary before the issue of substituent effects can be addressed, and so the initial study^{6,7} was directed at **C14**, **C15** and **C16**. The kinetics for the jump-rope reaction for **1** were determined by DNMR using the complete line shape (CLS) method.¹⁰ There are hazards in using such data to obtain reliable activation parameters. However, for several reasons, the naphthalenophanes are particularly well suited for the line shape method. Difficulties can arise because several factors other than the rate process of interest can affect line shapes. These include changes in field homogeneity at different temperatures and changes in solvent viscosity which alter molecular tumbling rates and thereby alter relaxation times. The naphthalenophanes, however, have an internal reference signal in each molecule (the aromatic protons for all three structures and additionally the protons on the central methylene of **C15**) that allowed reliable values for the natural line width, as measured by T_{2eff} , to be obtained.¹¹ Another problem is temperature-dependent chemical shifts. How-

ever, for all three compounds, the midpoint of the signal due to the γ protons (vida infra) which were used for the DNMR studies did not change. Finally, through a combination of high-field NMR (200- and 500-MHz) and the highly anisotropic environment provided by the naphthalene, quite large frequency separation ($\Delta\nu$) values were observed for the γ protons of all three compounds. Because of the large values of $\Delta\nu$, the coalescence occurred over a wide temperature range. Therefore, the early and late regions of coalescence were ignored, and only signals that were very substantially broadened were considered.¹² This minimized the contributions of factors other than chemical exchange to broadening. Because $\Delta\nu$ was large, this could be done while still leaving a wide temperature range for an Eyring analysis.

In addition, it should be noted that the saturation spin transfer (SST) method¹³ was also applied to **C14**. Such a study provides a check for systematic errors in the CLS study. Also, because the SST method operates in a different rate, and hence a different temperature range, a combination of CLS and SST methods allowed a very wide temperature range (114°) to be studied. The results from the SST method were in excellent agreement with those from the CLS study. The combined points all describe on the same line in the Eyring analysis.

Particular care was also taken in deriving the activation parameters and associated error limits. An iterative procedure which considers errors in both the rates and temperatures was used in the Eyring analysis.¹⁴ Excellent correlations were obtained for all three molecules. However, it is generally agreed that the standard deviations in ΔH^\ddagger and ΔS^\ddagger derived from an Eyring plot are poor measures of probable error.^{10,12} Thus, a method was used which

Table 1.1. Activation Parameters with Estimated Error Limits^{a,b}

structure	ΔG^\ddagger	ΔH^\ddagger	ΔS^\ddagger
C14	17.4 ± 0.2	10.4 ± 0.5	-23 ± 2
C15	13.4 ± 0.2	7.6 ± 0.7	-20 ± 2
C16	9.8 ± 0.2	8.8 ± 0.4	-3 ± 2

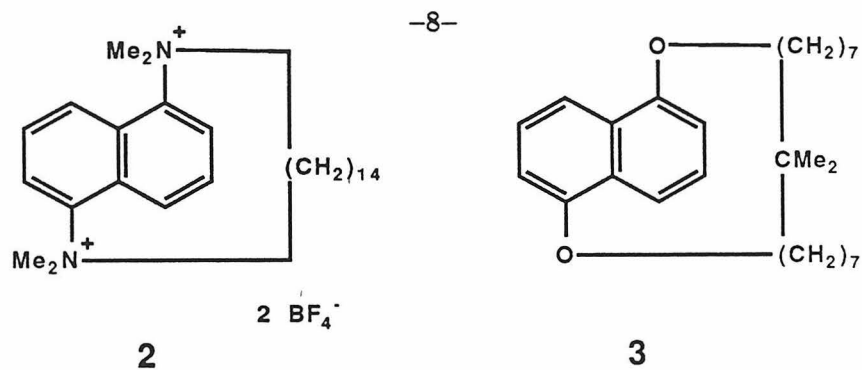
^a Units are kcal/mol and cal/mol·K. ^b from Ref. 7.

assumes maximal errors of 10% in rate constants and 1.0 K in temperatures to determine the maximal error in ΔG^\ddagger , and assumes the error in all points equals the maximal error in deriving errors for ΔH^\ddagger and ΔS^\ddagger .¹⁴ Using this approach, the best estimates for the activation parameters and error limits, as listed in Table 1.1, were obtained.

The results of this study are quite remarkable. The large negative activation entropies observed for **C14** and **C15** are consistent with the notion that these molecules are unrestricted and flexible in the ground state, but are quite restricted in the transition state. An activation entropy of this magnitude would not typically be expected for a unimolecular conformational process involving a hydrocarbon. For comparison, a Diels-Alder reaction, a stereospecific, bimolecular, concerted reaction would be expected to have an activation entropy of ca. -30 to -35 eu.¹⁵ Most surprising though, is the sharp contrast provided by **C16**, for which ΔS^\ddagger is very nearly zero. Note that an analysis based solely on ΔG^\ddagger would give the impression that the series **C14**, **C15**, and **C16** is well behaved and follows the obvious trend that a smaller chain gives a greater barrier. Finally, this study indicates that the ring sizes of **C14** and **C15** are the most appropriate for the studies of substituents and solvent effects.

In order to rationalize the dynamic properties of **C14**, **C15**, and **C16**, a molecular mechanics (MM) study has been undertaken. It was hoped that an understanding of the static stereochemistry, *i.e.*, the ground state conformations, would provide some insight into the dynamic behavior observed. In addition, such knowledge of the low-energy conformations for the parent system, **1**, will be valuable in understanding the effect of substituents. Two approaches have been taken. The first involves a systematic search for potential low-lying structures and focuses on determining what contribution a statistical entropy term might make to the large negative activation entropies observed. The second approach tests the applicability of some simple rules from the conformational analysis of large ring alkanes for predicting the low-energy structures of functionalized macrocycles such as **1**. From this second approach will come predictions about the preferred conformations adopted by **C14**, **C15**, and **C16**. All of these topics are addressed in Chapter 2.

In Chapter 3, experimental evidence supporting the predictions of MM will be presented. X-ray crystallography has been applied to all three structures, but only for **C16** was a complete structure obtained. For **C14** and **C15**, disorder prevented the resolution of the atoms in the polymethylene chain. In cases such as this, a second, easily applied experimental tool would be valuable. Thus, we were intrigued by the recent study of Möller on large ring alkanes which assigned ^{13}C shifts, as obtained by solid state CP-MAS ^{13}C NMR, to particular conformational environments.¹⁶ The applicability of using these shifts to identify the conformations of **C14**, **C15** and **C16** in the solid state was investigated and the results were compared with the predictions made by MM and the X-ray structure of **C16**. Taken together, the results of MM,



CP-MAS ¹³C NMR, and X-ray diffraction yield a consistent picture of the geometries of **C14**, **C15**, and **C16**.

In Chapter 4, a study using cyclophane **2** to probe for solvent effects will be presented. Specifically, we wished to assess what influence an aqueous environment exerts on the conformational properties of hydrophobic macrocycles. Enhanced folding of hydrocarbons has been predicted for hydrocarbons in aqueous media.¹⁷ In the area of synthetic host-guest chemistry, hosts with hydrophobic binding sites are used to bind small organic molecules in aqueous solution. The shape and rigidity of both host and guest, important in determining binding properties, may be altered from those expected in organic solvents. The results of the study of **2**, however, indicate that there is little or no change of the jump-rope reaction kinetics on going from organic solvents to water. A significant difference is noted between **2** and **C14**. MM calculations were applied to rationalize this change.

There is the possibility that some of the differences in the dynamic behavior between **2** and **C14** might be due to a gem-dimethyl effect.¹⁸ Gem-dimethyl substituents, such as those on the nitrogens of **2**, are thought to induce rigidity in hydrocarbons. A study of the jump-rope kinetics for cyclophane **3**, presented in Chapter 5, indicate that no changes are induced on going from **C15** to **3**.

REFERENCES

- (1) M. Dobler "Ionophores and Their Structure"; Wiley: New York, 1981.
- (2) For example: E.F. Gale, *et al.* "The Molecular Basis of Antibiotic Action", 2nd ed.; Wiley: London, 1981.
- (3) For an overview of the host-guest field, see: "Topics in Current Chemistry"; F. Vogtle, Ed.; Springer Verlag: Berlin, 1981 and 1982; Vol. 98 and 101.
- (4) J. Dale *Top. Stereochem.* **1976**, *9*, 199-270. F.A.L. Anet and T.N. Rawdah *J. Am. Chem. Soc.* **1978**, *100*, 7166-7171.
- (5) R. Breslow *Isr. J. Chem.* **1979**, *18*, 187-191.
- (6) M.H. Chang and D.A. Dougherty *J. Am. Chem. Soc.* **1983**, *105*, 4102-4103.
- (7) M.H. Chang, B.B. Masek, and D.A. Dougherty *J. Am. Chem. Soc.* **1985**, *107*, 1123-1133.
- (8) J.A. Marshall *Acc. Chem. Res.* **1980**, *13*, 213-218.
- (9) G. Binsch and J.D. Roberts *J. Am. Chem. Soc.* **1965**, *87*, 5157-5162.
- (10) For an overview of the DNMR method, see: J. Sandström "Dynamic NMR Spectroscopy"; Academic Press: New York, 1982.
- (11) U. Berg, S. Karlsson, and J. Sandström *J. Org. Magn. Res.* **1977**, *10*, 117-121.

- (12) G. Binsch and H. Kessler *Angew. Chem., Int. Ed. Engl.* **1980** *19*, 411-428.
- (13) See, for example: F.W. Dahlquist, K.J. Longmuir and R.B. DuVernet
J. Magn. Reson. **1975**, *17*, 406-10.
- (14) J.A. Irvin and T.I. Quickenden *J. Chem. Educ.* **1983** *60*, 711-712.
- (15) A. Wassermann "Diels-Alder Reactions"; Elsevier: Amsterdam, 1965; Ch. 4.
- (16) M. Möller, W. Gronski, H. Cantow, and H. Höcher *J. Am. Chem. Soc.* **1984**,
106, 5093-5099.
- (17) W.L. Jorgensen *J. Chem. Phys.* **1982**, *77*, 5757-5765. R.O. Rosenberg,
R. Mikkilineni and B.J. Berne *J. Am. Chem. Soc.* **1982**, *104*, 7647-7649.
- (18) N.L. Allinger and U. Zalkow *J. Org. Chem.* **1960**, *25*, 701-704. B. Capon and
S.P. McManus "Neighboring Group Participation"; Plenum Press: New York,
1976; Vol. 1, pp 59-70.

Chapter 2

Molecular Mechanics Studies
of Dioxo-(1,5)-Naphthalenophanes.

Introduction

The molecular mechanics (MM) method has proven reliable for predicting various properties of molecules up to a moderate size containing a variety of functional groups.¹ Geometries, relative energies, heats of formation, and barriers to interconversion of conformers are among the quantities which may be calculated by the method. For molecules the size of the cyclophanes, **1**, it is the only practical computational method available. Therefore, molecular mechanics calculations have been undertaken with several goals in mind. Part of the motivation for such a study was a desire to understand the sharp change in dynamic behavior on going from **C14** and **C15** to **C16**. Also, it was recognized that these structures provide a good example of a common situation in modern organic chemistry. With the discovery of ionophores² and macrolide antibiotics,³ and the continuing development of host-guest chemistry,⁴ macrocycles represent an important structural unit. In all these applications, it is important to understand the shape of the macrocycle, but this can be an extremely complex issue. Therefore, the ability and practicality of two different approaches to the problem of determining the preferred geometry and low-lying conformations for macrocyclic systems were evaluated using the cyclophanes, **1**, as a test case. Information on the preferred geometries obtained from such studies is vital to understanding both static and dynamic properties and to understanding changes induced in these properties by substituents.

As stated above, two approaches to the problem of generating possible low energy conformations of **1** have been taken. The first is an attempt at an unambiguous, systematic and complete method for generating all plausible input structures for the MM calculations.⁵ Because of the large number of

structures which need to be considered, a simplified MM method which does not explicitly treat hydrogen atoms will be used in conjunction with this approach. Such a MM method can greatly diminish the amount of computing time necessary for energy evaluations and geometry optimizations and is often used in MM studies of larger molecules such as proteins.⁶ In general, this method is expected to be less accurate than a full MM calculation, but is extremely useful in preliminary evaluation of complicated systems. In the second approach, we wished to test whether one can take a macrocycle with a well-defined structural subunit, such as that provided by the naphthalene system in **1**, and use that substructure along with a few simple principles from the conformational analysis of cycloalkanes as a starting point for a rational evaluation of a few likely low energy conformations. This would avoid the need to evaluate thousands of potential conformers. As will be shown, it appears, at least for the cyclophanes **1**, this less exhaustive approach can be successful. As only a few structures are being considered, the full MM treatment will be used. Predictions about the preferred geometries of **C14**, **C15** and **C16** will emerge from this second approach and, in Chapter 3, will be combined with experimental evidence to give a consistent picture of the ground state conformations of these molecules.

The Systematic Approach to Ring Generation

Inspection of molecular models and preliminary calculations indicated that a large number of structures with relatively low energies could be possible for the cyclophanes, **1**. One approach to finding the global minimum and all the low-lying conformations would be to search the entire conformational space. Because these molecules are not expected to be strained, only minimal deviations from standard bond lengths and valence angles are expected. The coordinates of relevance are the torsional or dihedral angles. To implement this approach, a computer program was written to search the entire torsional space of the polymethylene chain, looking for conformations which reach from one oxygen in **1** to the other.⁵ See Appendix A for a flow chart and source code. Starting at one oxygen and looping toward the other, the chain was built up using standard bonding parameters. The naphthalene system and the two oxygens were fixed at standard geometries.⁷ If the CH₂ attached to the ether oxygen is labeled α , and the carbon next to it is labeled β , etc., (see Figure 2.1) then the dihedral angles may be labeled in a similar manner. The first angle, α , is the C2-C1-O-CH₂ (or C6-C5-O-CH₂) angle, the β angle is C1-O-CH₂-CH₂ (or C5-O-CH₂-CH₂), etc. In this manner, the α angles position the α carbons, the β angles position the β carbons, etc. Each dihedral angle along the chain was allowed to be either gauche(+), gauche(-), or anti (C-C-C-C angles of 60, -60, or 180°, respectively). The only exception was α which was allowed to assume any value between -135 and +135° in 45° increments. To represent the naphthalene system, an ellipsoidal region into which the chain could not enter was used. This prevented the generation of structures for which the chain passed through the naphthalene.

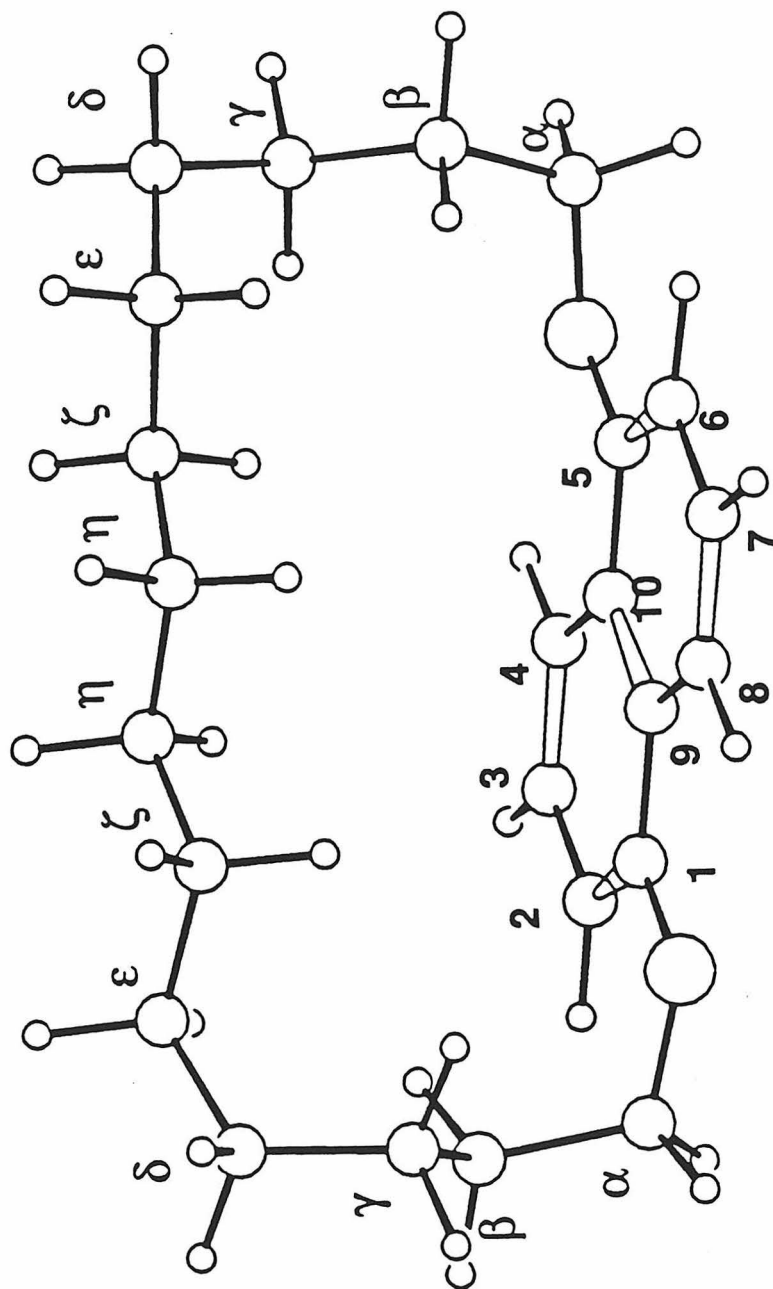


Figure 2.1. A molecular mechanics geometry of C₁₄ showing the labeling of the carbon atoms.

Any chain that terminated within a specified distance (the closure criterion) of the terminal oxygen was retained. All such structures were then submitted to a closure optimization procedure. The goal of this process was to make the C-O bond length and the CH₂-CH₂-O and CH₂-O-C1 bond angles of the closure conform to standard bonding parameters. This was accomplished by allowing the dihedral angles along the chain to deviate slightly from the standard values and by retaining any deviation that led to a decrease in the energetics of the ring closure. These energetics were evaluated using the standard MM terms for the three parameters described above. After this procedure, all generated structures had standard bond lengths and valence angles along the entire chain. Finally, each structure generated in this manner was subjected to an initial energy evaluation using MM. As mentioned, a simplified MM treatment was used, the particular parameters being those of the NOH (no-hydrogen) field developed by Still and implemented in the program MODEL.⁸

The number of unique structures generated in the above manner was surprisingly large. The initial studies emphasized **C12** as the smallest structure that, according to models, still seemed reasonably flexible in the ground state. For example, with the closure criterion at 3.5 Å, all viable **C12** structures were generated and then the ring closure was optimized. The steric energy of each structure was then evaluated and only structures with steric energies less than 200 kcal/mol were retained. The energy of the most stable structure, E₀, was 55 kcal/mol. Using this approach, 1906 unique **C12** input guesses were obtained. In this context, unique implies having a different value of the conformational descriptor assigned by describing each dihedral angle (α , β , γ ,...) as either g⁺, g⁻, or anti. The 200 kcal/mol energy cutoff may seem overly generous,

but preliminary studies clearly showed that structures with energies this high could, upon complete optimization, attain energies comparable to those of the most stable conformers.

Because it was impractical to perform a geometry optimization on all 1906 structures generated above, the above procedure was repeated for **C12** with a closure criterion of 2.5 Å. This led to a total of 838 unique **C12** structures with initial energies less than 200 kcal/mol. The geometries of all these structures were optimized to 0.1 kcal/mol convergence using the Newton-Raphson optimization algorithm implemented in MODEL. The naphthalene was frozen at the standard geometry. This resulted in 778 unique minima. The steric energies of these minima relative to the lowest energy structure, E_{rel} , ranged from 0 to 47 kcal/mol, but the vast majority (626) were less than 14 kcal/mol above the "ground state". It must be emphasized that the NOH field with a 0.1 kcal/mol convergence criterion is a crude level of optimization.

The magnitude of the problem thus became clear, especially when one considers a larger and presumably more flexible structure such as **C16**, for which the number of feasible conformers would likely be astronomical. The preliminary studies on **C12** indicate that a complete enumeration of all possible conformations using such an approach is infeasible. But, by using restrictive closure and energy criteria, a large but manageable number of structures is obtained. However, it is not certain that the global minimum or other very low-lying conformations will be among the structures generated. The following approach was therefore adopted. Rather than attempt to quantitatively reproduce the ΔH^\ddagger and ΔS^\ddagger values of Table 1.1, we sought to rationalize the trends in the data. More specifically, the large number of structures encountered for

C12 suggest that a statistical term might account for at least part of the large negative ΔS^\ddagger observed for **C14** and **C15**.

The contribution of a statistical entropy

There are, in principle, two effects that contribute to ΔS^\ddagger for reactions such as the enantiomerization of **C14-C16**. The first is due to the difference in entropy content of the ground and transition states. This is merely the entropy difference between two conformers of the same molecule and will be given by differences in the partition function associated with internal degrees of freedom, that is, the vibrational and rotational modes. This shall be referred to as the intrinsic entropy of activation ΔS_{int}^\ddagger . As discussed below, for the jump-rope reaction there may be many “ground states” and even several transition states. This will lead to a large number of reaction paths, each with its own ΔS_{int}^\ddagger .

The second contributor to ΔS^\ddagger is a statistical term, ΔS_{stat}^\ddagger . This arises from the fact that there is not just one ground state conformation and one transition state, but rather there may be large numbers of both. If, as a first approximation, all the low-lying “ground state” conformers found are considered to be degenerate and likewise for the “transition states”, then ΔS_{stat}^\ddagger is as given in equation 1, in which g_1 is the degeneracy of the ground state and g_2 is the degeneracy of the transition state.

$$(1) \quad \Delta S_{stat}^\ddagger = R \ln g_2/g_1.$$

It is useful to first consider the values g_1 and g_2 must have if ΔS_{stat}^\ddagger is the major contributor to ΔS^\ddagger . For example, a ΔS^\ddagger of -20 eu would require $g_1/g_2 = 24,000$. More significantly, if the -20 eu *difference* in ΔS^\ddagger values between **C15** and **C16** is due entirely to ΔS_{stat}^\ddagger , then the ratio of the g_1/g_2 ratios for **C16** and **C15** would have to be 24,000. Thus one of the primary goals has been to search for a dramatic change in the statistics of ground state vs. transition state conformations for **C14** and **C15** vs. **C16**. Only a very substantial change could make a sizable contribution to ΔS^\ddagger .

The systematic structure generating program can be used evaluate the degeneracies of the ground and transition states. In such a study, the crucial consideration is to apply a *consistent level of theory* to all structures calculated. In this way, the trends in experimental data can be analyzed, even though precise quantitative agreement is not obtained.

The first step was to analyze **C14**–**C16** in a manner similar to the above treatment of **C12**. Table 2.1 summarizes the structure-generation results for these molecules. In order to keep the problem manageable, a more severe closure criterion (1.0 \AA) was adopted. As expected, the longer the chain, the greater the number of viable structures that were generated. At this level, only 26 structures were generated for **C12**. While a substantially larger number of structures was generated for **C16** than for **C15** or **C14**, the difference was less than a factor of 5. This would seem to be a first indication that ΔS_{stat}^\ddagger is not a major reason for the $\Delta\Delta S^\ddagger$ between **C15** and **C16**.

Table 2.1. Results of Structure Generation and Minimization

structures	<u>ground states</u>		<u>transitions states</u>	
	guesses ^a	minima	guesses ^c	transition states
C12	26	26	44	6
C14	326	326	266	35
C15	592	590	594	77
C16	2619		1738	327
C16	810 ^b	805		

^aClosure criterion = 1.0 Å; energy cutoff = 200 kcal/mol.

^bEnergy cutoff = 100 kcal/mol.

^cClosure criterion = 2.0 Å; energy cutoff = 500 kcal/mol.

Table 2.1 also shows the number of minima obtained from these input guesses. Unfortunately, all 2619 **C16** structures could not be optimized, and so only the 810 structures with initial energies less than 100 kcal/mol ($E_0 = 60$ kcal/mol) were optimized. As with **C12** most input structures led to unique minima.

Since ΔS_{stat}^\ddagger depends not only on the number of ground state structures, but also on the number of transition states (eq 1), we wished to determine whether there was a dramatic difference between **C14/C15** and **C16** in this respect. We therefore needed a way to evaluate relative transition state degeneracy for the three structures. This was accomplished through a modification of the structure generation program.

We first assumed that transition state structures would in general have the aliphatic chain roughly in the plane of the naphthalene. That is, the chain would be looping around the edge of the ring system, rather than across one face. Thus, with the naphthalene ring fixed in the xy plane, all carbons of the chain were forced to have an absolute value of $< 2.0 \text{ \AA}$ for their z coordinates. Additionally, instead of treating the steric exclusion volume of the naphthalene as an ellipsoid, it was treated as an infinitely tall box, thereby preventing passage of the chain over the naphthalene. Structures were then generated in the usual manner and subjected to the closure optimization procedure as above, except that the closure criterion was opened up to 2.0 \AA , and the initial energy cutoff was expanded to 500 kcal/mol . These structures were then optimized (NOH, 0.1 kcal/mol convergence) and, based on the following criterion, transition state representatives were chosen from the resulting minima. With the naphthalene still in the xy plane, the z coordinates of the chain carbons were averaged, and this average was required to be $< 0.25 \text{ \AA}$. Note that positive z values will cancel with negative z values in the summation, thereby producing a small average z . Additionally, structures with at least four carbons on each side of the ring were retained. Both these criteria were intended to limit the list of transition state structures to only those conformations in which the chain really does wrap around the edge of the naphthalene. The actual numerical criteria are somewhat arbitrary, but the important point is that they were applied consistently throughout the series. It must be remembered that the structures so obtained are not transition states. In fact, they are true minima. However, the energetics and statistics of such structures can provide a useful, qualitative model for the actual transition states. Two views of a typical "transition state" structure for **C12** are given in Figure 2.2.

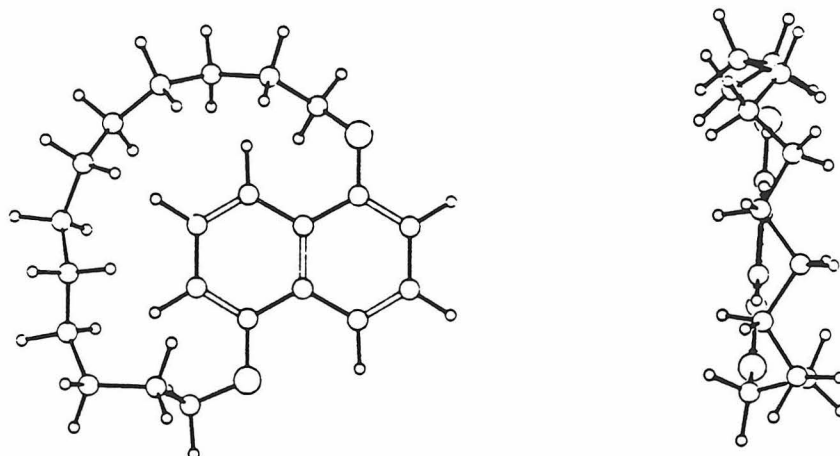


Figure 2.2. Two views of a typical “transition state” for **C12**.

The results of this study are summarized in Tables 2.1 and 2.2. A fairly large number of guess structures were generated, but upon optimization, a large number of conformers optimized to give structures that failed to meet the various transition state criteria. Still, significant numbers of transition state structures were obtained. As expected, the longer the chain, the greater the number of transition states. Concerning the above statistical arguments, the substantial increase in the number of viable ground state conformations for **C16** relative to **C14-C15** is paralleled by an increase in transition state structures. This holds true whether one considers the total number of structures or only the relatively low-lying ones. Thus, g_1/g_2 for **C16** should not be dramatically different from that for **C14-15**. We therefore conclude that ΔS_{stat}^\ddagger is *not* the dominant contributor to the ΔS^\ddagger observed.

To conclude this section, a systematic approach to searching out low-lying conformations of the cyclophanes, **1**, could not be exhaustively applied. However, a large but limited search was practical. Such a search was valuable in evaluating whether or not a statistical entropy term was contributing to the

Table 2.2. Distribution of Ground and “Transition” States
as a Function of Energy^a

E_{rel}	<u>C14</u>		<u>C15</u>		<u>C16</u>	
	GS	TS	GS	TS	GS ^b	TS
0-2	5	0	3	0	5	0
2-4	10	0	5	0	22	2
4-6	34	0	21	2	63	1
6-8	37	0	54	2	125	13
8-10	61	1	83	4	203	16
10-12	53	3	114	2	181	30
12-14	53	1	101	12	127	35
14-16	35	7	93	12	56	36

^aEnergies in kcal/mol. GS = ground state; TS = transition state.

^bOnly the 810 structures below 100 kcal/mol were optimized.

unique dynamic behavior observed for **C14–C16**. Because we concluded that ΔS_{stat}^\ddagger is **not** responsible for the large negative activation energies observed, we infer that it is ΔS_{int}^\ddagger which is. The answer to how well a limited search did at finding the lowest energy conformations will be deferred to the next section where a comparison between the systematically generated structures and those generated in a rational manner will be made.

A Rational Approach to the Elucidation of the Low-Lying Conformations of Macrocycles

In this section, a rational approach to considering probable low energy conformations will be tested. Predicting the conformations of macrocycles is a challenging and complex task. The conformational properties of large ring alkanes are fairly well understood.⁹ However, most macrocycles of interest are not simple $(\text{CH}_2)_n$ molecules, but contain substantial perturbations to the basic ring structure. In the present case, the naphthalene system provides a perturbing structural subunit to the macrocycle. Starting with the conformational preferences of such a substructure and then applying simple principles from the conformational analysis of cycloalkanes, can the preferred geometry of a macrocyclic system be predicted? For the cyclophanes, **1**, such an approach is successful.

Conformational Analysis

In his pioneering work on the conformational analysis of medium- and large- ring alkanes, Dale arrived at two simple rules which are useful in constructing geometries for large rings.⁹ For a ring to be formed, a certain number of gauche dihedral angles must be introduced. First, Dale found that a sequence of two gauche dihedral angles of the same sign was an efficient way to achieve chain bending. The energy cost of this deformation should be additive, *i.e.*, twice the value of a single gauche interaction. This type of bend, which we shall call a normal corner, is found in unstrained diamond-lattice type conformations of large rings.¹⁰ Secondly, in even-membered rings, conformations with four normal corners, and therefore four sides, are found.

For odd-membered rings, it is impossible to fit together four sides so as to form normal corners, and three- or five-sided conformations are adopted.

We wished to test whether these principles could be extended to substituted or functionalized macrocyclic systems such as **1**, in order to predict low energy conformations in these systems. By considering six atoms of the dioxanaphthalene system to be part of a macrocyclic ring (C1, C9, C10, C5 and both oxygens, Fig. 2.3), **C14**, **C15**, and **C16** are found to be 20-, 21-, and 22-membered rings respectively. Thus **C14** and **C16**, being even-membered macrocycles, would be predicted to adopt conformations with four normal corners, while **C15** might adopt conformations with either three or five corners. This assumes the dioxanaphthalene system is not too different from a polymethylene chain. The three bonds of the naphthalene ring (C1-C9, C9-C10, and C10-C5) are equivalent to three anti bonds in a cycloalkane, and thus, do not represent a major deviation from a conformation normally expected of a polymethylene chain.

The conformational preference of the aromatic ether functionality is also compatible with cycloalkane conformational preferences. Anisole strongly prefers a planar geometry;¹¹ therefore, the first methylene of the cyclophanes will prefer to lie in the plane of the naphthalene ring. The methylene will eclipse C2 of the naphthalene system as opposed to C9 where it would encounter adverse nonbonded interactions with the peri hydrogen on C8. MM2 calculations confirm these predictions (*vide infra*). In this conformation, the naphthalene system and the α methylenes become equivalent to a sequence of five anti dihedral angles in a cycloalkane.

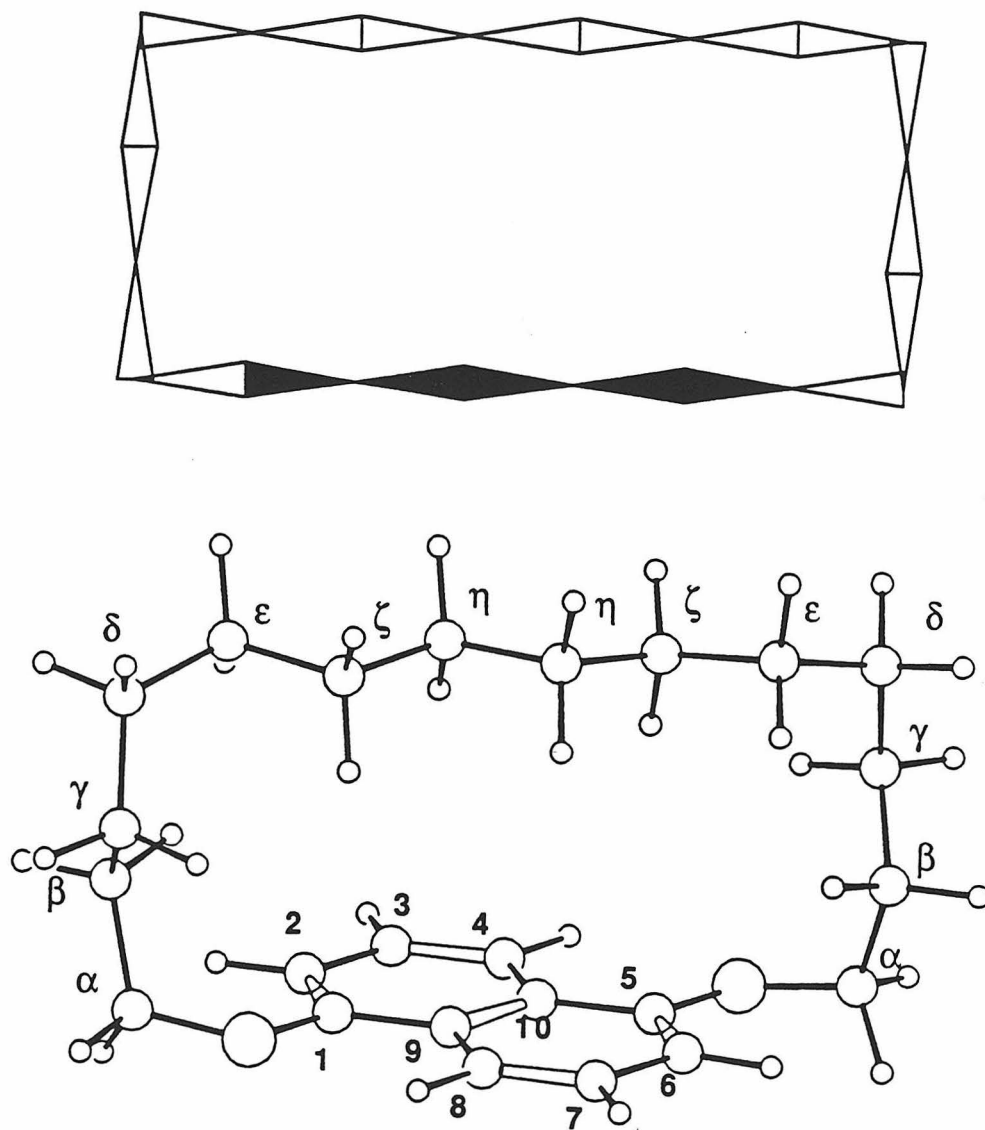


Figure 2.3. Dale projection (top) and MM2 geometry (bottom) of the [7373] geometry of C14. Filled wedges in the Dale projection are part of the diox-anaphthalene. Oxygen atoms are at the borders between the filled and open wedges.

With the first methylene eclipsing C2, there are two conformations about the O-CH₂ bond, gauche (+ or -) or anti. However, the gauche conformation is destabilized by a nonbonded interaction with the hydrogen on C2 of the naphthalene ring, and so one would predict a moderate preference for the anti conformation about this bond. In 1-ethoxynaphthalene, MM2 calculations predict the anti conformation to be preferred by 2.1 kcal/mol. Thus, in the absence of ring constraints, both the first and second methylenes have a preference to lie in the plane of the naphthalene ring. In this conformation, the naphthalene system plus the α and β methylenes is equivalent to a sequence of seven anti dihedral angles in a cycloalkane, and would give rise to a side nine bonds long according to Dale's rules.

Conformations of large rings are conveniently described using Dale's nomenclature.⁹ Each "side" is defined as the region between two corners and assigned a number corresponding to the number of bonds between the corners. For example, Figure 2.3 shows a Dale projection of the [7373] conformation of C14 with a drawing of the MM2 geometry for this conformation. Both Dale projections and Dale's nomenclature will be used in this thesis.

Molecular Mechanics

Using the above considerations, we will try to rationally choose the best candidates for the global minimum for each structure. Because only a minimal number of structures will be considered, a full MM treatment will be used. Geometry optimizations and energy evaluations were carried out using the MM2^{1,12} force field as implemented by the program BIGSTRN3.¹³ Normal mode analysis insured that all the structures discussed below are in fact minima

on the potential energy surface. The undefined parameters^{14a} for MM2 were chosen so as to reproduce both the experimental barrier for rotation in anisole and the existing structural data for anisole and related compounds.^{14b}

Some valuable insights can be obtained from Figure 2.4 which shows the torsional profiles for anisole and 1-methoxynaphthalene as calculated using both MM2 and NOH fields. The more accurate MM2 procedure predicts an 8 kcal/mol barrier for rotation of a methoxy group past the peri hydrogen on C8 of the naphthalene. This is quite similar to the ΔH^\ddagger values observed for **C14-C16**. In an idealized enantiomerization pathway, one end of the chain would go past the peri position and the other past the 2 position. This suggests that a major contributor to ΔH^\ddagger is this peri interaction, with relatively little steric strain due to interactions involving the remainder of the chain wrapping around the naphthalene.

C14. For cycloeicosane, Dale proposed [7373] and [6464] conformations as probable ground states. For **C14**, along with these two conformations, one should consider the conformation with the first and second methylenes in the naphthalene plane, the [9353] conformation. However, in a 20-membered ring this leads to a large discrepancy between the length of the two opposite long sides, and this conformer would be expected to be of higher energy. A compromise would be the [8363] conformation which allows one β and both α methylenes to be placed in their preferred positions. The results of MM2 calculations are shown in Table 2.3. The [8363] conformation is found to be the ground state with the [7463] conformation 1.4 kcal/mol above it in energy. Dale projections of the two lowest energy conformations are shown in Figure 2.5.

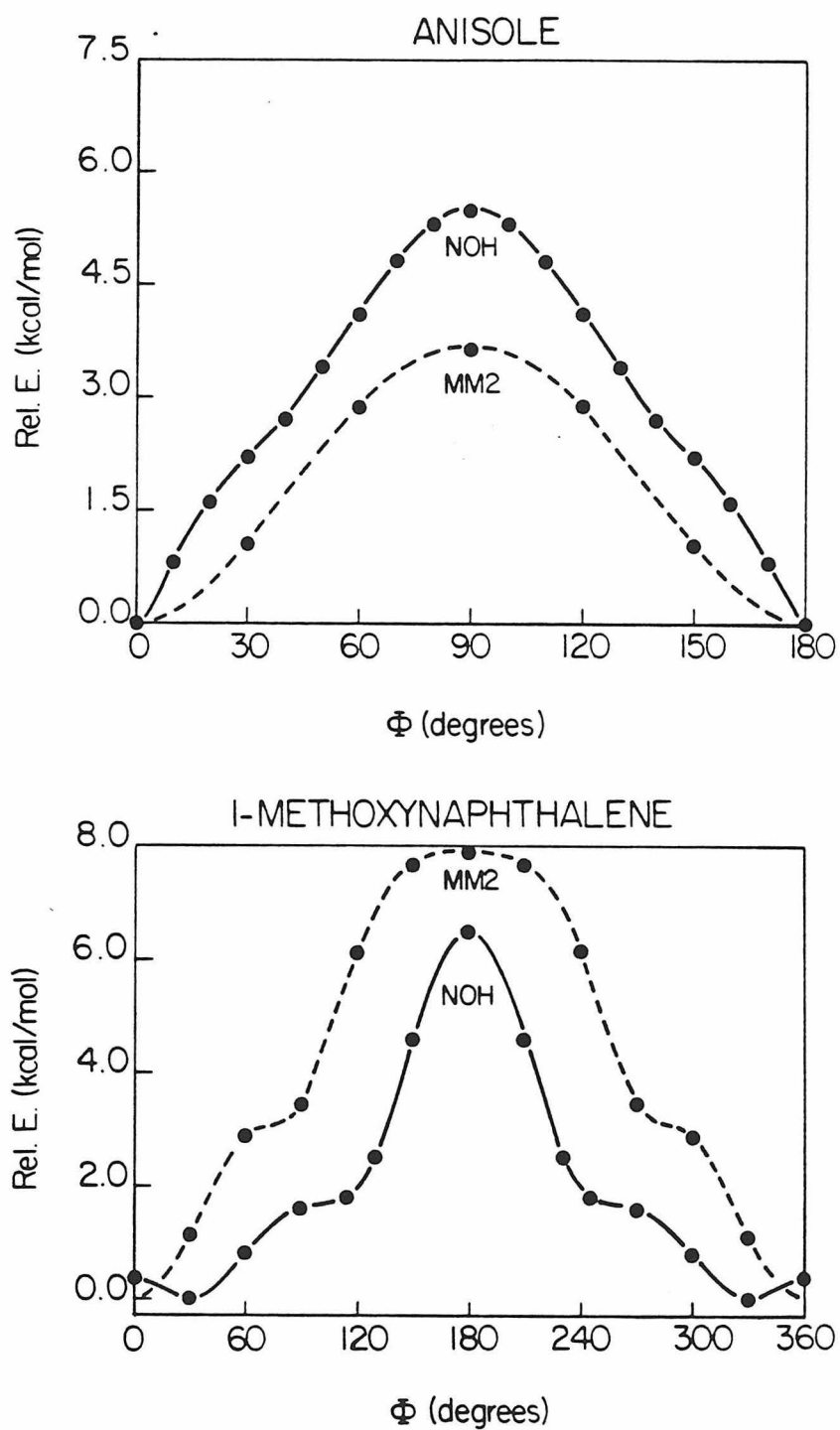


Figure 2.4. The torsional profiles of anisole and 1-methoxynaphthalene as calculated by MM2 and NOH. The dihedral angle Φ is the C2-C1-O-CH₃ angle for both structures.

C15. Because C15 is an odd-membered macrocycle, it might adopt conformations with either three or five normal corners. Dale also states that five-sided conformations having a side one bond long are closely related to quadrangular conformations of the even-membered rings immediately above or below in size.⁹ Such conformations are derived from the conformations of the even-membered rings by insertion of one bond at a corner of the lower homologue or by cutting off a corner ring atom in the higher homologue. Such conformations have one "nonstandard" corner. A variety of standard trigonal, standard quinquangular, and ring expanded or contracted quinquangular conformations were considered. The results are shown in Table 2.3. Dale projections of the low energy conformations are shown in Figure 2.5. The lowest energy structure found, [83163], is derived for the [8363] conformation of **C14** by ring expansion, while the next lowest structure, [83712], is obtained by cutting a corner off the **C16** [8383] structure (*vida infra*).

C16. For cyclodocasane, Dale proposed three low energy conformations, [8383], [7474] and [6565]. One might expect that for **C16** these would also be low-lying conformers. The trapezoidal [9373] conformation should also be considered as it allows the α and β methylenes to be placed in their preferred positions. The results of the MM2 calculations are shown in Table 2.3. The [9373] and [8383] conformations shown in Figure 2.5 are of nearly the same energy with the other conformations at higher energies.

Table 2.3. Relative Energies^a for Various Conformations of **C14**, **C15**, and **C16**.

<u>C14</u>		<u>C15</u>		<u>C16</u>	
Conf.	E_{rel}	Conf.	E_{rel}	Conf.	E_{rel}
[8363] ^b	0.0	[83163]	0.0	[9373]	0.0
[7463]	1.4	[83712]	0.3	[8383]	0.6
[7373]	2.8	[92163]	1.2	[8473]	1.6
Non-Dale ^{b,c}	3.2	[82173]	1.6	[8374]	2.3
Non-Dale ^{b,c}	3.5	[93153]	1.6	[8464] ^b	2.5
[9353]	4.3	[83613]	2.7	[9274] ^b	2.7
[6464]	4.7	[966]	2.8	[7474]	4.8
		Non-Dale ^{b,c}	2.8	[6565]	7.5
		[876]	3.4		
		[867]	4.1		
		[73443]	4.4		
		[73434]	5.0		
		[777]	5.3		
		[74334]	5.7		

^aEnergies in kcal/mol.^bFound by the systematic structure search.^cContains multiple single-gauche and other non-normal corners.

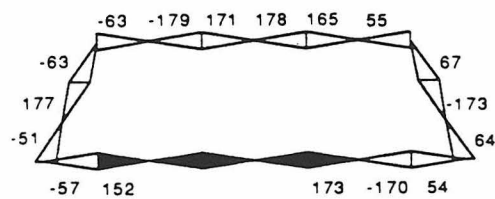
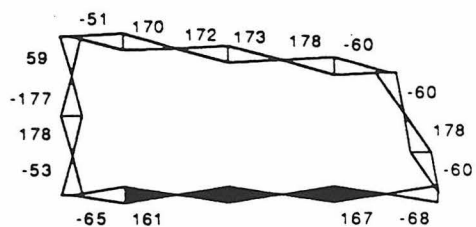
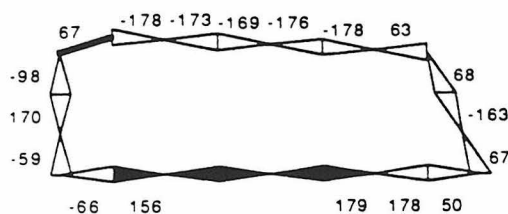
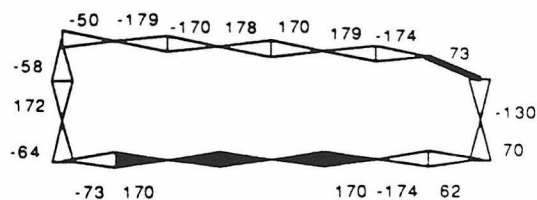
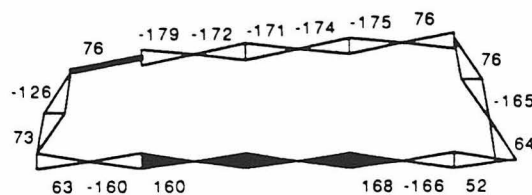
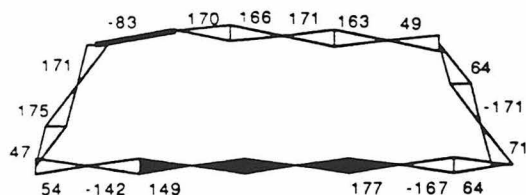
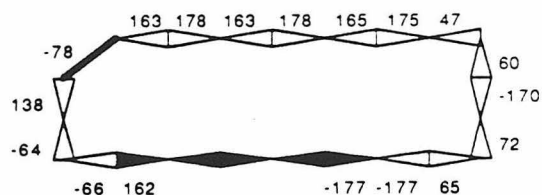
C14**[8363]****[7463]****C15****[83163]****[83712]****[92163]****[93153]****[82173]**

Figure 2.5. Dale projections of the low energy conformations of C14, C15, and C16. Blackened bonds are part of the dioxanaphthalene. Oxygen atoms are at the borders between filled and open wedges. Dihedral angles listed are MM2 (X-ray) values. For conformations with C_2 symmetry, only half the angles are given.

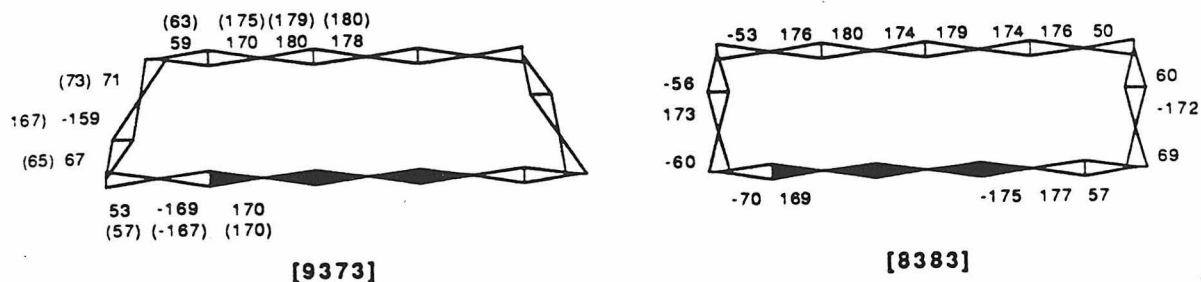
C16

Figure 2.5 continued.

We can now compare the systematic approach to structure generation with the results of the rational approach just described. Thus, the five best structures generated systematically were geometry optimized using the full MM treatment. The low energy structures that resulted are listed in Table 2.3 along with those mentioned above. For C14, the lowest energy structure, [8363], was found with both methods. It should also be noted that the systematic approach generated two low-lying conformations that defy description using Dale's nomenclature. For C15 and C16, both Dale and non-Dale low-lying conformations were found by the systematic approach. However, the global minima and many other low-lying structures were missed. Clearly, the limited systematic search did much worse than a rational approach at predicting the geometries of the cyclophanes, **1**.

With steric energies for fully optimized structures in hand, the assumption that these naphthalenophanes are essentially strain-free can be tested. This was done by evaluating ΔH° for the homodesmotic reaction¹⁵ shown in Figure 2.6. A normal corner should induce ca. 1.6 kcal/mol of strain giving

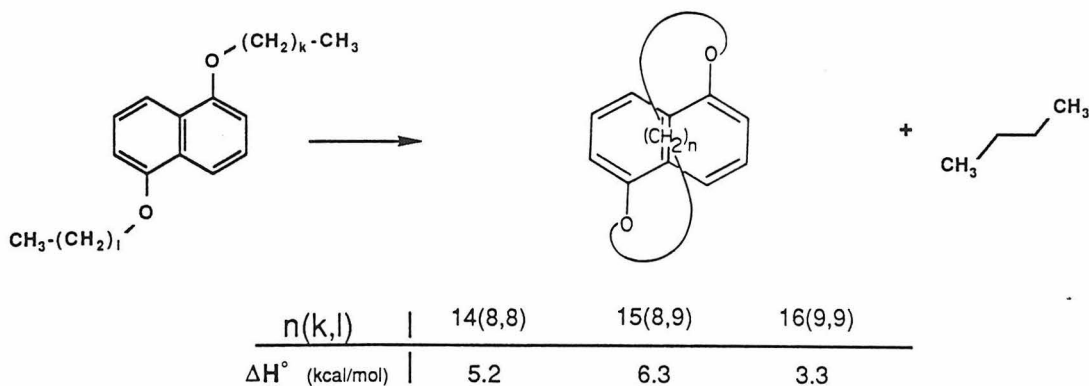


Figure 2.6. Calculating the strain energies of C14, C15 and C16.

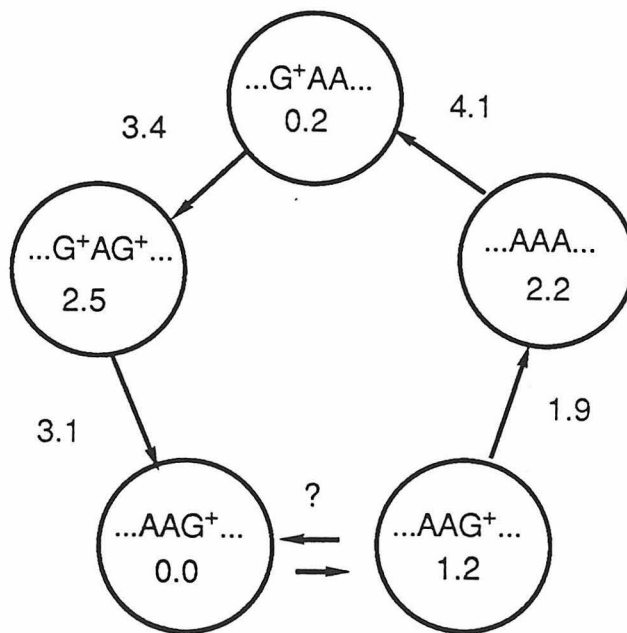
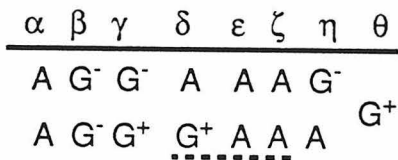


Figure 2.7. The results of angle driving calculations on C12. Energies (kcal/mol) are relative to the lowest conformation shown. Arrows indicate direction angle was driven.

a predicted strain of ca. 6.4 kcal/mol for a four-cornered conformation. The strain energies obtained are slightly lower than expected. This is probably due to the proximity of the ether oxygen to two of the corners, lowering the strain induced at these two corners.¹⁶

Finally, the topic of conformational interconversions will be briefly discussed. In macrocycles, it might be expected that individual dihedral angles are not freely rotating as in an open-chain molecule, but are constrained by the ring. Thus, conformational changes may involve a concerted change in several dihedral angles. The corner move^{9,17} is an important process for large rings involving a simultaneous change in three dihedral angles, and will be discussed more fully in Chapter 3. Other concerted motions, such as the Schatzki crankshaft motion have been studied for systems such as polymers.¹⁸ Another such motion is the gauche migration, which involves a change of the sequence ($G^{\pm}AA$) to the sequence (AAG^{\pm}).¹⁹ Because of its smaller size, the ring constraints are perhaps more severe for **C12**. Therefore, standard angle-driving calculations using the full MM treatment were undertaken for two low-lying conformations of **C12** related by a gauche migration. The results are shown in Figure 2.7. These calculations indicate the barriers to interconversions are quite small (< 4 kcal/mol), and that rotations along the chain are not necessarily coupled. For example, a single angle can be changed from gauche to anti and the rest of the chain will simply readjust. Also, it should be noted that two distinct minima were found that have the same conformational descriptor.

Conclusion

Two approaches to the elucidation of the low energy conformations of **1** have been described. Though the systematic approach did poorly at finding the ground states of these molecules, it was useful in showing that ΔS_{stat}^\ddagger is not a major contributor to ΔS^\ddagger for the jump-rope reaction. Predictions about the ground states of **1** can be made using a rational approach to the consideration of possible low-lying conformations. Starting with the constraints enforced by the naphthalene, adding the conformational preferences of aryl ethers, and then applying Dale's simple analysis leads to relatively few probable conformers. For **C16**, MM predicts two potential ground states, [9373] and [8383], the 0.6 kcal/mol energy difference between them being within the generally accepted error limits for the MM method. For **C15**, the lowest energy structures, [83163] and [83712], are derived from higher or lower homologues by cutting off a corner or inserting a bond at a corner. For **C14**, the Dale analysis, followed by MM leads to the prediction of the [8363] conformation as the ground state. MM calculations indicate that, as expected, these molecules are relatively strain-free, with many low-lying conformations that can rapidly interconvert at room temperature. In Chapter 3, experimental evidence will be presented which will support or confirm these predictions.

REFERENCES

- (1) U. Burkert and N.L. Allinger "Molecular Mechanics"; American Chemical Society: Washington, D.C., 1982.
- (2) M. Dobler "Ionophores and Their Structure"; Wiley: New York, 1981.
- (3) For example: E.F. Gale, *et al.* "The Molecular Basis of Antibiotic Action", 2nd ed.; Wiley: London, 1981.
- (4) For an overview of the host-guest field, see: "Topics in Current Chemistry"; F. Vogtle, Ed.; Springer Verlag: Berlin, 1981 and 1982; Vol. 98 and 101.
- (5) A similar approach is used in the program RINGMAKER: W.C. Still and I. Galykner *Tetrahedron* **1981**, *37*, 3981-96.
- (6) For example: M.R. Pincus and H.A. Scheraga *Acc. Chem. Res.* **1981**, *14*, 229-306
- (7) D.W.J. Cruickshank and R.A. Sparks *Proc. R. Soc. London.* **1960**, *258*, 270-285.
- (8) W.C. Still, unpublished results.
- (9) J. Dale *Acta. Chem. Scandi.* **1973**, *27*, 1115-1129, 1130-1148, 1149-1158.
J. Dale *Top. Stereochem.* **1976**, *9*, 199-270. J. Dale *J. Chem. Soc.* **1963**, 93-111.

- (10) F.A.L. Anet and A.K. Cheng *J. Am. Chem. Soc.* **1972**, *94*, 9250-9252. *ibid* **1975**, *97*, 2420-2424.
- (11) G.M. Anderson, P.A. Kollman, L.N. Domelsmith, and K.N. Houk *J. Am. Chem. Soc.* **1979**, *101*, 2344-2352.
- (12) N.L. Allinger *J. Am. Chem. Soc.* **1977**, *99*, 8127-8134. N.L. Allinger, S.H.M. Chang, D.H. Glaser, and H. Hönl *Isr. J. Chem.* **1980**, *20*, 51-56.
- (13) H.B. Burgi, W.D. Hounshell, R.B. Nachbar Jr., and K. Mislow *J. Am. Chem. Soc.* **1983**, *105*, 1427-1438.
- (14a) Bond stretching: 4-12; $K = 771.63 \text{ kcal/mol}\cdot\text{\AA}^2$, $R_0 = 1.36 \text{ \AA}$. Angle bending: 12-12-4, $K = 79.21 \text{ kcal/mol}\cdot\text{rad}^2$, $\Theta_0 = 121.4^\circ$; 12-4-2, $K = 110.85 \text{ kcal/mol}\cdot\text{rad}^2$, $\Theta_0 = 106.8^\circ$; 12-4-5, $K = 50.39 \text{ kcal/mol}\cdot\text{rad}^2$, $\Theta_0 = 106.8^\circ$.
Torsions (kcal/mol):

angle	V_0	V_1	V_2	V_3
12-12-12-4	14.736	-0.270	-15.0	0.0
4-12-12-1	15.0	0.0	0.0	-15.0
12-12-4-5	0.0	0.0	0.0	0.0
12-4-2-2	0.347	0.400	-0.520	0.467
12-4-2-1	0.530	0.0	0.0	0.530

Dipole, 12-4; 0.44 D.—where 1 = H, 2 = C, 4 = O, 5 = lone pair,
12 = C_{aryl} .

- (14b) In ref. 11, the X-ray structures of 30 planar, unhindered methoxy-substituted aromatics were examined. Bond lengths and valence angles were found to be comparable for the compounds considered and are listed below. The unknown stretching ($C_{aryl}-O$) and bending ($C_{aryl}-C_{aryl}-O$ and $C_{aryl}-O-C$) parameters were adjusted to reproduce this data, as shown.

	X-ray ¹¹	MM2
$C_{aryl}-O$	1.37 Å	1.38 Å
$O-CH_3$	1.43 Å	1.42 Å
$C_{aryl}-C_{aryl}-O$	124.0°	126.2°
$C_{aryl}-O-CH_3$	117.3°	115.4°

Ab-initio calculations on anisole¹¹ indicate that in the perpendicular conformation ($C_{aryl}-C_{aryl}-O-CH_3 = 90^\circ$) the $C_{aryl}-C_{aryl}-O$ angle relaxes to 120° and the $C_{aryl}-O-CH_3$ angles closes to 110.2° . These values are also reproduced by the bending and stretching parameters chosen. The ab-initio study predicts a 1.55 kcal/mol barrier to rotation of the methoxy group and places the perpendicular conformation in a very shallow minima. Instead, we chose to reproduce the experimental barrier of 3.6 kcal/mol^{14c} with the perpendicular conformation as the transition state to rotation.

- (14c) G. Allen and S. Fewster "Internal Rotation in Molecules";
W.J. Orville-Thomas, Ed.; Wiley-Interscience: New York, 1974 pg 275.
- (15) P. George, M.T. Trachtman, C.W. Bock, and A.M. Brett *Tetrahedron* **1976**, *32*, 317-323.

- (16) MM2 calculations on methylpropyl ether indicate that the C-C-C-O bond prefers anti to gauche by only 0.3 kcal/mol.
- (17) F.A.L. Anet and T.N. Rawdah *J. Am. Chem. Soc.* **1978**, *100*, 7166-7171..
- (18) T.F. Schatzki *Polymer Preprints*, **1965**, *6*, 646-51.
- (19) E. Helfand *J. Chem. Phys.* **1971**, *54*, 4651-61.

Chapter 3

The Conformations of C14, C15, and C16

as Determined by

Solid State CP-MAS ^{13}C NMR and X-ray Diffraction.

Introduction

In Chapter 2, it was shown that a Dale analysis produces relatively few potential ground state conformers for **C14-C16**. These few structures were easily evaluated by molecular mechanics, leading to predictions of the preferred geometries of these macrocycles. In order to assess the success of the Dale/MM analysis, experimental information about the conformations of these molecules was needed. To this end, two techniques have been applied: X-ray diffraction and CP-MAS ^{13}C NMR. X-ray diffraction is perhaps the most powerful method for the determination of molecular structure. It is capable of providing precise positions for the constituent atoms of a molecule. However, as can be the case with large floppy macrocycles, disorder prevented the determination of the full structures for **C14** and **C15**. A second technique based on ^{13}C chemical shifts, as observed in the solid by CP-MAS ^{13}C NMR spectroscopy, was also applied. These results provide support for the MM predictions made in Chapter 2.

Results and Discussion

X-ray Diffraction

As previously stated, cyclophanes **1** are chiral, having at most C_2 symmetry. For all three compounds, the enantiomers are rapidly interconverting in solution at room temperature, the temperature at which the crystals used for X-ray diffraction work were grown. It is interesting that all three compounds give crystals which belong to a chiral space group ($P4_12_12$) with only one enantiomer present in a given crystal.

C16. The molecular structure of **C16** is presented in Figure 3.1. The conformation found in the crystal is [9373], the conformation predicted by MM2 to be the ground state. The overall molecular symmetry is constrained by a crystallographic C_2 axis which is perpendicular to the naphthalene and intersects the midpoints of the C9-C10 and C_θ - C_θ bonds. Dihedral angles are listed in Table 3.1 along with the values from MM2 for comparison. It can be seen that the MM2 values are in excellent agreement with experiment. Bond lengths and valence angles are listed in Tables 3.2 and 3.3 along with the MM2 values. As can be seen, due to large amplitude motions in the crystal, the experimental bond lengths are slightly short and thus unreliable

The crystal packing is illustrated in Figure 3.2 and will be briefly described. As previously mentioned, the molecule has C_2 symmetry, with the naphthalene planes lying perpendicular to crystallographic C_2 axes. These run along the ab diagonals, and intersect both the C9-C10 and the C_θ - C_θ bonds at their midpoints. As can be seen from Figure 3.1, the molecule has a trapezoidal shape when viewed from the side. There is a crystallographic 2-fold screw axis coincident with the c axis which passes very near the midpoints of the C_γ - C_δ bonds. The molecule therefore packs along the c axis in columns with the short sides of the trapezoids abutting. Alternating molecules in the column are flipped by 180° about the c axis. The plane of the naphthalenes in this column are parallel to the (110) set of planes. There is a second such column, related by the 4_1 axes at $x = 1/2$ or $y = 1/2$, that is coincident to the 2_1 axis parallel to c which runs through the center of the unit cell. The planes of the naphthalenes in this second column are rotated by 90° with respect to the first column, *i.e.*, they are parallel to the $(\bar{1}10)$ set of planes. The molecules in this

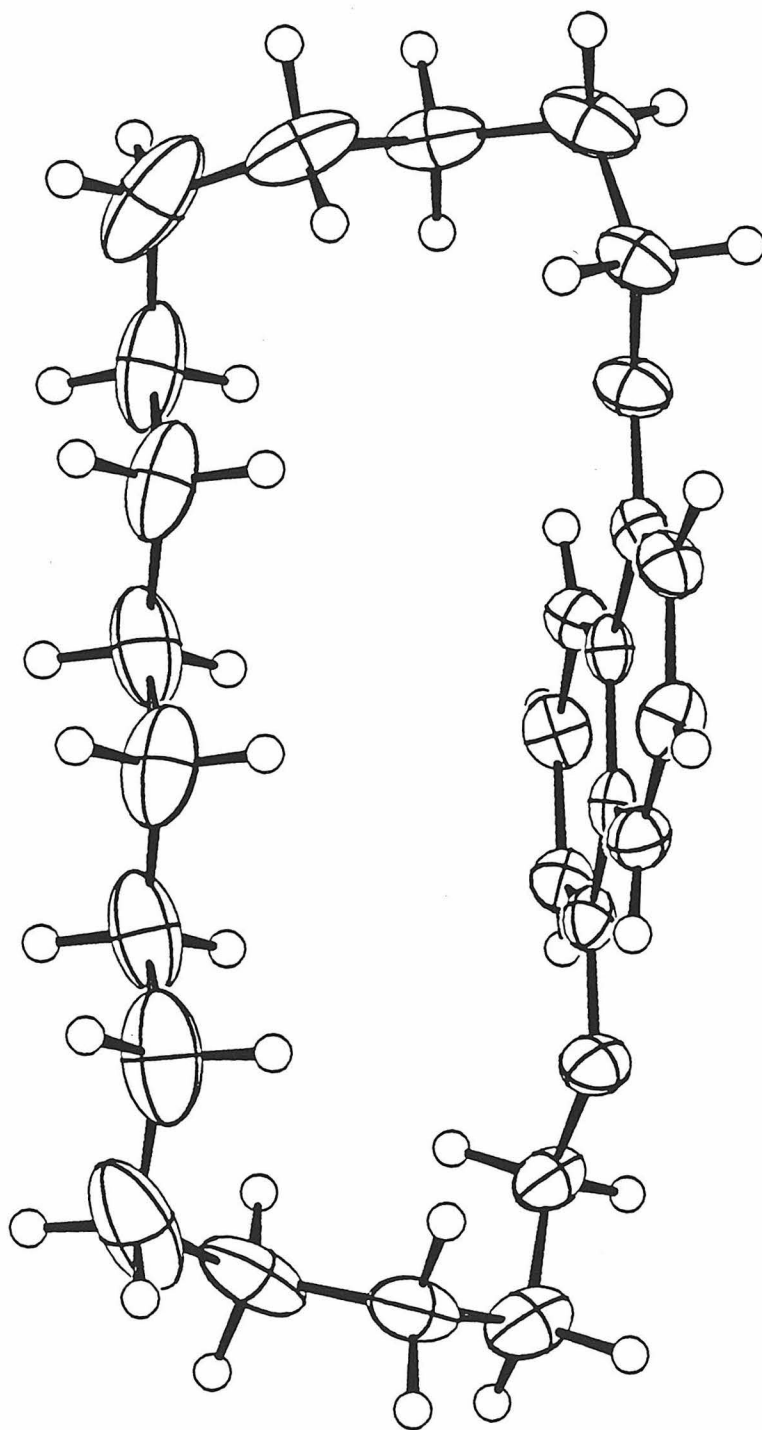


Figure 3.1. ORTEP drawing of the X-ray structure of **C16**. 20% probability ellipsoids are shown.

Table 3.1 Dihedral Angles of **C16** from X-ray Diffraction and MM2.^a

angle	X-ray	MM2
9-1-O- α	169.7(5)	169.9
1-O- α - β	-166.7(6)	-168.7
O- α - β - γ	57.2(9)	53.2
α - β - γ - δ	64.7(11)	67.1
β - γ - δ - ϵ	-166.9(10)	-158.9
γ - δ - ϵ - ζ	72.6(14)	70.5
δ - ϵ - ζ - η	63.4(15)	59.3
ϵ - ζ - η - θ	175.3(10)	170.4
ζ - η - θ - θ	179.2(9)	179.6
η - θ - θ - η	-179.7(8)	177.5

^a Values listed are in degrees (standard deviation of the last digit).

Table 3.2. Bond Lengths of **C16** from X-ray Diffraction and MM2.^a

bond	X-ray	MM2	bond	X-ray	MM2
O-1	1.364(8)	1.381	α - β	1.489(11)	1.542
O- α	1.417(8)	1.422	β - γ	1.509(13)	1.541
1-2	1.349(10)	1.402	γ - δ	1.499(15)	1.538
1-9	1.412(9)	1.410	δ - ϵ	1.505(18)	1.538
2-3	1.394(11)	1.395	ϵ - ζ	1.520(19)	1.542
3-4	1.370(11)	1.394	ζ - η	1.492(16)	1.539
4-10	1.381(10)	1.402	η - θ	1.526(14)	1.538
9-10	1.413(8)	1.405	θ - θ	1.503(14)	1.539

^aLengths given in Å (standard deviation of the last digit).

Table 3.3 Valence angles of **C16** from X-ray Diffraction and MM2.^a

angle	X-ray	MM2	angle	X-ray	MM2
O-1-2	125.3(6)	124.5	1-O- α	116.5(5)	116.9
O-1-9	114.4(6)	117.3	O- α - β	106.8(6)	108.4
9-1-2	120.3(6)	118.2	α - β - γ	113.7(7)	113.8
3-2-1	120.4(7)	120.9	β - γ - δ	114.0(8)	113.9
4-3-2	120.2(7)	120.0	γ - δ - ϵ	115.9(10)	113.6
10-4-3	121.1(7)	120.8	δ - ϵ - ζ	113.5(11)	115.3
10-9-1	119.3(6)	121.6	ϵ - ζ - η	116.8(11)	114.1
8-9-1	122.1(6)	119.9	ζ - η - θ	114.1(9)	112.5
9-10-4	118.6(6)	118.5	η - θ - θ	113.4(8)	112.0

^aValues given are in degrees (standard deviation of the last digit).

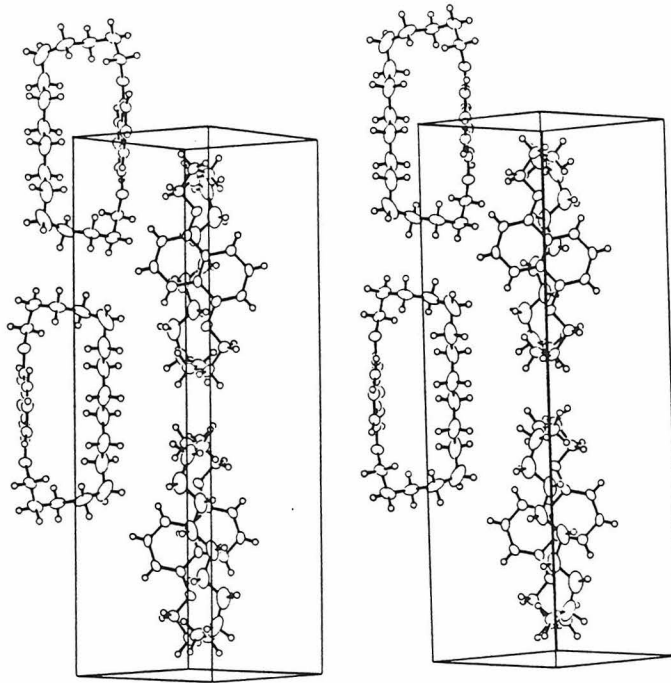


Figure 3.2. A stereoview of the molecular packing in the crystal.

column are displaced 1/4 along the c axis (one-half the molecule's length along c) with respect to the first column.

C14 and C15. For **C14** and **C15**, complete structures could not be determined. Perhaps the first indication that these structures would be disordered came from parameters derived from the Wilson plots.¹ The values obtained for 2B were 23 Å² for **C14** and 19 Å² for **C15**. For comparison, the value of 2B obtained from the Wilson plot for **C16** was 11 Å². All three data sets were collected for $1^\circ \leq \Theta \leq 20^\circ$ using Mo K α radiation.

As with **C16**, solution by direct methods was attempted for both **C14** and **C15**. In both cases, the naphthalene and the α carbon were found in the same position as for **C16**. Fourier maps (see Appendix B) revealed a continuous band or tube of electron density running ca. 4.0 Å above the naphthalene ring in roughly the position occupied by the chain for **C16**. However, disorder prevented the resolution of the positions of the carbon atoms along the chain and, therefore, full refinement of these structures was not possible.

Molecular mechanics calculations predict ground states with C_1 symmetry for both **C14** and **C15**. The lowest energy C_2 structures are 2.8 kcal/mol higher in both molecules. A C_1 structure which occupies the lattice site with two-fold disorder would produce the observed crystallographic C_2 axis and would account for the disorder of the polymethylene chain. Therefore, this seems a likely explanation. Such a disorder could be static or dynamic. If the disorder is due to the degenerate interconversion of a C_1 structure, giving rise to apparent C_2 symmetry (see Figure 3.8 for an example involving **C14**), then by cooling the crystal such motion might be frozen out and a full structure ob-

tained. However, attempts to study **C14** at low temperatures were discontinued because the crystals fractured on cooling.

Finally, it should be noted that **C14** could also be crystallized from ethanol to give orthorhombic crystals, space group *Pccn*. The naphthalene was found to lie perpendicular to a crystallographic C_2 axis and the polymethylene chain was disordered.

Solid State CP-MAS ^{13}C NMR

We have shown that a Dale analysis produces relatively few potential ground state structures for **C14-C16**, which can be evaluated by MM easily. For **C16**, X-ray diffraction confirms the ground state prediction. For **C14** and **C15**, disorder prevented the determination of the full structure. It would be useful to have an easily applied experimental tool that could provide support for the Dale/MM predictions. This is especially true in situations where X-ray diffraction does not provide a complete answer. Thus, we were intrigued by the recent studies of Möller² on the solid state ^{13}C chemical shifts in polymethylene chains. By studying cycloalkanes with both low temperature X-ray diffraction and low temperature CP-MAS ^{13}C NMR, it was found that the chemical shifts of the various carbons depended on the conformations about the two bonds on either side of a given methylene. The chemical shifts assigned to various conformational sequences are given in Table 3.4. Two shifts are distinctive, being reasonably well separated from the rest, and at each extreme, upfield and downfield: the shift associated with the sequence AA.AA at 35.5 ppm and the shift associated with $G^\pm A.G^\pm G^\pm$ at 23.6 ppm. These could be especially useful tools for determining where the corners are in a molecule.

Table 3.4. Solid State ^{13}C Shifts as a Function of Conformation.^a

$\text{G}^{\pm}\text{A} .\text{G}^{\pm}\text{G}^{\pm}$	23.6
$\text{G}^{\pm}\text{A} .\text{A} \text{G}^{\mp}$	25.0
$\text{G}^{\pm}\text{G}^{\pm}.\text{A} \text{A}$	27.9
$\text{A} \text{G}^{\pm}.\text{G}^{\pm}\text{A}$	28.7
$\text{A} \text{A} .\text{A} \text{G}^{\pm}$	30.4
$\text{A} \text{A} .\text{A} \text{A}$	35.5

^aFrom ref 2.

For a given conformation of **1**, the appearance of the solid state ^{13}C NMR spectrum can be predicted on the basis of the results in Table 3.4. For example, consider the [8363] conformation of **C14**, Figure 3.3. For the methylene labeled γ , the conformational sequence associated with the two bonds to either side is $\text{G}^+\text{G}^+.\text{A}\text{G}^+$, which would be expected to give rise to a peak at 23.6 ppm. Likewise for the methylene labeled γ' (which is *not* symmetry equivalent to γ in this conformation), the conformational sequence is $\text{G}^-\text{A}.\text{G}^-\text{G}^-$ and again a peak at 23.6 is predicted. In a similar fashion, the chemical shifts of all the methylenes can be predicted. Note that in such spectra, peak intensities often accurately reflect atomic ratios. By studying a variety of organic compounds, Grant found that signal intensities agreeing with atomic ratios were obtained from ^{13}C CP-MAS spectra if a contact time of about 2.25 ms was used, and often with a contact time as short as 1.0 ms.³ Möller also obtained quantitative spectra for cycloalkanes using a 3.0 ms contact time.² We have used a 2.0 ms contact time. Because the carbons of interest are on the aliphatic chain and all have two directly attached protons, they should be cross-polarized easily, and we can reasonably expect signal intensities to reflect atomic ratios.

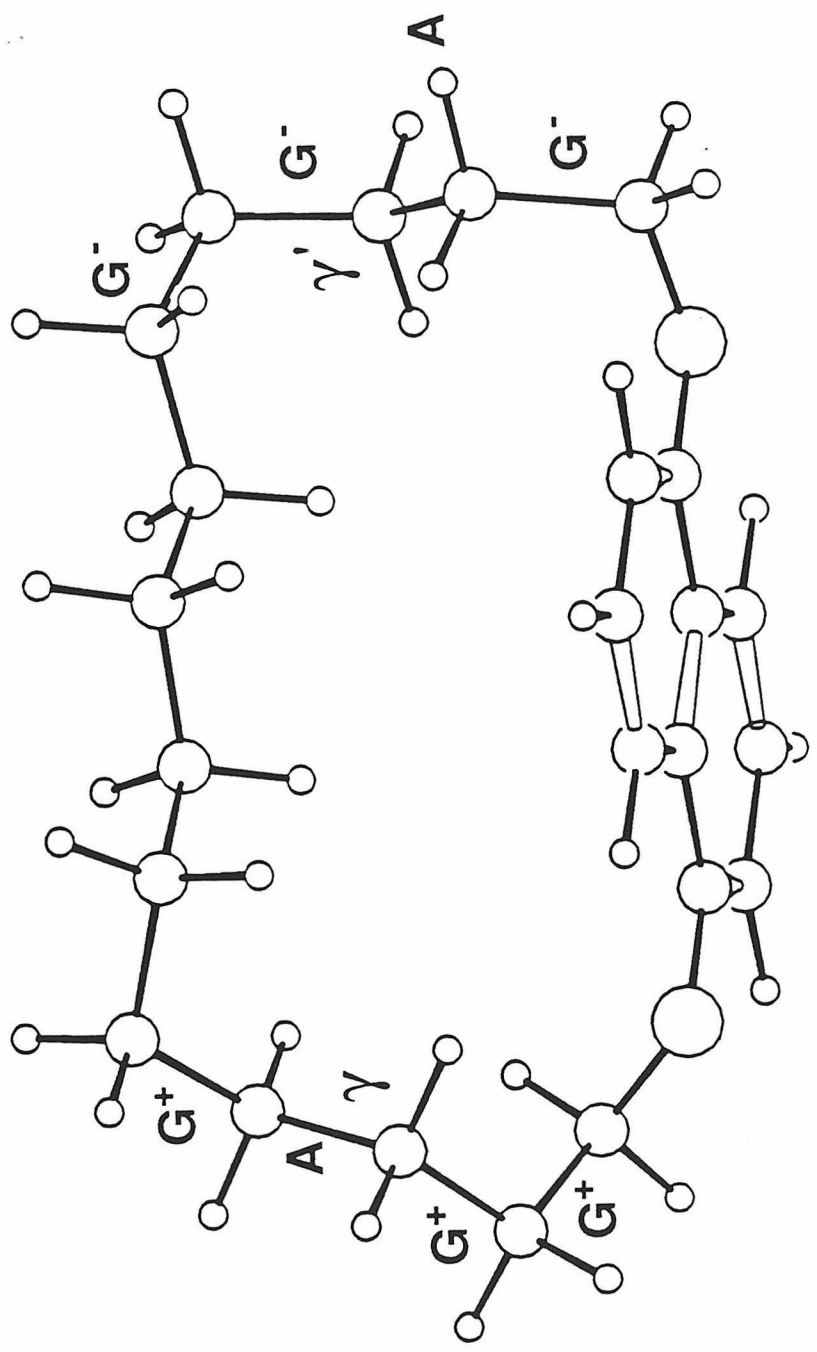


Figure 3.4. The [8363] conformation of C14.

Figure 3.4 shows the aliphatic region of both solid and solution state ^{13}C NMR spectra for **C14**, **C15**, and **C16**. For all three compounds, crystals of the tetragonal lattice were used. In addition, for **C14**, the orthorhombic lattice was investigated, but the two spectra were identical, so our discussion will emphasize the tetragonal. The entire spectra are given in Appendix C.

Because the ^1H NMR spectra have been previously assigned, heteronuclear ^{13}C - ^1H shift-correlated 2D NMR⁴ allows complete assignment of the ^{13}C peaks in the solution spectra. All methylene groups for **C14** and **C16**, and all but the central methylene group for **C15**, consist of a diastereotopic pair of protons. Each pair is interconverted by the jump-rope reaction. For **C15** and **C16**, the jump-rope reaction is fast on the NMR time scale at room temperature. Each CH_2 group produces only one signal in the ^1H spectrum and after consideration of the C_2 symmetry, eight aliphatic signals are expected. In the 2D NMR spectra of **C16** and **C15** (Figures 3.5 and 3.6), we have expanded the region containing the seven signals due to the $\beta - \theta$ methylenes. For **C14**, the jump-rope reaction is slow on the NMR time scale at room temperature and for the six methylenes, $\beta - \eta$, twelve signals would be expected in the ^1H NMR. Two signals in the ^1H spectrum should correlate to each peak in the ^{13}C spectrum. Only eight ^1H signals are resolved, as can be seen from Figure 3.7. The two protons of the δ methylene have nearly the same chemical shift and therefore a single multiplet correlates to one peak in the ^{13}C NMR. The same is true for the ϵ methylene. Also, the signals due to the ζ and η protons overlap giving rise to three, not four multiplets. As can be seen in the 2D NMR, the peak at 0.58 ppm (^1H) correlates to two peaks in the ^{13}C spectrum and is due to a proton on each of these two methylenes.

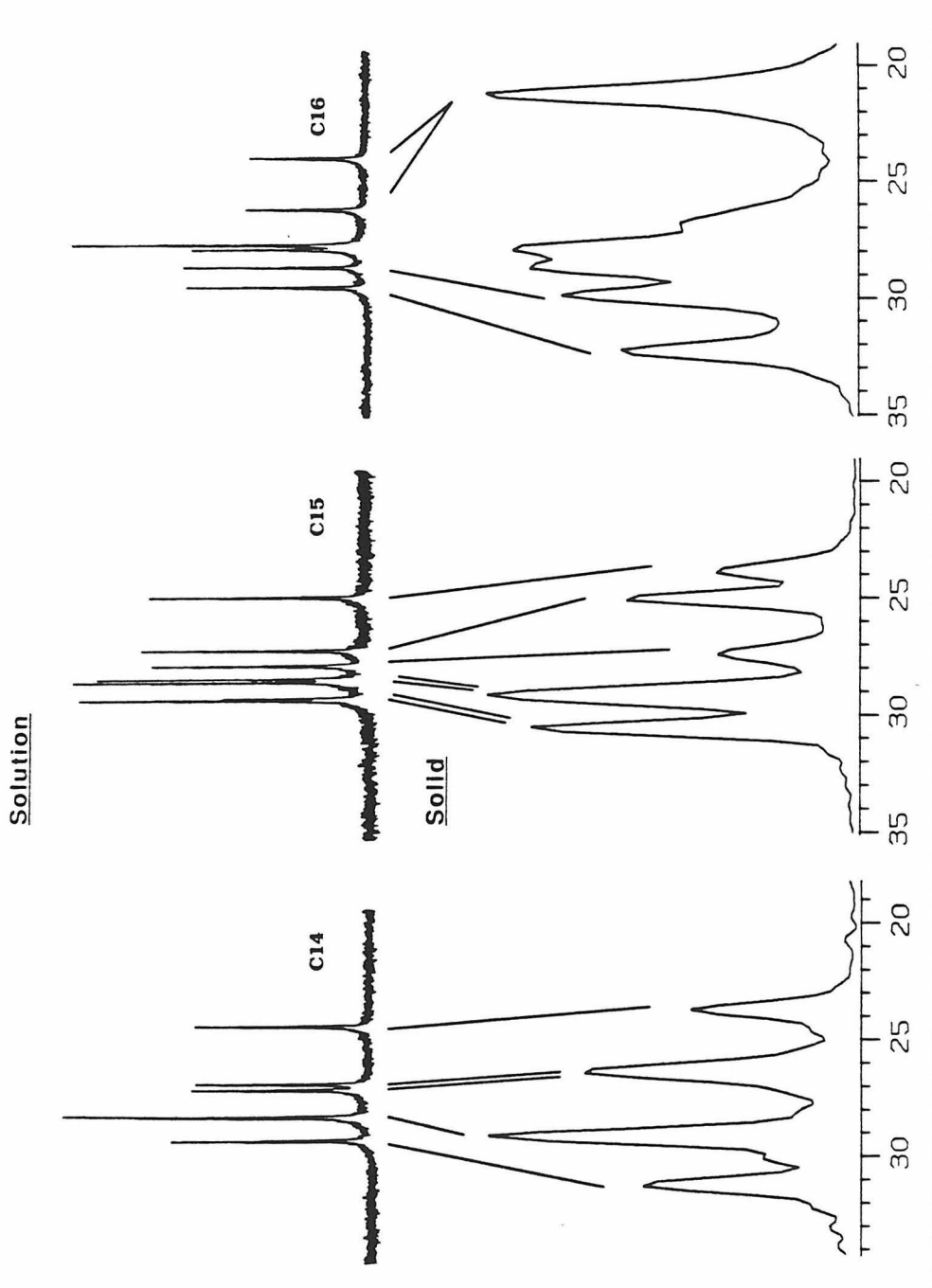


Figure 3.4. Aliphatic region of the ^1H -decoupled ^{13}C NMR spectra in CDCl_3 solution (top) and CP-MAS ^{13}C NMR spectra in the solid phase (bottom) of **C14**, **C15**, and **C16**.

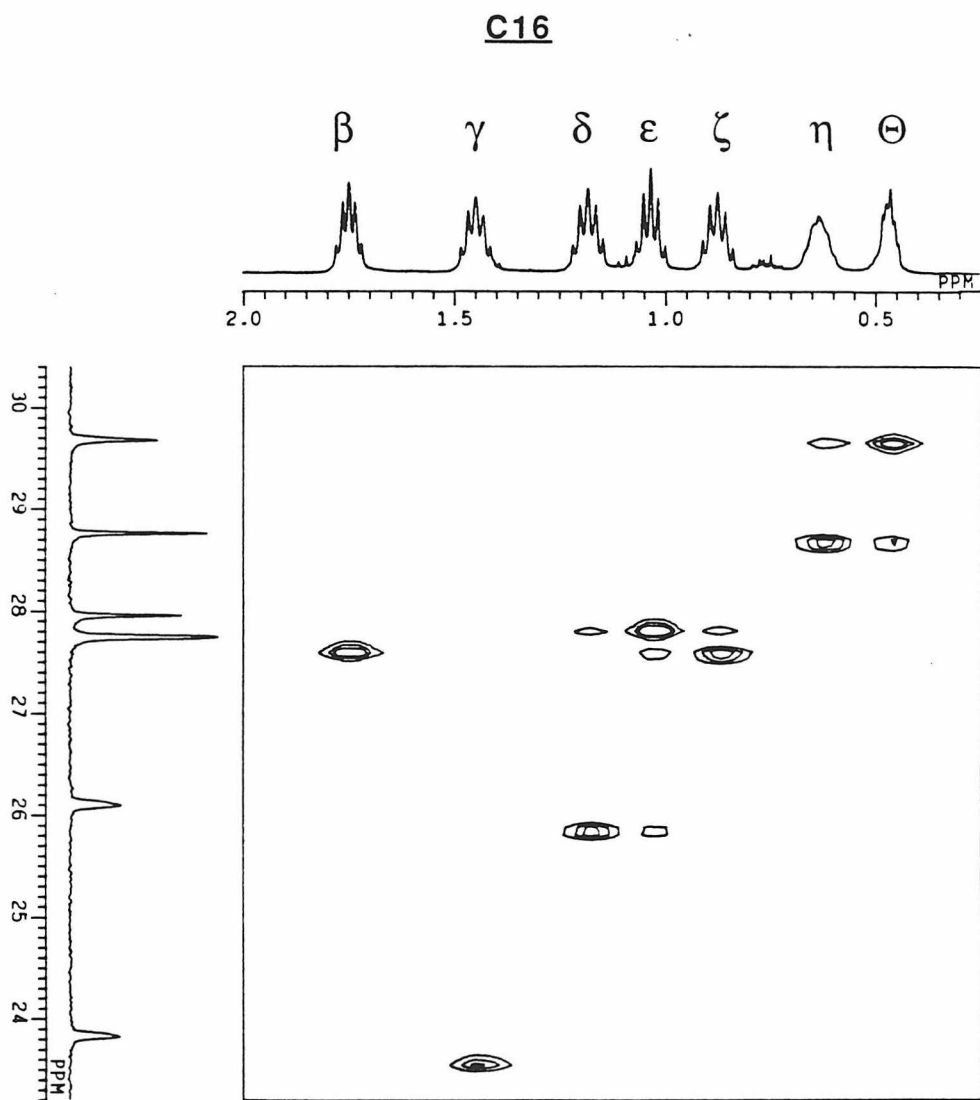


Figure 3.5 The aliphatic region of the heteronuclear ^{13}C - ^1H shift-correlated 2D NMR of C16.

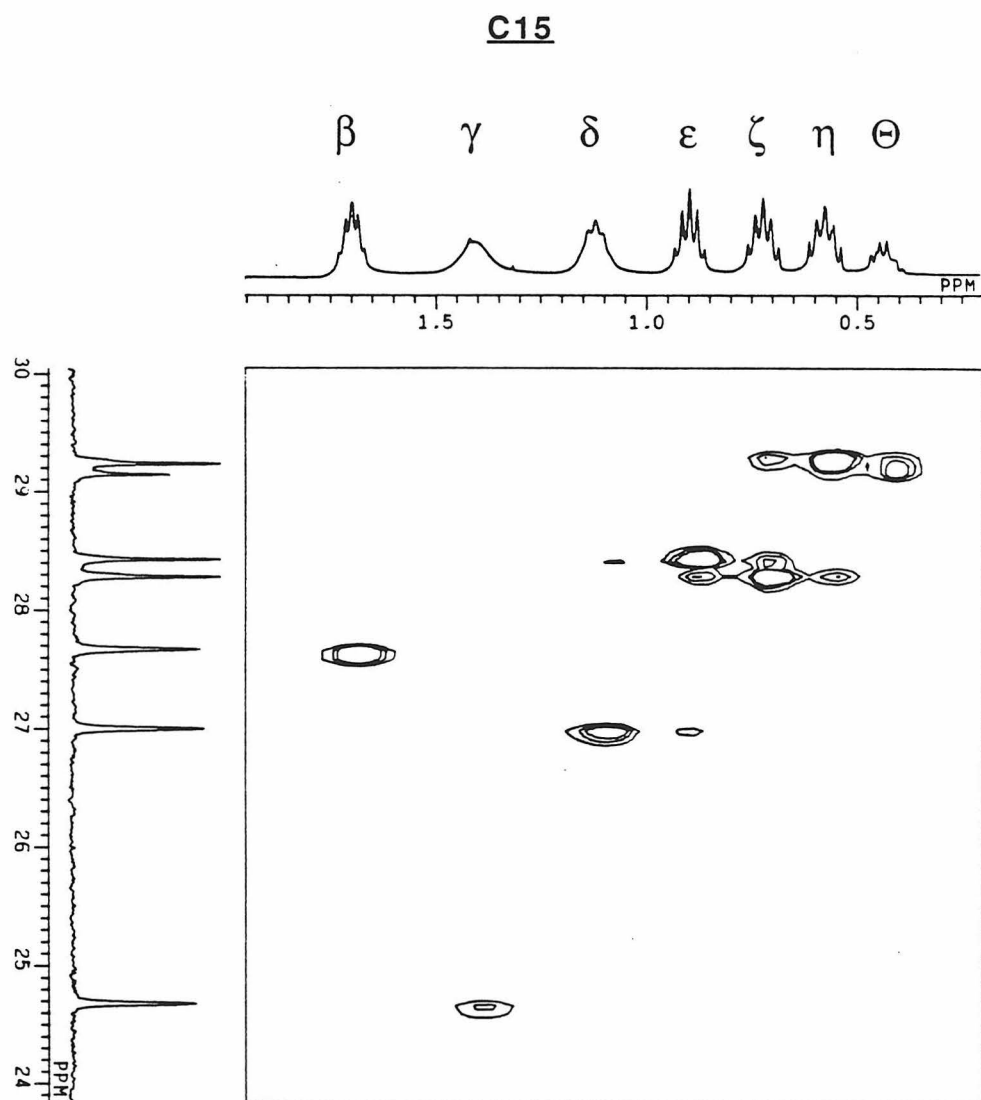


Figure 3.6 The aliphatic region of the heteronuclear ^{13}C - ^1H shift-correlated 2D NMR of C15.

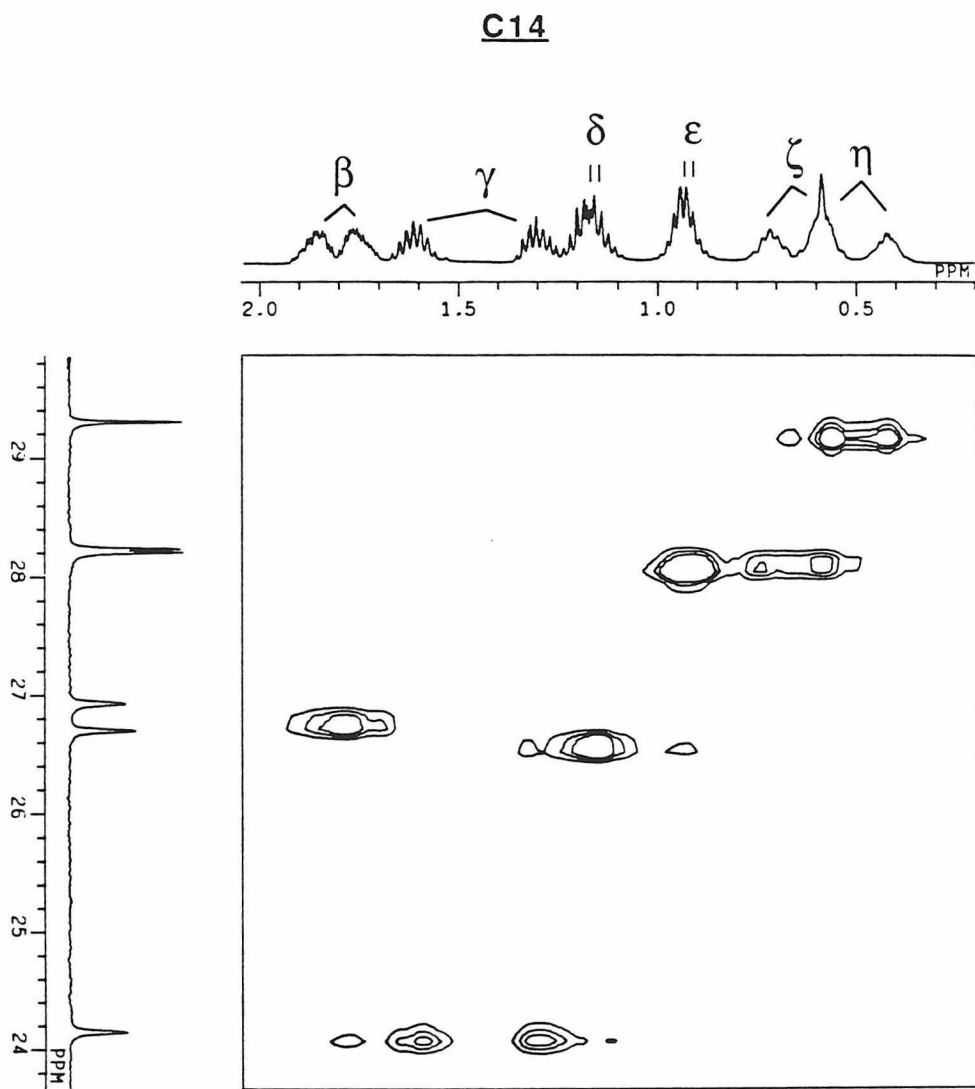


Figure 3.7 The aliphatic region of the heteronuclear ^{13}C - ^1H shift-correlated 2D NMR of C14.

The progression of the signals for the methylenes in the ^1H spectra, moving from left to right (downfield to upfield) is the same as the progression of the methylenes along the chain; *i.e.*, the α protons are the most downfield, the β protons are the next most downfield, etc.⁵ Note, this pattern is not carried over to the ^{13}C spectra. For all three compounds, it is the γ carbon which gives the most upfield signal. The carbons in the center of the chain, η and θ , give the most downfield signal of the methylenes, excluding α .

C14. It is apparent from Figure 3.4 that the solution and solid state spectra are quite similar. We can use this similarity to assign the peaks in the solid state spectrum as shown. Deconvolution of the aliphatic region of the solid state spectrum (see Appendix C) indicates that the peaks at 26.3 ppm and 29.1 ppm have twice the area of the peaks at 23.7 ppm and 31.2 ppm, consistent with the above assignments. The solid state shifts assigned to the various carbons are listed in Table 3.5 along with the shifts predicted for the various low energy conformations found by MM2.

The lowest energy conformation, [8363], has C_1 symmetry, and is inconsistent with the C_2 symmetry indicated by solution ^{13}C and ^1H NMR, by the solid state ^{13}C NMR, and by the site symmetry in the crystals. However, rapid interconversion on the NMR time scale of the two equivalent [8363] forms would lead to time-averaged C_2 symmetry. A potential pathway for this interconversion is outlined in Figure 3.8. The elementary step involved, $\text{G}^+\text{G}^+\text{A}$ changing to AG^-G^- , is a corner moving process that has been proposed to explain the dynamic behavior of other large-ring compounds, both in solution and in the solid state.^{2,6,7,8} The barrier to such a corner move has been calculated for cyclododecane by MM and found to be 7.9 kcal/mol, in good agreement

Table 3.5. Solution, Solid, vs. Predicted ^{13}C Chemical Shifts for **C14**.

Carbon	Solution ^a	Solid	Time Avg.		
			C ₂ [8363]	C ₂ [7463]	C ₂ [7373]
α	67.4	67.2	—	—	—
β	27.2	26.3	—	—	—
γ	24.4	23.7	23.6	24.2	23.6
δ	27.0	26.3	26.2	28.3	28.7
ϵ	28.5	29.1	28.3	28.3	27.9
ζ	28.5	29.1	29.2	29.2	30.4
η	29.6	31.2	33.0	33.0	35.5
Relative Energy ^b			0.0	1.4	2.8

^a CDCl_3 . ^b kcal/mol.

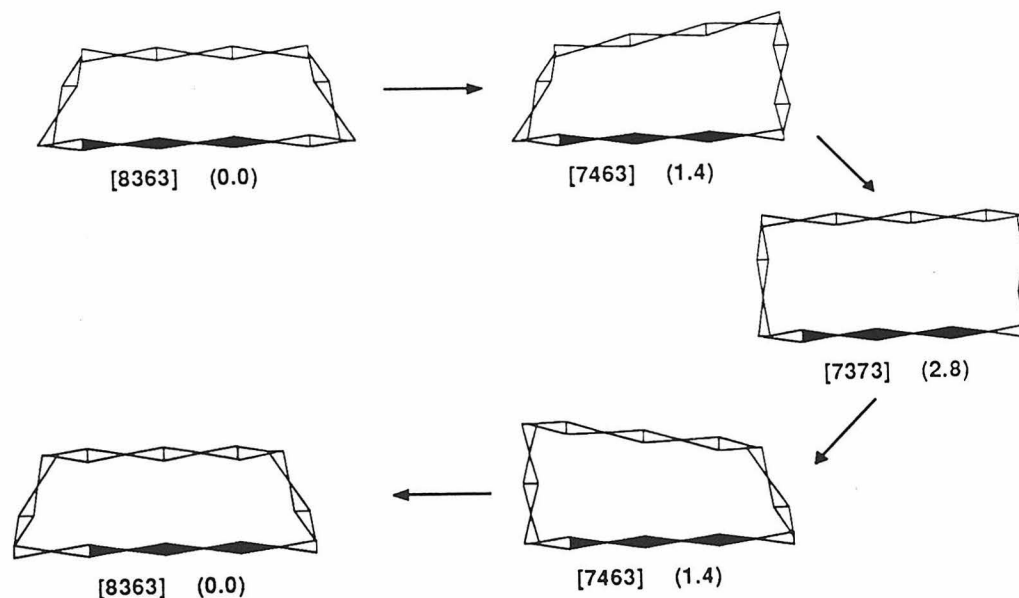


Figure 3.8. A pathway for the degenerate interconversion of the [8363] conformation of **C14**. Energies listed in parenthesis are in kcal/mol relative to [8363].

with the experimental free energy barrier of 7.3 kcal/mol in solution.⁷ Möller has made the intriguing observation that the same process occurs in the solid state and with essentially the same barrier as in solution.² A time-averaged [8363] structure therefore seems quite feasible, and it is included in Table 3.5. One should also consider the next lowest energy conformation, [7463] (C_1 symmetry). It is on the pathway outlined in Figure 3.8 and thus a time-averaged C_2 symmetry is feasible. As can be seen from Table 3.5, the shifts predicted for the [8363] and [7463] conformations (after "time-averaging") differ only for the γ and δ carbons. For both these carbons, the shift predictions for the [8363] are in excellent agreement with the observed shift data. The match for the [7463] conformation is much less satisfactory. We take this as evidence that the preferred conformation in the solid is [8363]. Additional evidence of the dynamic structure of **C14** in solution is provided by solution phase ^{13}C NMR on cooling to 153 K, see Figure 3.9. We know the broadening observed is due to chemical exchange because signals for the aromatic carbons (*m*, *p*, *ipso*) remain sharp (see Appendix C). If we take the coalescence temperature to be about 153 K and assume $\Delta\nu$, the frequency difference between the two coalescing peaks, to be about 3 ppm (300 Hz), then a crude estimate of about 6.8 kcal/mol for the free energy of activation of the process causing exchange can be made.⁹ This is similar to the barrier observed for corner moving in other systems.

C15. A comparison of the solution and solid state spectra again shows a great deal of similarity. This similarity was used to assign the peaks in the solid state spectrum, as shown in Figure 3.4. Because there is only one θ carbon and two of every other ($\alpha - \eta$), the peak assignments should give rise to the ratio 1.5:2:1:1:1 for the areas of the aliphatic peaks (moving left to right

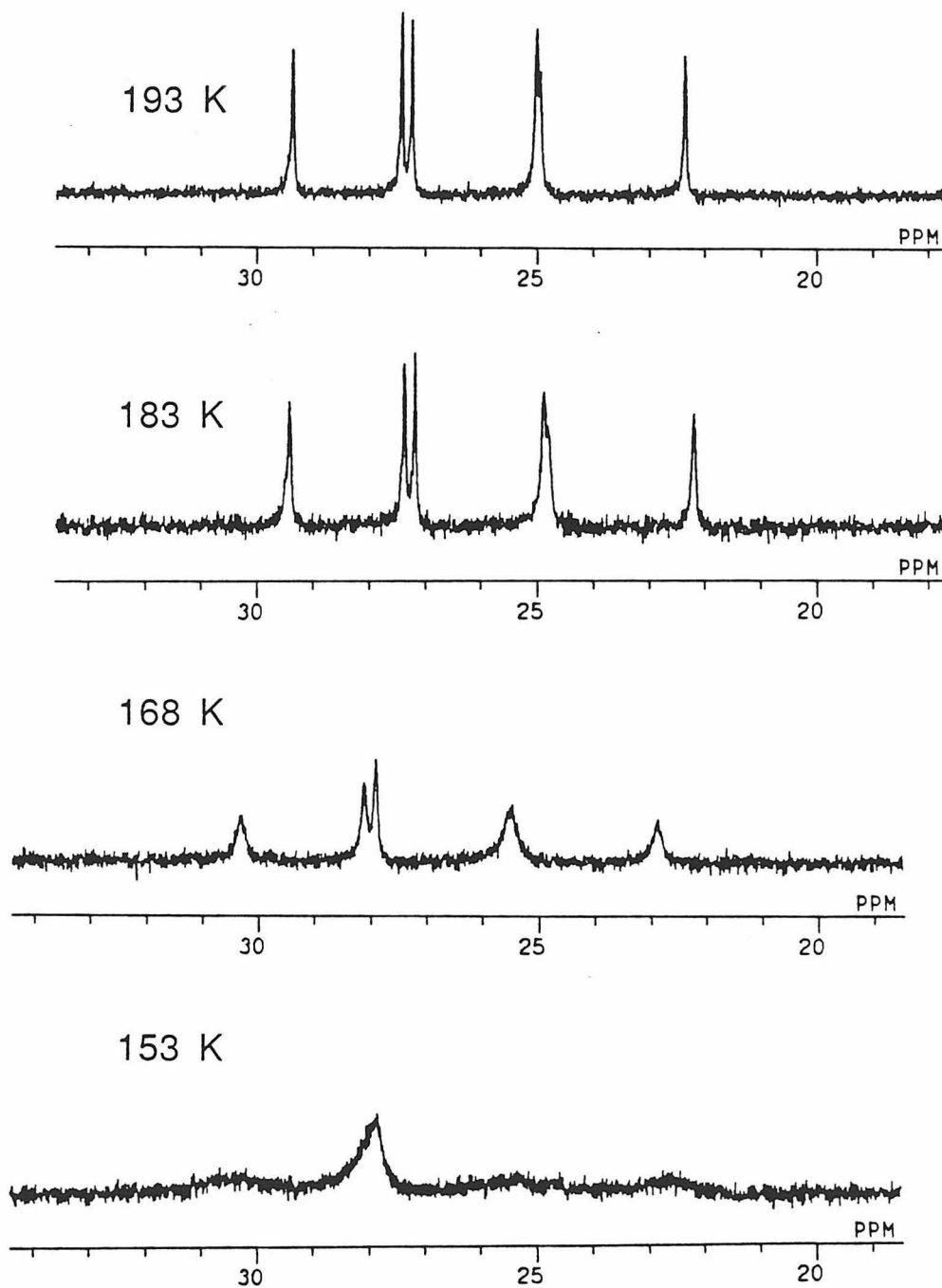


Figure 3.9. The aliphatic region of variable temperature ^1H -decoupled ^{13}C NMR spectra of C14 in a 1/3 $\text{CD}_2\text{Cl}_2/\text{CFCl}_3$ solution.

(downfield to upfield)). Deconvolution of the aliphatic region (see Appendix C) gives the expected ratio. Because all of the predicted low energy conformations have one nonstandard corner, and Möller studied only even-membered cycloalkanes having normal corners, it is not possible to make a quantitative prediction of the shifts for these conformations. However, qualitatively the trend is clear. As with **C14** and **C16** (vide infra), the γ carbon is the most upfield at 23.9 ppm. This suggests a carbon in the sequence $G^\pm A.G^\pm G^\pm$, putting the γ carbon in a side three bonds long. More informative, the η and θ carbons are the most downfield (as with **C14** and **C16**), indicating they are embedded in a sequence of anti dihedral angles (AA.AA). This rules out the regular trigonal and quinquangular conformations (*e.g.* [966], [876], [73443], etc.), but is consistent with the ring expanded or contracted structures which are predicted to be of lower energy. So, while the solid state ^{13}C chemical shift data does not allow the selection of a particular conformation, it does rule out several classes of conformations, and is most consistent with the ring expanded or contracted structures, the structures predicted to be the low energy conformations by MM2.

C16. As can be seen from Figure 3.4, a comparison of the solution and solid state NMR spectra again shows some similarity. In the solution state spectrum, a peak at 28.0 ppm can be seen by heteronuclear ^{13}C - ^1H shift-correlated 2D NMR to be a coincidence of two peaks, the peaks for the β and ζ carbons (Figure 3.5). However, deconvolution of the solid state spectrum (see Appendix C) indicates that it is the peak at 21.6 ppm in the solid which is the double peak. Of the two low-energy conformations found by MM2, only one, the [9373] conformation would be predicted to have double intensity for

Table 3.6. Solution, Solid, vs. Predicted ^{13}C Chemical Shifts for **C16**.

Carbon	Solution ^a	Solid	Time Avg.	
			C ₂ [9373]	C ₂ [8383]
α	66.7	65.9	—	—
β	28.0	27.2, 28.3 or 29.0	—	—
γ	24.0	21.6	23.6	23.6
δ	26.3	21.6	23.6	26.2
ϵ	28.2	27.2, 28.3 or 29.0	28.7	28.3
ζ	28.0	27.2, 28.3 or 29.0	27.9	29.2
η	29.0	30.2	30.4	33.0
θ	29.9	32.6	35.5	35.5
Relative Energy ^b			0.0	0.6

^a CDCl_3 . ^b kcal/mol.

the most upfield peak (see Table 3.6). As already stated, single crystal X-ray diffraction shows the conformation to be [9373]. Based on analogy to the solution spectrum, the two most downfield aliphatic peaks of the solid state spectrum can also be assigned, as shown in Figure 3.4. It is, however, difficult to assign the middle three peaks to particular carbons, as the shifts are so close to each other. Any assignment of these peaks would result in a satisfactory agreement between both solution and solid spectra and between the solid state spectrum and that predicted for the [9373] conformation.

The differences between the solid and solution NMR spectra may be due to the presence of a second conformation in solution. MM2 calculations predict the [8383] conformation is 0.6 kcal/mol higher in enthalpy than [9373]. However, because [8383] is of lower symmetry (C_1) than [9373] (C_2), the former will be favored by an entropic factor of $R \cdot \ln 2$ or ca. 0.4 kcal/mol at room temperature. Thus the two conformations are likely to be very close in energy, and both may be significantly populated at room temperature. Interconversion by a corner moving process would be expected to occur very rapidly on the NMR time scale and thus a time-averaged spectrum is observed in solution. This would lead to a downfield shift of the δ carbon in solution, as is observed.

Conclusion

Experimental data supporting the Dale/MM predictions of Chapter 2 have been obtained. For **C16**, MM predicts two low-energy structures, [9373] and [8383]. The solid state ^{13}C NMR contains an upfield signal of double intensity consistent only with [9373]. This assignment is confirmed by the X-ray structure. The solution ^{13}C NMR differs from that in the solid state in a way that is fully consistent with a rapid equilibrium between the two low-energy conformations. For **C15**, the lowest lying structures are predicted to belong to the ring expanded or ring contracted type of conformations. This prediction is strongly supported by the NMR data, although it is not possible to identify the ground state conformation. For **C14**, the [8363] conformation is predicted to be the ground state. The solid state NMR data support this conclusion.

For both **C14** and **C15**, the ground states have C_1 symmetry. However, solution ^1H and ^{13}C NMR, solid state ^{13}C NMR, and X-ray diffraction indicate C_2 symmetry. A rapid interconversion in both solution and solid, giving rise to time-averaged C_2 symmetry, is proposed. This is supported by variable temperature solution ^{13}C NMR for **C14**, and is consistent with the disorder observed by X-ray diffraction for both **C14** and **C15**.

We note that all three molecules share common features. The ordering of the signals in the ^1H NMR spectra are the same for all three compounds.⁵ In the ^{13}C NMR spectra, the γ carbons always give the most upfield signals, and the central carbons (η and θ) always give the most downfield signals. The predicted conformations all have a basically rectangular shape, with two long and two short sides. In all the conformations, the γ carbons reside in the short sides with one proton pointed in at the naphthalene, with its ring currents, and the other proton pointed out away. This explains why, for all three compounds, the γ protons consistently show a large chemical shift difference.⁵ Similarly, the carbons in the center of the chains of all three compounds form a zig-zag parallel to the plane of the naphthalene, and this points one proton down at the naphthalene and one up and away. Again large chemical shift separations are observed for the central methylenes.⁵

Overall, these results are quite encouraging. There is complete consistency among the data and the MM predictions. It is remarkable that the simple Dale/MM analysis can produce the correct conformations of such large flexible molecules. For the cyclophanes, **1**, solid state CP-MAS ^{13}C NMR was successful in providing useful information unavailable by X-ray diffraction. The shifts determined by Möller² provide a tool which should prove valuable in stud-

ies of other molecules containing polymethylene chains. It would appear that large-ring conformational analysis is not unmanageable if there is a structural element that provides some measure of order.

Experimental Section

General

The preparation of **C14**, **C15**, and **C16** has been described elsewhere.⁵ Routine ¹H and ¹³C NMR spectra and the 2D NMR spectra were taken on a JEOL-GX400 spectrometer.

X-ray Diffraction

Crystals of all three cyclophanes have been grown from acetonitrile and are transparent, multifaceted prisms. For both **C14** and **C16**, oscillation photographs and zero-level and first-level Weissenberg photographs¹ were taken as part of a preliminary investigation to determine the space group. Symmetry elements were evident in the photographic workup and indicated that the crystals belong to the tetragonal system. In both cases, the crystals were mounted along the *c* axis, which coincides with the long axis of the crystal. From the systematic absences observed in the intensity data (00*l* absent for $l \neq 4n$; *h*00 and 0*k*0 absent for *h* or *k* odd), the space group, $P4_12_12$ (# 92),¹¹ is unambiguously determined. The cell constants are: $a = b = 9.168(4), 9.143(2), 9.126(5)$ Å; $c = 26.23(2), 27.254(5), 28.071(9)$ Å; $Z = 4$ for **C14**, **C15**, and **C16**, respectively. They were determined by least-squares refinement of 25 2θ values: $10^\circ < 2\theta < 16^\circ$ for **C16**, $10^\circ < 2\theta < 26^\circ$ for **C15**, and $13^\circ < 2\theta < 22^\circ$ for **C14**. The intensity data for all three compounds were collected on an Enraf-Nonius CAD-4 diffractometer with a graphite monochromator using $\text{MoK}\alpha$ radiation with $2^\circ \leq 2\theta \leq 40^\circ$. A scan rate of $1^\circ/\text{min.}$ for scans of ω was used. For **C16**, one full quadrant (+*h*, +*k*, ±*l*) plus part of an additional quadrant (+*h*, -*k*, ±*l*) of data was collected. For **C15**, all but one quadrant (±*h*, -*k*, -*l*) of data was

collected. For **C14**, a hemisphere ($\pm h, +k, \pm l$) of data was collected. During data collections, three standard reflections that were checked every 5000 seconds showed no loss of intensity. The crystal used for data collection for **C14** was 0.43 x 0.43 x 0.43 mm. in size. The crystal used for data collection for **C15** was 0.36 x 0.36 x 0.36 mm. in size. The size of the crystal used for **C16** was not recorded, but was similar.

The structure of **C16** was solved in a lower symmetry space group ($P4_1$, # 76) by direct methods using the program MULTAN.¹⁰ This allowed the coordinates of the naphthalene group, the oxygen atoms, and twelve of the carbon atoms in the polymethylene chain to be determined. The positions of the remaining four carbons were determined by subsequent phasing and Fourier synthesis. Full-matrix least-squares refinement was carried out in the higher symmetry ($P4_12_12$) space group, minimizing the function $\sum \omega [F_o^2 - (F_c/k)^2]^2$. The asymmetric unit contains half the molecule, with the other half related by a crystallographic C_2 axis. The scale factor, the coordinates and anisotropic Gaussian ellipsoids for the carbon and oxygen atoms, plus the coordinates and isotropic temperature factors for the hydrogen atoms of the naphthalene were included in the refinement giving a total of 139 parameters. The hydrogen atoms on the carbon atoms of the polymethylene chain were not refined, but were simply placed in calculated positions. The scattering factors were taken from Ref. 11. The final cycle yielded a goodness-of-fit of 2.3 for 717 reflections; the R value obtained was 0.075 for $I_{obs} > 0$ and 0.054 for $I_{obs} > 3\sigma$. The final values of all the parameters, *i.e.*, coordinates, temperature factors, etc., are given in Appendix B with the structure factor amplitudes. All calculations were carried out on a VAX 11/750 computer using MULTAN or the CRYM

system of programs.

CP-MAS ^{13}C NMR

The NMR data were obtained on a home-built spectrometer operating at a carbon frequency of 50.4 MHz and equipped with a CP-MAS probe from Doty Scientific with 7 mm o.d. sapphire rotors. The samples were generally spun at speeds of 3.2-4.2 kHz. The ^1H 90° -pulse length was usually $5\mu\text{s}$. Cross-polarization contact times were 2.0 ms, and the Hartmann-Hahn matching condition was set using an adamantane standard, whose methylene peak also furnished a chemical shift reference at 38.56 ppm from TMS.¹² The cross-polarization pulse program incorporated spin-temperature inversion¹³ to suppress artifacts, and "flipback" of the ^1H magnetization to decrease the recycle delay. A "rolling baseline" in some spectra was eliminated by left-shifting the free-induction decay and by using a baseline fit routine on the Nicolet 1280 computer. Deconvolution of peak intensities was carried out using the Nicolet NMC software.

REFERENCES

- (1) For an introductory discussion, see: G.H. Stout and L.H. Jensen
"X-ray Structure Determination"; MacMillan Publishing: New York, 1968.
- (2) M. Möller, W. Gronski, H. Cantow, and H. Höcker *J. Am. Chem. Soc.* **1984**,
106, 5093-5099.
- (3) L.B. Alemany, D.M. Grant, R.J. Pugmire, T.D. Algers, and K.W. Zilm
J. Am. Chem. Soc. **1983**, *105*, 2133-2141, 2142-2147.
- (4) "Two Dimensional Nuclear Magnetic Resonance in Liquids"; A. Bax, Ed.;
Delft University Press: Holland, 1982.
- (5) M.H. Chang, B.B. Masek, and D.A. Dougherty *J. Am. Chem. Soc.* **1984**,
107, 1124-1133.
- (6) J. Dale *Acta. Chem. Scandi.* **1973**, *27*, 1130-1148.
- (7) F.A.L. Anet and T.N. Rawdah *J. Am. Chem. Soc.* **1978**, *100*, 7166-71.
F.A.L. Anet, A.K. Chang, and J.J. Wagner *J. Am. Chem. Soc.* **1972**, *94*,
9250-9252.
- (8) F.A.L. Anet and A.K. Cheng *J. Am. Chem. Soc.* **1975**, *97*, 2420-2424.
- (9) At coalescence, the rate constant for the process causing exchange is given by
 $k = (\pi \cdot \Delta\nu) / \sqrt{2}$. See: J. Sandström "Dynamic NMR Spectroscopy"; Academic
Press: New York, 1982.

- (10) G. Germain, P. Main, and M.M. Woolfson *Acta. Crystallogr., Sect. A* **1971**, *A27*, 368-376.
- (11) "International Tables for X-ray Crystallography"; Kynoch Press: Birmingham, England, 1974; Vol. IV.
- (12) W.L. Earl and D.L. Vanderhart *J. Magn. Reson.* **1982**, *48*, 35-54.
- (13) E.O. Stejskal and J. Schaefer *J. Magn. Reson.* **1975**, *18*, 560-563.

Chapter 4

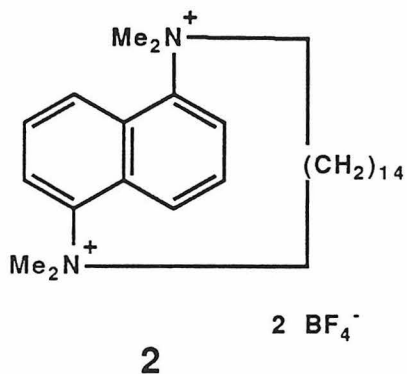
The Enantiomerization Kinetics of an
N,N,N',N'-Tetramethyldiamino-(1,5)-Naphthalenophane.

Introduction

The hydrophobic effect has been invoked to rationalize such diverse phenomena as the formation of micelles and the cell wall,¹ the capricious behavior of hydrolysis kinetics in water-rich binary solutions,² and the folding of proteins.³ The latter represents an example of the perturbation of the conformational properties of a molecule by the unique environment of aqueous solution. In the area of hydrophobic host-guest chemistry, the water-soluble hosts provide a greasy cavity in which hydrophobic guests can bind.⁴ Shape is presumably important in determining binding properties. However, because the host molecules are often macrocyclic, with some degree of flexibility, the conformation adopted in aqueous solution may differ from that predicted for the gas phase or a hydrocarbon solution. It is desirable to understand the influence the aqueous environment has on the conformational properties of such structures in order to better control their binding properties.

The relative energies of the various conformations of a hydrophobic hydrocarbon molecule in aqueous solution can be different from those in the gas phase or the liquid. For example, Monte Carlo simulations indicate that the population of gauche butane increases on going from liquid butane to butane dissolved in water.⁵ Enhanced folding is also predicted on the basis of surface area calculations. It has been shown that the solubilities of hydrocarbons correlate to the "water accessible surface area"; the larger the surface area, the larger the free energy of hydration.⁶ Thus, conformations with a smaller surface area are predicted to be stabilized relative to large surface area conformations, and folding is predicted to be enhanced.

As previously stated, naphthalenophanes such as **1** are ideal for the study of solvent effects on the dynamic properties of macrocycles for several reasons. First, the jump-rope reaction they undergo is an unambiguously defined process involving a large ring. Second, the rates for this process can be accurately measured. And finally, the synthesis of these molecules is relatively simple.



In order to assess the influence of the aqueous environment on the jump-rope reaction, the same probe molecule should be studied both in water and organic solvents. Clearly, cyclophanes **1** are inappropriate because of their very limited solubility in water. Instead, tetramethyldiamino-(1,5)-naphthalenophane **2** was chosen as the target molecule. Quaternary nitrogens replace the oxygens in order to enhance the water solubility. Methyl groups were chosen, as opposed to hydrogens, in order to avoid the complications of proton exchange. Also, because the methyl groups are diastereotopic and exchange sites via the jump-rope reaction, just as the protons on each methylene do, they can be used as a probe in dynamic NMR (DNMR) experiments. This removes the need for deuterating the hydrocarbon chain. The fourteen carbon chain was chosen because, by analogy to the ethers, **1**, it was hoped that coalescence would occur in the temperature range amenable to study in aqueous solutions, that is 30-60 °C.

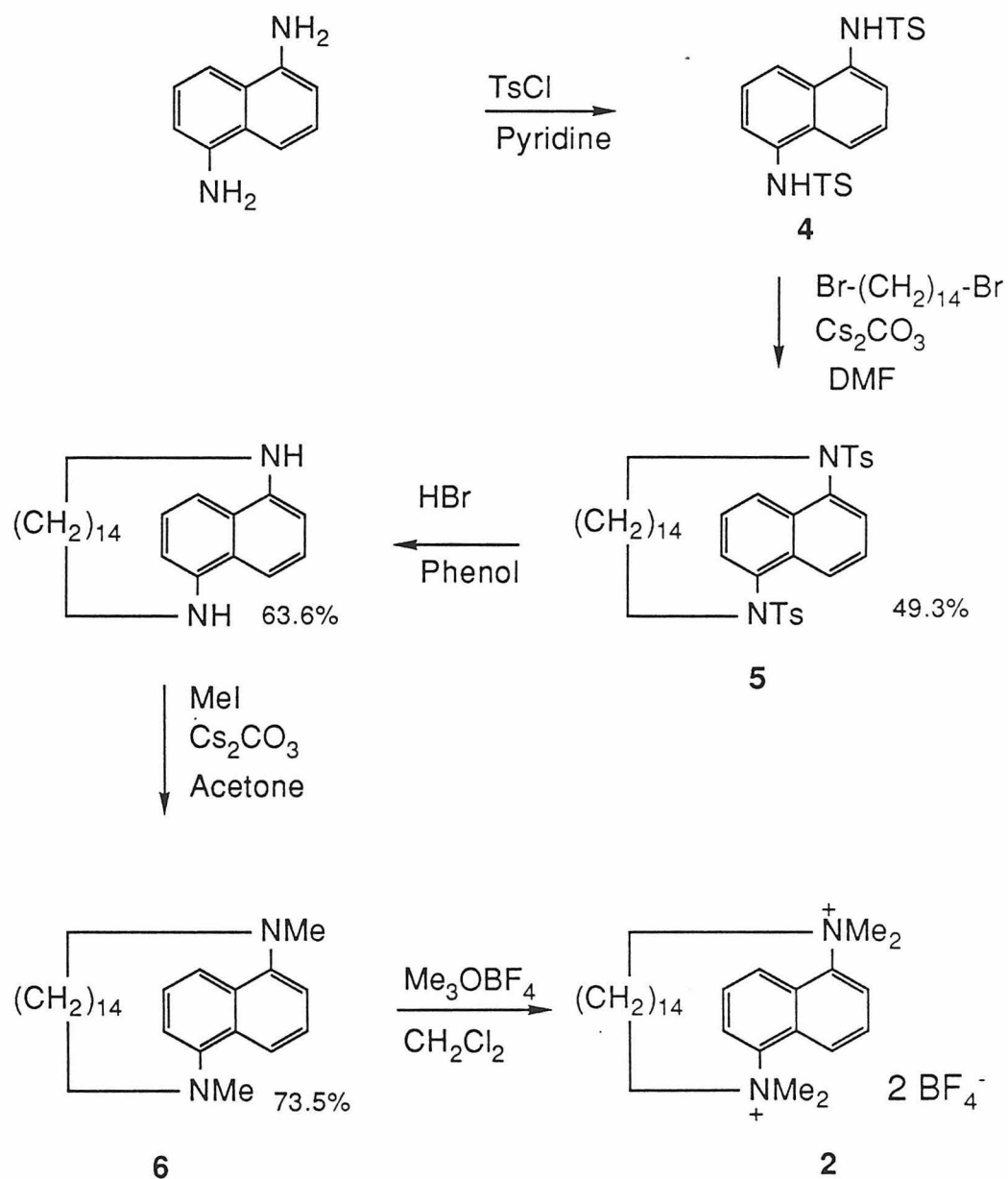
Synthesis

The synthesis of **2** is outlined in Scheme 4.1. 1,5-Diaminonaphthalene is protected against multiple alkylation by formation of the tosylamide, **4**. Alkylation of the tosylamide with 1,14-dibromotetradecane affords the desired macrocycle, **5**, in reasonable yield. Deprotection followed by methylation gives the target cyclophane, **2**. It should be noted that the methylation must be carried out in two steps. Alkylation with methyl iodide gives the tertiary amine, **6**. Presumably, quaternization is hampered by steric hinderance from the peri hydrogen of the naphthalene ring. However, after thorough drying, **6** can be alkylated with Meerwein's reagent to give **2** as the bis-tetrafluoroborate salt.

DNMR Results

The ambient temperature 400-MHz ^1H NMR of **2** in D_2O is shown in Figure 4.1. Similar spectra are obtained in methanol, acetonitrile, dimethylsulfoxide (DMSO) and acetone. These spectra indicate the jump-rope reaction is slow on the NMR timescale at room temperature. The two singlets at 3.8 ppm are assigned to the two diastereotopic methyl groups. The triplet at 4.8 ppm integrates for two protons and on the basis of chemical shift can be assigned to one-half of an AB pattern (plus additional coupling) due to the set of diastereotopic protons on the α carbons. The other half of this AB pattern is under the methyl peaks at 3.8 ppm. This is indicated by integration and by the fact that the AB pattern is partially resolved from the methyl peak in other solvents. The broad multiplets at 0.6–1.6 ppm are due to the remainder of the aliphatic chain.

SCHEME 4.1



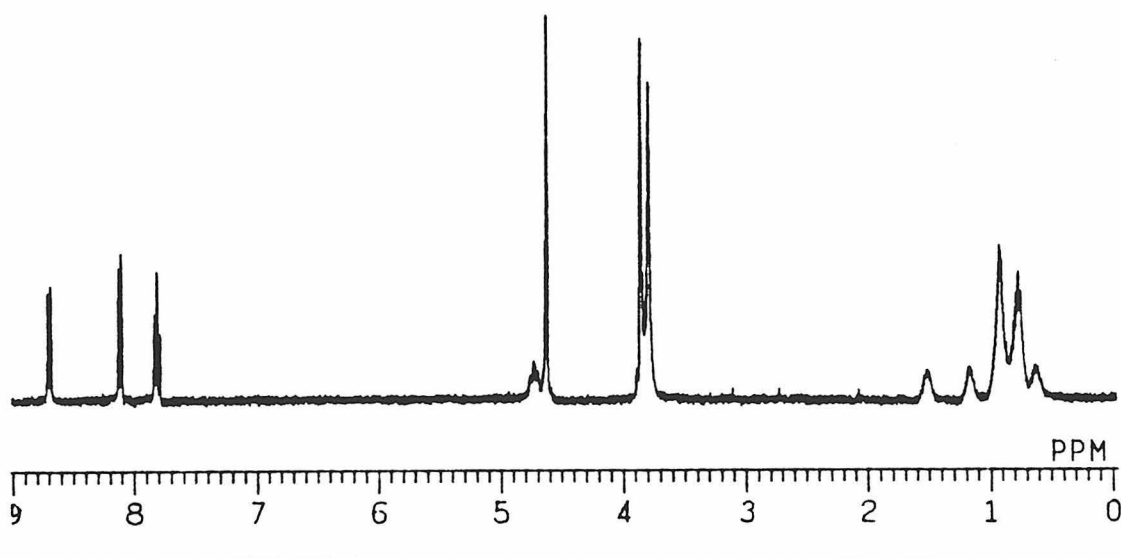


Figure 4.1. The 400-MHz ^1H NMR spectrum of **2** in D_2O at ambient temperature.

Because **2** is an amphiphile, containing both hydrophilic (quaternary nitrogen) and hydrophobic (naphthalene plus chain) groups, aggregation in aqueous solution might be expected. A plot of many physical properties (light scattering, ^1H chemical shifts) as a function of concentration will show inflections near the aggregation concentration.⁸ Therefore, the ^1H NMR spectra of **2** in D_2O were taken at saturation (≈ 0.9 mM) and at 0.09 mM. A sufficient signal to noise ratio could not be obtained in a reasonable amount of time for more dilute solutions. The chemical shift of all the peaks are essentially the same, indicating that these concentrations are either well below or above the aggregation concentration.

To simulate spectra of systems undergoing chemical exchange, the complete line shape method⁹ requires three parameters: the rate of exchange, k , the separation of the signals undergoing exchange, $\Delta\nu$ (in hertz), and the

effective line width, as indicated by T_{2eff} . Because both $\Delta\nu$ and T_{2eff} can be determined, the line shape observed is a function of only one unknown parameter, the rate, k . The value of T_{2eff} can be obtained from the line width of a signal not affected by chemical exchange. In this case, the low field aromatic doublet (δ 8.35) was used. The frequency separation, $\Delta\nu$, is generally determined by cooling well below the slow exchange limit. A linear plot of $\Delta\nu$ as a function of temperature can then be extrapolated into the region where chemical exchange causes broadening. Unfortunately, this was not possible for the aqueous solution of **2** because the signals for the methyl groups become completely decoalesced at about 15 °C. Thus, only one or two data points were obtained before the sample froze. Instead, spectra were obtained at two different fields¹⁰ on 400-MHz and 200-MHz spectrometers. If the spectra are obtained at the same temperature, the rates, k , will be the same. Also, the $\Delta\nu$'s of the two spectra are related. On the 200-MHz spectrometer, $\Delta\nu$ will be half that on the 400-MHz spectrometer. Since there are two observations (spectra) and only two independent variables, k and $\Delta\nu$, a unique solution can be obtained for k . Only one k and one $\Delta\nu$ are consistent with both spectra.

The 400- and 200-MHz spectra of the methyl protons of **2** in D₂O at various temperatures are shown in Figures 4.2a and 4.2b along with the simulated spectra. All simulated spectra were obtained with the program DNMR3¹¹ and the optimal fit was judged visually by overlapping the actual and simulated spectra on a light table. By varying the parameters from the optimal values, an estimate of the span of rates which still allow reasonable fits can be obtained as an indication of the error in the rate constants. The rates and estimated errors are listed in Table 4.1. The jump-rope reaction kinetics were also studied in

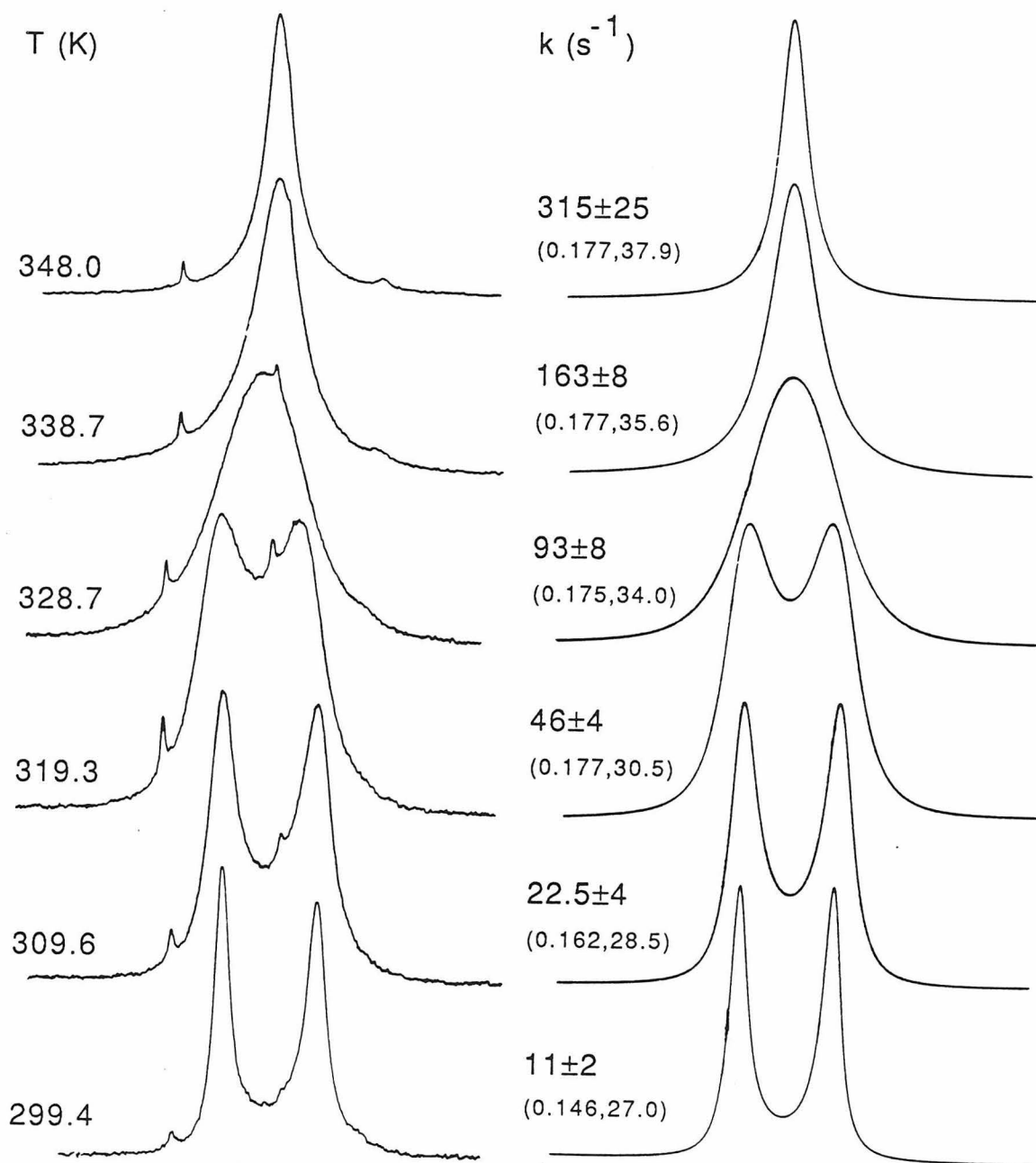


Figure 4.2a. 400-MHz, variable temperature, ¹H NMR spectra of the methyl protons of **2** in D₂O. The values in parenthesis are T_{2eff} and Δν.

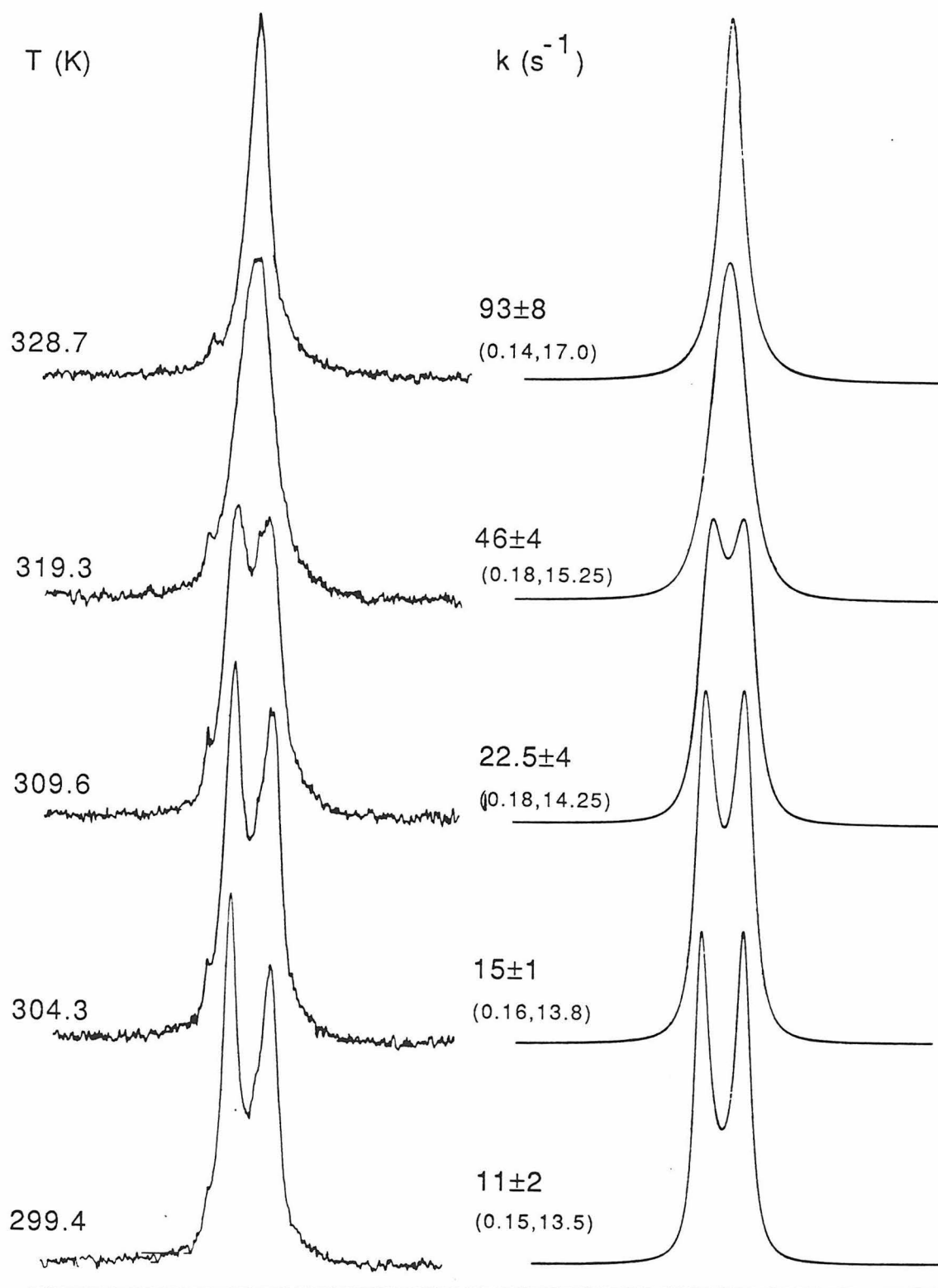


Figure 4.2b. 200-MHz, variable temperature, ^1H NMR spectra of the methyl protons of **2** in D_2O . The values in parenthesis are $T_{2\text{eff}}$ and $\Delta\nu$.

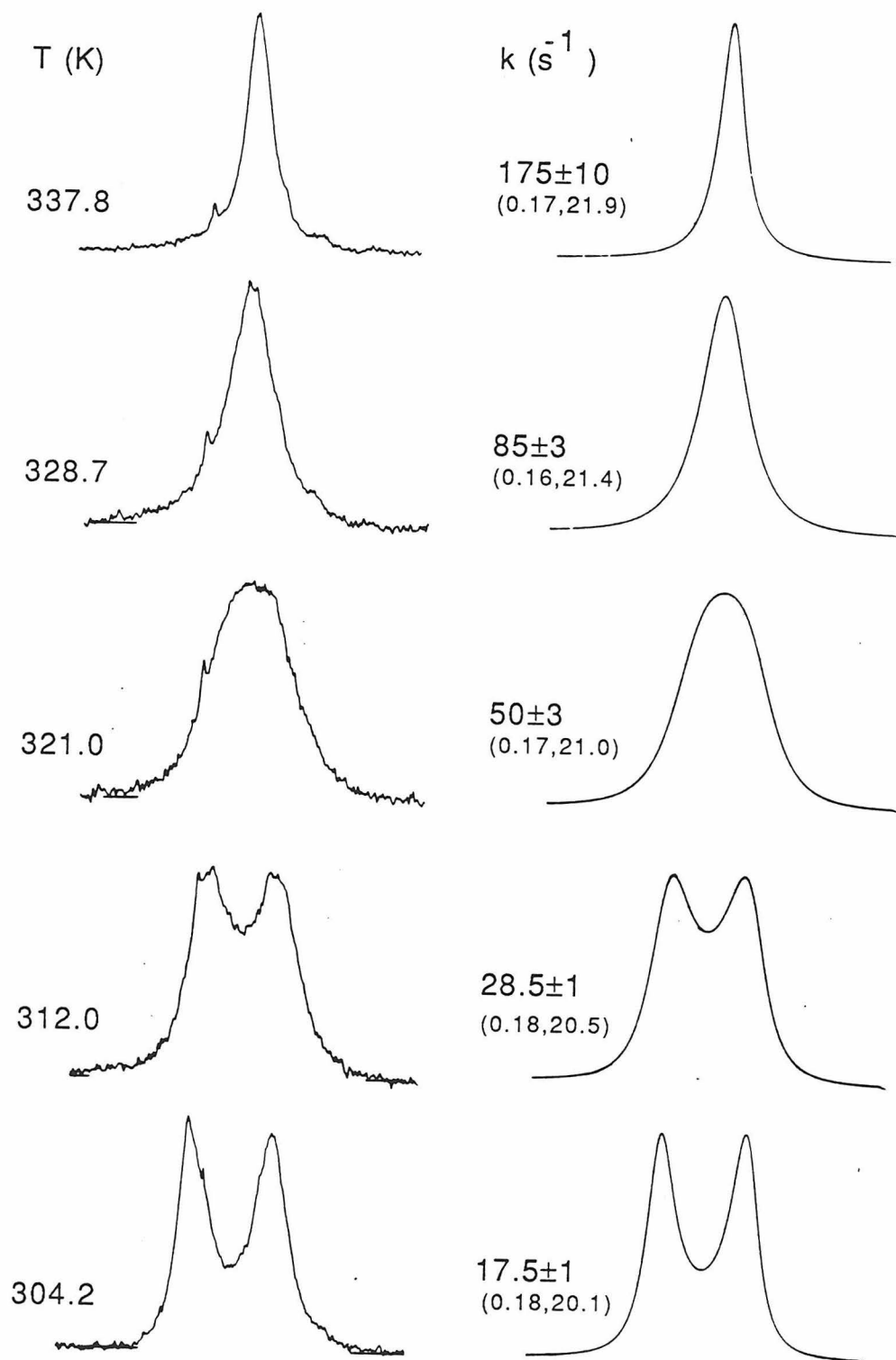


Figure 4.3. 200-MHz, variable temperature, ^1H NMR spectra of the methyl protons of **2** in CD_3CN . The values in parenthesis are T_{2eff} and $\Delta\nu$.

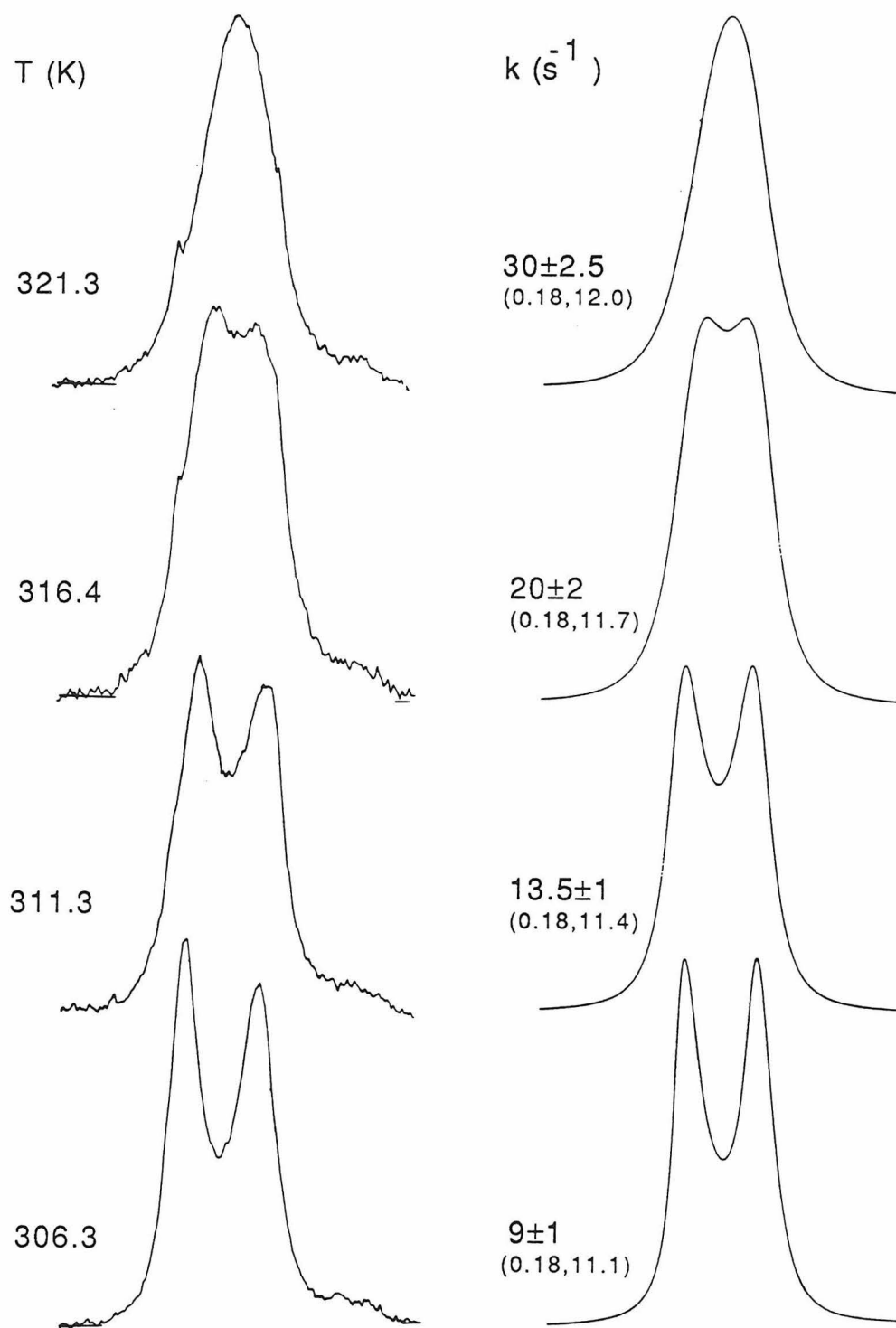


Figure 4.4. 200-MHz, variable temperature, ^1H NMR spectra of the methyl protons of **2** in MeOH. The values in parenthesis are T_{2eff} and $\Delta\nu$.

Table 4.1. Enantiomerization Rates of **2**.

solvent	T (K) ^a	k (s ⁻¹)
D ₂ O	299.4	11 ± 2
	304.3	15 ± 1
	309.6	23 ± 4
	319.3	46 ± 4
	328.7	93 ± 8
	338.7	163 ± 8
	348.0	315 ± 25
CD ₃ CN	304.2	17.5 ± 1
	312.0	28.5 ± 1
	321.0	50 ± 3
	328.7	85 ± 3
	337.8	175 ± 10
MeOH d ₄	306.3	9 ± 1
	311.3	13.5 ± 1
	316.4	20 ± 2
	321.3	30 ± 2.5

^a ± 1 K

Table 4.2. Activation Parameters for the Jump-Rope Reaction of **2** in various solvents.

	$\Delta G_{298}^{\ddagger a}$	$\Delta H^{\ddagger a}$	$\Delta S^{\ddagger b}$	ρ^c	$\sigma \Delta H^{\ddagger d}$	$\sigma \Delta S^{\ddagger d}$	pts. ^e	ΔT^f
D ₂ O	16.1	13.8	-7.8	.9996	0.2	0.5	7	48.6
CD ₃ CN	16.1	13.3	-9.3	.9959	0.7	2.2	5	33.6
MeOH	16.6	15.0	-5.2	.9997	0.2	0.8	4	15.0

^akcal/mol. ^bcal/mol·K. ^cCorrelation coefficient. ^dStandard deviation.

^eNumber of data points. ^fTemperature range.

acetonitrile and in methanol (see Figures 4.3 and 4.4). In both these cases, $\Delta\nu$ could be determined from the low temperature spectra. Because both these solvents have low boiling points, it was not possible to obtain spectra over the entire coalescence region on the 400-MHz spectrometer. Therefore, the 200-MHz spectrometer was used. The rates and estimated errors are listed in Table 4.1. Kinetics were not determined in DMSO because $\Delta\nu$ was very small and it was doubtful whether accurate activation parameters could be obtained.

Eyring plots of the data for the various solvents are given in Figure 4.5. The activation parameters and associated data were obtained using an iterative procedure that considers the errors in both the rates and the temperatures¹² and are listed in Table 4.2. Temperatures were considered accurate to ± 2 K.

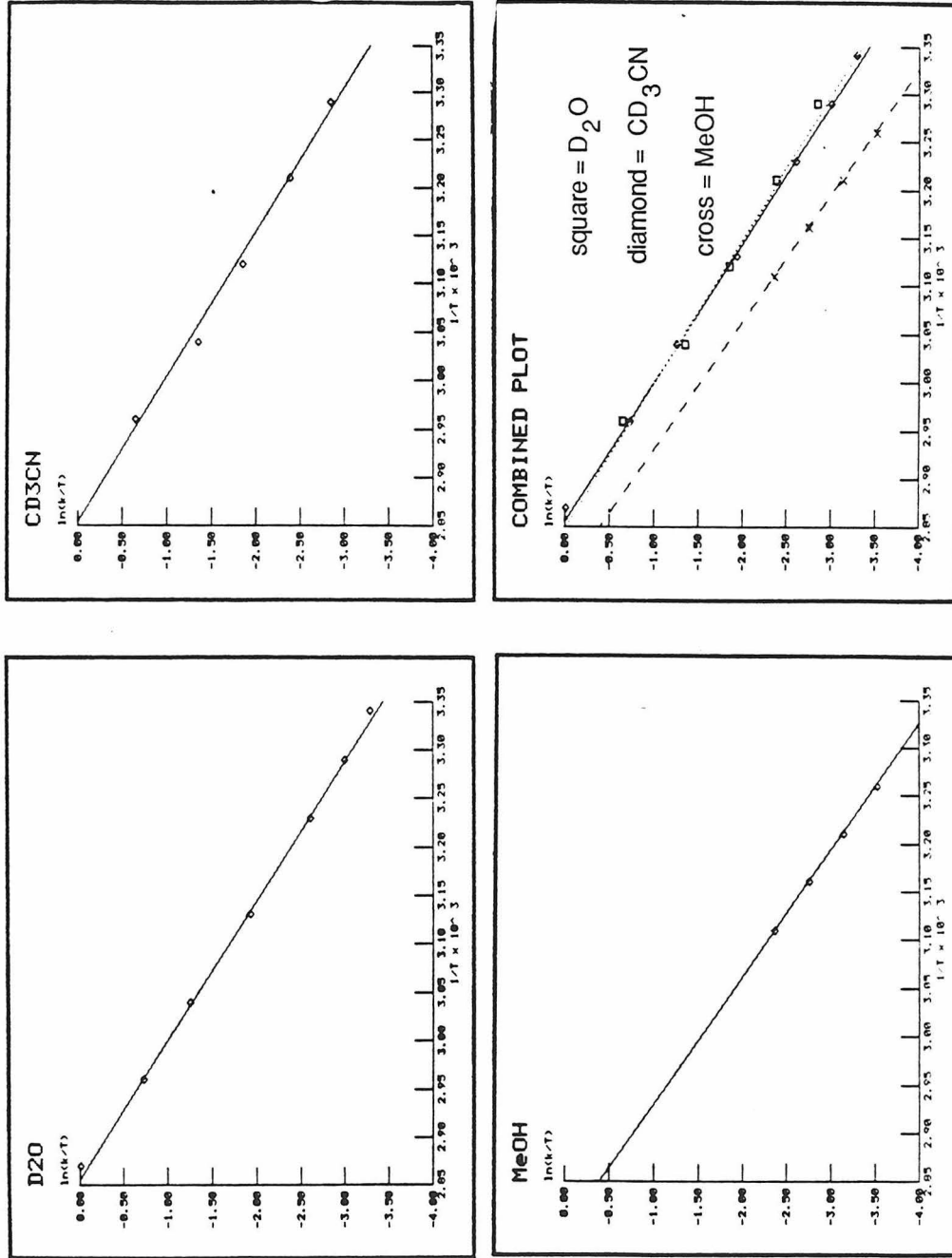


Figure 4.5. Eyring plots for 2 in D₂O, CD₃CN, CD₃OD, and a combined plot.

It is generally agreed that given the possibilities for systematic error in DNMR studies, the standard deviations in ΔH^\ddagger and ΔS^\ddagger derived from an Eyring plot are inadequate measures of probable error.^{9,13} As with the cyclophanes, **1**, the approach suggested by Sandström has been adopted.¹⁴ This method assumes maximal errors of 10% in rate constants and 1 K in temperatures to determine a maximal error in ΔG^\ddagger , and assumes the error in all points equals the maximal error in deriving errors for ΔH^\ddagger and ΔS^\ddagger . Using this approach, the best estimates for the activation parameters, listed in Table 4.3, are obtained.

The study in D₂O covers a 49 K temperature range. The seven data points span a 30-fold range of rates, and the activation parameters can be derived with some confidence. On the other hand, the study in methanol covers a mere 15 K temperature range, with only four data points covering a 3-fold rate range. Note, the small standard deviations in Table 4.2 derive from a good agreement amongst a small amount of data and are not a good indicator of the actual quality of the activation parameters. The study in acetonitrile covers a 34 K temperature range, the five data points spanning a 10-fold rate range. The larger error limits indicate the mediocre quality of the data. More accurate activation parameters could be obtained by increasing $\Delta\nu$, either by increasing the magnetic field or, in this case, by using the signals from a methylene group, some of which show very large $\Delta\nu$'s. The larger $\Delta\nu$ is, the greater the range over which coalescence occurs and so the greater the temperature range over which reliable rates can be obtained.¹³ Unfortunately, the greater $\Delta\nu$ is, the higher the temperature that is required for coalescence. For both methanol and acetonitrile, this will be a problem. A larger $\Delta\nu$ will cause a significant amount

Table 4.3. Activation Parameters with Estimated Error Limits.

	$\Delta G_{298}^{\ddagger a}$	$\Delta H^{\ddagger a}$	$\Delta S^{\ddagger b}$
2 (D ₂ O)	16.1 ± 0.2	13.8 ± 0.9	-8 ± 3
2 (CD ₃ CN)	16.1 ± 0.2	13.3 ± 1.2	-9 ± 4
2 (MeOH)	16.6 ± 0.2	15.0 ± 2.5	-5 ± 8
C14 (Nitrobenzene d ₅)	17.4 ± 0.2	10.4 ± 0.5	-23 ± 2

^akcal/mol. ^bcal/mol·K.

of the coalescence region to occur above the boiling point of the solvent.

Discussion

As can be seen from Table 4.1, the rates for the jump-rope reaction of **2** in various solvents at similar temperatures are very similar. An Eyring plot for the three data sets on the same axes shows the similarity (Figure 4.5). It is not surprising, then, that the activation parameters for **2** in various solvents (Table 4.3) all fall within experimental error of each other. No solvent effect on ΔG^{\ddagger} is observed although an effect of ca. 1 kcal/mol in magnitude should have been detectable. Because the error limits of ΔH^{\ddagger} and ΔS^{\ddagger} in both methanol and acetonitrile are large, the small differences in these activation parameters cannot be considered to be significant.

How do these results compare to predictions based on solvent accessible surface area calculations? As previously mentioned, the free energy of hydration of a saturated hydrocarbon is proportional to the area of its water accessible surface.⁶ This surface is defined as the area that would be traced out by the center of a probe sphere (radius = 1.45 Å for water) representing the solvent as it is rolled over the Van der Waals surface of the molecule of interest.^{6,15a} By calculating the difference in the water accessible surface area of the ground state and transition state for the jump-rope reaction, a prediction of the effect of water on ΔG^\ddagger might be made. C14 was used as the model compound for the calculations of water accessible surface areas. The program used was written by Connolly^{15b} and also allows the calculation of the surface area associated with the separate parts of the molecule. The total surface area, the area associated with the fourteen methylenes of the chain, and the area associated with the rest of the molecule (the naphthalene and the oxygens) are given in Table 4.4. The ground state of **2** is predicted to be the [5555] conformation (vide infra), and so the various surface areas of the [5555] conformation of C14 were calculated. As models for the transition state, the surface areas of the four best "transition states" of C14 (Chapter 2) were used. As can be seen (Table 4.4), on going from the ground state to the transition state, the total surface area decreases. Note, the aliphatic surface areas in the transition states are significantly larger than that of the ground state, while the surface area due to the aromatic group is much larger in the ground state than in the transition states. The free energy cost of exposing saturated hydrocarbon to water is ca. 30 cal/mol·Å².⁶ For aromatic hydrocarbons, the free energy of hydration per unit area is expected to be less,^{1,6a} but an exact value has not been obtained. On going from the ground state to the transition state, an increase in

Table 4.4. The water accessible surface areas of **C14**.^a

Conformation	Total ^b	Aromatic ^c	Aliphatic ^d
[5555]	629	224	405
TS1 ^e	593	163	430
TS2 ^e	603	163	440
TS3 ^e	603	157	447
TS4 ^e	601	163	438

^aUnits are Å². ^bsurface area of the entire molecule. ^csurface area of the naphthalene and the oxygens. ^dsurface area of the fourteen methylenes. ^ethe four lowest energy “transition states” from Chapter 2.

the solvation energy associated with the chain is predicted; however, a decrease in the solvation energy associated with the aromatic group is also predicted. The net result may be that the solvation energies of both the ground and transition states are nearly the same. No solvent effect on the reaction would be expected. This is consistent with the experimental results.

Although we observe no solvent effects on the jump-rope reaction of **2**, on comparing **2** with **C14**, substantial differences in the activation parameters for the enantiomerization are noted (Table 4.3). On going from **C14** to **2**, ΔH^\ddagger increases by 3.4 kcal/mol. However, ΔS^\ddagger becomes more positive by 15 eu., leading to a net lowering of ΔG^\ddagger for **2**. Can these differences be rationalized?

In Chapter 2, we calculated the barrier to rotation of the methyl group past the peri-hydrogen in 1-methoxynaphthalene to be 8.0 kcal/mol. We noted that this was similar to the values of ΔH^\ddagger observed for **C14-C16**. In an idealized enantiomerization pathway, one end of the chain would go past the peri-hydrogen and the other past C2. This seemed to suggest that a major contributor to ΔH^\ddagger is the peri-interaction, with relatively little strain in the transition state due to interactions involving the rest of the chain wrapping around the naphthalene. By analogy, the barrier to rotation of the *t*-butyl group in 1-*t*-butylnaphthalene has been calculated to be 4.0 kcal/mol using MM2. On going from 1-methoxynaphthalene to 1-*t*-butylnaphthalene, the barrier to rotation is predicted to *decrease*. On going from **C14** to **2**, ΔH^\ddagger is observed to *increase*. This indicates that the peri-interaction is not the only contributor to ΔH^\ddagger .

Replacing the oxygen in **C14** with dimethyl substituted nitrogen is expected to have a dramatic influence on the geometry of **2**. In **C14**, the α methylene has a strong preference to lie in the plane of the naphthalene eclipsing C2. Now consider **2**. In 1-*t*-butylnaphthalene, the preferred geometry has one methyl group in the plane of the naphthalene eclipsing C2, with the other two methyl groups symmetrically positioned above and below the plane. On going to cyclophane **2**, one of the methyl groups becomes a methylene. In the absence of ring constraints, no strong energetic preference for placing the methylene in either position exists. Thus, the α methylene may lie in the plane of the naphthalene as in **C14**, or it can, at no cost in energy, lie above or below the plane and, in so doing, create a corner at nitrogen. Thus, a corner can be built at the nitrogen without the usual 1.6 kcal/mol energy cost. The

Table 4.5. The relative energies of various conformations of **2a**^b and **C14**.^a

	2	C14
[5555]	0.0	11.2
[8363]	10.8	0.0
[7463]	7.3	1.4
[7373]	7.3	2.8

^akcal/mol. ^bi.e., **2** with nitrogen replaced by carbon.

[5555] conformation places corners at both the nitrogens and would therefore be expected to be of low energy for **2**. As a model for **2**, we used **2a**, in which the nitrogen atoms have been replaced by carbon atoms. The results of MM2 calculations on **2a** are shown in Table 4.5 along with those on **C14** for comparison. The [5555] conformation, which was of very high energy in **C14**, is predicted to be the preferred conformation of **2a** by a large margin.

CONCLUSION

The enantiomerization of **2** has been studied in D₂O, CD₃CN, and MeOH. No changes in the activation parameters for the reaction are observed, although small effects on the activation enthalpy or entropy might not be discernible because of the uncertainty in these parameters. When **2** is compared with **C14**, a dramatic difference in the activation parameters is noted. This difference could be rationalized by the fact that **C14** and **2** are predicted to have different preferred geometries. In addition, **2** is a gem-dimethyl substituted molecule. Such substituents are thought to enhance the rigidity of polymethylene chains. The effects of gem-dimethyl substituents are further investigated in Chapter 5.

Experimental Section

A. Methods:

Routine NMR spectra were recorded on a Varian EM-390 or a JEOL FX-90Q spectrometer. High-field NMR spectra were recorded on a Varian XL-200 or a JEOL GX-400 spectrometer. Chemical shifts are referenced to residual solvent peaks. Temperature controllers on both probes were calibrated during each run using MeOH (low temperature) or ethylene glycol (high temperature) and the standard Van Geet relationship.¹⁶ Line shape analysis was performed using the program DNMR3.¹¹ Elemental Analyses were obtained at the Caltech Analytical Facility. Melting points were determined on a Thomas-Hoover Unimelt and are uncorrected. Ultraviolet-visible absorption spectra were obtained with a Hewlett-Packard 8451A diode array spectrophotometer. Standard inert atmosphere techniques were applied for all reactions.

B. Materials:

DMF was distilled from CaO under vacuum and stored over a mixture of freshly regenerated 3 and 4 Å molecular sieves for at least one week before use. Me₃OBF₄ was stored in a dry box under inert atmosphere. Flash chromatography¹⁷ (diameter x length) was carried out with 230-400 mesh silica gel.

Preparation of 4. 1,5-Diaminonaphthalene (2.5 g, 16 mmol) and tosyl chloride (6.0 g, 32 mmol) were combined in a dry 250 mL round-bottomed flask. Dry pyridine (125 mL) was added via canula and the reaction mixture stirred for 5 h. The mixture was then added to 150 mL absolute EtOH, then

300 mL H₂O were added to give a light gray precipitate. A small portion was recrystallized from acetone/water to give the desired product. mp > 270° C; ¹H NMR (DMSO d₆) δ 2.0 (s, 3H), 6.8-7.8 (m, 7H), 9.8 (s, 1H).

Preparation of 5. Bis-tosylate **4** (0.373 g, 0.800 mmol) and 1,14-dibromotetradecane (0.285 g, 0.800 mmol) were combined in a dry 1 L round-bottomed flask. Dry DMF (800 mL) was added via canula and Cs₂CO₃ (1.0 g, 3.1 mmol) was quickly added. The reaction mixture was stirred at 50-60 °C for 3 days. The solvent was removed by rotary evaporation under reduced pressure and the residue washed with 5% HCl and CH₂Cl₂. The aqueous layer was extracted with CH₂Cl₂ (3 x 25 mL). The combined organic layers were dried with MgSO₄ and filtered. Flash chromatography (35 x 80 mm) eluting with 1/4 Et₂O/petroleum ether with collection of a 75 mL pre-run and 100 x 8 mL fractions gave 0.261 g (49.3%) of the desired product in fractions 50-60. ¹H NMR (CDCl₃) δ 0.8-1.4 (m, 12H), 2.4 (s, 3H), 3.2 (m, 1H), 4.0 (m, 1H), 6.7 (d, J=5 Hz, 1H), 7.3 (d, J=6 Hz, 2H), 7.4 (t, J=5 Hz, 1H), 7.6 (d, J=6 Hz, 2H), 8.4 (d, J=5 Hz, 1H); ¹³C NMR (CDCl₃) 143.21, 136.15, 134.87, 129.20, 128.02, 125.30, 125.22, 124.96, 52.80, 27.79, 27.33, 27.05, 25.81, 21.87.

Diamino-(1,5)-naphthalenophane. Macrocycle **5** (0.451 g, 0.682 mmol), phenol (0.53 g, 5.6 mmol) and ca. 15 mL 48% HBr were refluxed together for 1 day; the mixture was cooled and added dropwise to 45 mL 25% KOH with stirring and cooling. Extraction with Et₂O (3 x 25 mL) afforded the crude product in the organic layer. Flash chromatography (50 x 100 mm) eluting with 1/9 Et₂O/petroleum ether and collection of a 200 mL pre-run and 40 ca. 30 mL fractions gave 0.236 g (94%) crude product in fractions 7-11. Flash chromatography (50 x 85 mm) of the crude product eluting with benzene and

collection of a 100 mL pre-run and 36 x 40 mL fractions gave 0.153 g (63.6%) pure product in fractions 20-30. ^1H NMR (CDCl_3) δ 0.5-1.5 (m, 11H), 1.95 (br s, 1H), 3.25 (br s, 1H), 3.60 (br s, 1H), 4.50 (s, 1H), 6.60 (d, 1H), 7.05 (d, 1H), 7.25 (quartet, 1H); ^{13}C NMR (CDCl_3) 143.20, 124.78, 124.07, 107.89, 105.13, 43.32, 29.79, 28.37, 28.18, 27.51, 26.13, 24.70.

Preparation of 6. Diamino-(1,5)-naphthalenophane (0.153 g, 0.435 mmol), Cs_2CO_3 (0.9 g, 3 mmol) and MeI (5 mL) in 15 mL of acetone were refluxed together overnight, cooled, filtered, and the solvent removed on a rotovap. Flash chromatography (30 x 95 mm) eluting with 1/1 benzene/petroleum ether with ca. 0.5% Et_3N and collection of 8 mL fractions gave 0.121 g (73.5%) product in fractions 9-45. ^1H NMR (CDCl_3) δ 0.8-1.5 (m), 2.85 (s), 3.15 (br d), 7.0 (d), 7.35 (t), 7.95 (d).

Preparation of 2. Cyclophane **6** (0.121g, 0.320 mmol) was dried for 1 h at 80 °C under high vacuum. Me_3OBF_4 (0.260 g, 1.80 mmol) was added in a dry box and the flask fitted with a septum. When 2 mL CH_2Cl_2 was added, gas evolved and a precipitate slowly formed. The mixture was stirred for 2.5 hrs, then filtered, washed with CH_2Cl_2 , then with EtOH to give 0.188 g (100%) of a white precipitate. Recrystallization from MeOH/ H_2O gave the desired product. mp > 310°C with dec.; ^1H NMR see text; ^{13}C NMR (CD_3CN) 141.00, 128.47, 128.14, 127.16, 124.43, 69.72, 58.86, 58.50, 28.60, 28.57, 27.61, 27.47, 26.04, 25.19; Analysis ($\text{C}_{28}\text{H}_{46}\text{N}_2\text{B}_2\text{F}_8$); Calculated: C, 57.56; H, 7.94; N, 4.79. Found: C, 57.26; H, 7.65; N, 4.79.

Concentration of 2 in D₂O. The concentrations of **2** in D₂O were determined spectrophotometrically. A series of standard solutions of known concentration were found to obey Beer's Law in the concentration range 0.156–0.0312 mM. Thus 9.10 mg of **2** was placed in a 25 mL volumetric flask and doubly distilled water was added, with stirring, to the mark to give a 0.624 mM stock solution. Aliquots (500, 350, 200, and 100 μ L) of the stock solution were placed in 2 mL volumetric flasks and diluted to the mark to give a series of standard solutions at concentrations of 0.156, 0.109, 0.0624, and 0.0312 mM respectively. The vis-uv spectra of the standards show peaks at 224 ($\epsilon = 53000$), 282 ($\epsilon = 7200$), and 320 nm ($\epsilon = 950$). A program provided with the spectrophotometer to apply Beer's Law was used to determine the concentration of the NMR samples over a range of wavelengths (260–320 nm). The concentration of the DNMR sample used was found to be ca. 1.8 mM.

REFERENCES

- (1) C. Tanford "The Hydrophobic Effect"; John Wiley and Sons: New York, 1980.
- (2) J.B.F.N. Engberts "Water, A Comprehensive Treatise"; F. Franks, Ed., Plenum Press: New York, 1979; Vol. 6, Ch. 4.
- (3) T.E. Creighton "Proteins, Structure and Molecular Properties"; W.H. Freeman: New York, 1983; Ch. 4.
- (4) I. Tabushi and K. Yamamura *Topics in Current Chemistry* **1983**, *113*, 145-183.
- (5) W.L. Jorgensen *J. Chem. Phys.* **1982**, *77*, 5757-5765.
R.O. Rosenberg, R. Mikkilineni, and B.J. Berne *J. Am. Chem. Soc.* **1982**, *104*, 7647-7649.
- (6) a) R.B. Herman *J. Phys. Chem.* **1972**, *76*, 2754-2759.
b) *ibid* **1975**, *79*, 163-169.
c) R.B. Herman *Proc. Natl. Acad. Sci.* **1977**, *74*, 4144-4155.
d) J.A. Reynolds, D.B. Gilbert, and C. Tanford *ibid* **1974**, *71*, 2925-2927.
e) G.L. Amidon, S.H. Yalkowski, S.T. Anik, and S.C. Valvani *J. Phys. Chem.* **1975**, *79*, 2239-2246.
f) S.C. Valvani, S.H. Yalkowski, and G.L. Amidon *ibid* **1976**, *80*, 829-835.
- (7) M.H. Chang, B.B. Masek, and D.A. Dougherty *J. Am. Chem. Soc.* **1984**, *107*, 1124-1133.

- (8) E.S. Fendler, V.G. Constien, and J.H. Fendler *J. Phys. Chem.* **1975**, *79*, 917-926. P. Mukerjee and K.J. Mysels, *Natl. Stand. Ref. Data Ser., Natl. Bur. Stand.* **1971**, No 36.
- (9) For an excellent overview of the DNMR method, see: J. Sandström "Dynamic NMR Spectroscopy"; Academic Press: New York, 1982.
- (10) A similar approach was used by H.S. Gutowsky and H.N. Cheng *J. Chem. Phys.* **1975**, *63*, 2439.
- (11) D.A. Kleier and G. Binsch *Q.C.P.E.* **1979**, *11*, 165.
- (12) J.A. Irvin and T.I. Quickenden *J. Chem. Educ.* **1983**, *60*, 711-712.
- (13) G. Binsch and H. Kessler *Angew. Chem., Int. Ed. Engl.* **1980**, *19*, 411-428.
- (14) U. Berg, S. Karlsson, and J. Sandström *Org. Magn. Reson.* **1977**, *10*, 117-121.
- (15) a) M.L. Connolly *Science* **1983**, *221*, 709-713.
b) M.L. Connolly *Q.C.P.E. Bull* **1981**, *1*, 75.
- (16) A.L. Van Geet *Anal. Chem.* **1970**, *42*, 679-680. *ibid* **1968**, *40*, 2227-2229.
- (17) W.C. Still, M. Kahn, and A. Mitra, *J. Org. Chem.* **1977**, *42*, 3761-3764.

Chapter 5

The Effect of Gem-Dimethyl Substituents on the
Jump-Rope Reaction of a (1,5)-Naphthalenophane.

Introduction

In Chapter 4, the jump-rope reaction of cyclophane **2** was used to probe the effects that an aqueous environment might exert on the dynamic properties of macrocycles. Although no differences between water and organic solvents were observed, significant differences were noted on comparing the ether, **C14**, to the quaternary amine, **2**. Simple changes in a functional group induced important changes in the dynamic properties. In this chapter, further attempts to understand and quantitate the changes induced by substituents will be presented. Information about how substituents affect both the shape and rigidity of a macrocyclic system would be valuable both in understanding the properties of naturally occurring macrocycles^{1,2} and in designing new synthetic host molecules.³

A change in the preferred geometry has been predicted on going from **C14** to **2**. This change in the static geometry might explain the changes observed in the dynamic behavior. Additionally, part of the differences observed may be due to the effect of the gem-dimethyl substituents. It has long been known that gem-dimethyl substituents enhance the rate of ring formation in cyclization reactions as well as favoring the cyclic form at equilibrium. This has come to be known as the gem-dimethyl effect.^{4,5} Thermodynamic data for both 5- and 6-membered rings indicates that both the enthalpy and entropy of ring closure become more favorable upon substitution, each contributing roughly equally to the observed enhancements.⁴ Allinger has rationalized both the enthalpic and entropic effects observed for a series of substituted hexanes.⁵ The enthalpic enhancement observed could be calculated by considering the change in the number of gauche interactions induced by cyclization. The entropy en-

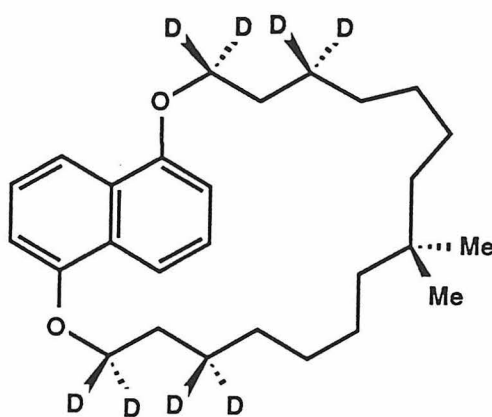
hancement was predicted using a simplified expression derived from statistical mechanical considerations. After taking into account the differences in symmetries, it was found that the rigidity induced in the ring upon substitution was less than that induced in the open chain, and thus the ring closure is also entropically favored.

Changes in the conformational properties of the cycle or ring might be expected upon gem-dimethyl substitution. Dale has analyzed the consequences of gem-dimethyl substituents on both the energy ordering of the various conformations and the barriers to conformational interconversions for the C₉ to C₁₆ cycloalkanes.⁶ The gem-dimethyl substituted carbons preferentially occupy corner positions, thereby reducing transannular contacts. Also, with respect to the ring skeleton, no energy difference between gauche and anti is expected in the bonds adjacent to the substituted carbon atom, and a corner can be built at this atom without the usual energy cost of ca. 1.6 kcal/mol. In fact, MM2 calculations on 3,3-dimethylpentane indicate that the preferred conformation is G[±]G[±] and that the AA conformation is 0.8 kcal/mol less stable. Thus, in a cycloalkane, a conformation which has the substituted carbon at a corner position will be stabilized by at least 2.4 kcal/mol over a conformation which places the substituted carbon along a side. When a single ring carbon is substituted, the energy ordering of the various conformations is not expected to change.⁶ The substituted carbon is free to occupy the corner sites in all the conformations, and no one conformation will be stabilized with respect to the others. However, an increase is expected in the barriers for conformational interconversions that involve pathways which move the gem-dimethyl substituted carbon from the corner position.⁶ Qualitatively, this suggests that gem-dimethyl substituents

make large rings more rigid. When two ring carbons are substituted, both the energy ordering and the barriers to interconversion may be affected.⁶ Depending on the relative positioning of the substituted carbons, one conformation may become strongly preferred, with the barriers to interconversion also increasing. Again, qualitatively, gem-dimethyl substituents have made the ring more rigid.

The enantiomerization or jump-rope reaction of **1** could be a sensitive probe to rigidity induced in the polymethylene chain by gem-dimethyl substituents. The large negative activation entropies observed, ca. -20 eu, for **C14** and **C15** indicate that in the unsubstituted molecule the chain is quite floppy in the ground state, but that significant rigidity is induced in the transition state. If gem-dimethyl substituents are introduced, rigidity induced in the ground state would be reflected as a decrease in the activation entropy for the jump-rope reaction. Indeed, as was discussed in Chapter 4, replacing the two oxygens of **C14** with gem-dimethyl substituted nitrogens to give **2** leads to a dramatic decrease in ΔS^\ddagger . A question arises as to the origin of the decrease in ΔS^\ddagger . Is it a result of rigidity induced in the alkyl chain, or a result of changing the preferred geometry, or both?

It was therefore desirable to design a second probe which would embed the gem-dimethyl substituted atom in the polymethylene chain. Molecule **3** is such a probe. The 15-carbon chain length allows a single substitution to be made without breaking the constitutional C_2 symmetry. By analogy to **C15**, it is expected that the γ protons will exhibit the greatest chemical shift difference, allowing the most accurate line shape study possible. Therefore, **3** was deuterated at the β and δ carbons so that the AB pattern of the γ protons would be fully isolated.



3

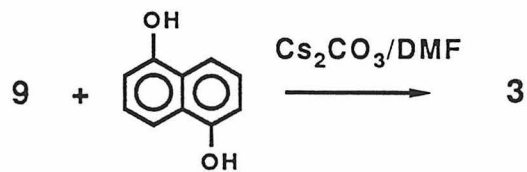
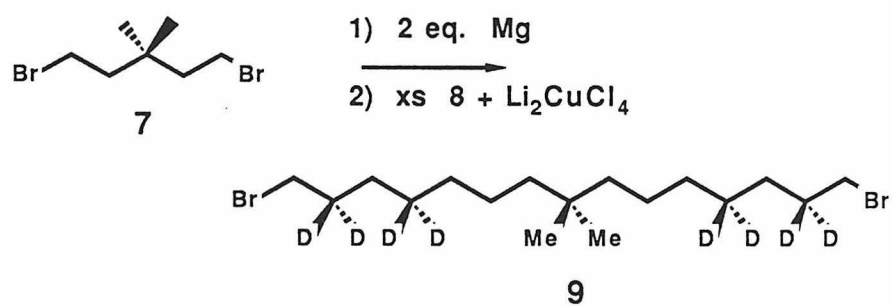
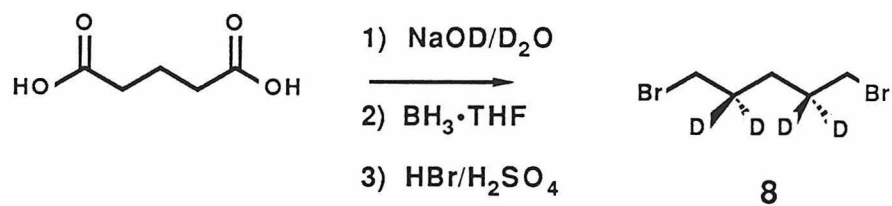
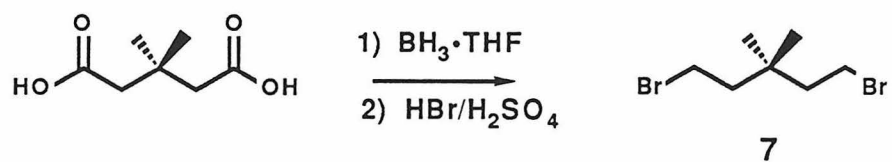
Synthesis

The synthesis of **3** is outlined in Scheme 5.1. 1,5-dibromo-3,3-dimethyl pentane can be obtained from 3,3-dimethylglutaric acid by reduction to the diol and conversion of the diol to the dibromide. In a fashion analogous to that used to synthesize **C15**,⁷ 1,5-dibromo-3,3-dimethylpentane is coupled to deuterated 1,5-dibromopentane to give the substituted pentadecane dibromide deuterated in the desired positions. A one step macrocyclization reaction gives the desired cyclophane.

DNMR Results

The ambient temperature 400-MHz ¹H NMR spectrum of **3** (non-deuterated) is shown in Figure 5.1. It is identical to that of **C15**⁷ in every respect but one; the most upfield multiplet of **C15** is gone and is replaced by a sharp singlet at 0.55 ppm due to the methyl groups.

Scheme 5.1



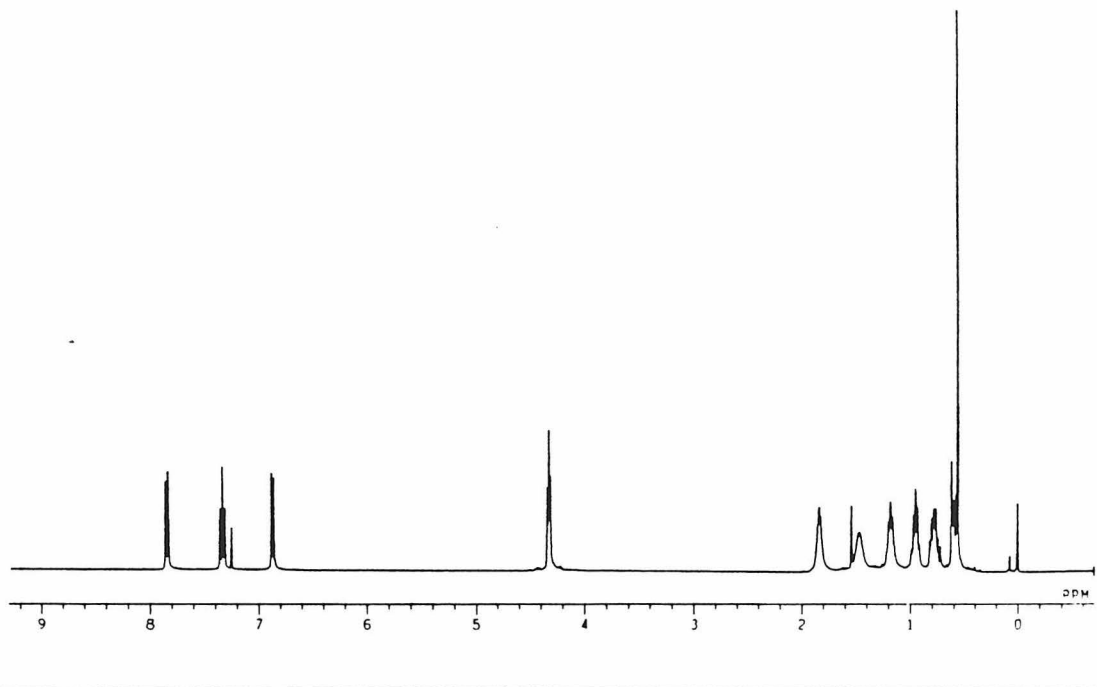


Figure 5.1 The 400 MHz ^1H NMR spectrum of **3** at ambient temperature.

Application of the complete line shape method⁸ at 400-MHz to **3** proceeded smoothly (see Figure 5.2 and Table 5.1). As with **C15**, the chemical shift separation of the two signals ($\Delta\nu$) was nearly temperature independent. However, $\Delta\nu$ for **3** (69.1 Hz at 400-MHz \Rightarrow 0.173 ppm) is smaller than for **C15** (116.7 Hz at 500-MHz \Rightarrow 0.233 ppm).⁷ An Eyring plot of the data for **3** is shown in Figure 5.3. As with **1** and **2**, the activation parameters and associated data listed in Table 5.2 were obtained using an iterative procedure that considers the errors in both the rates and the temperature.⁹ Temperatures were considered accurate to ± 1 K. The study covered a 44 K temperature range. The eight data points span a 10-fold range in rates, and the activation parameters were derived with confidence. As with **1** and **2**, the method of Sandström¹⁰ was adopted to obtain the best estimates of these error limits, as listed in Table 5.3.

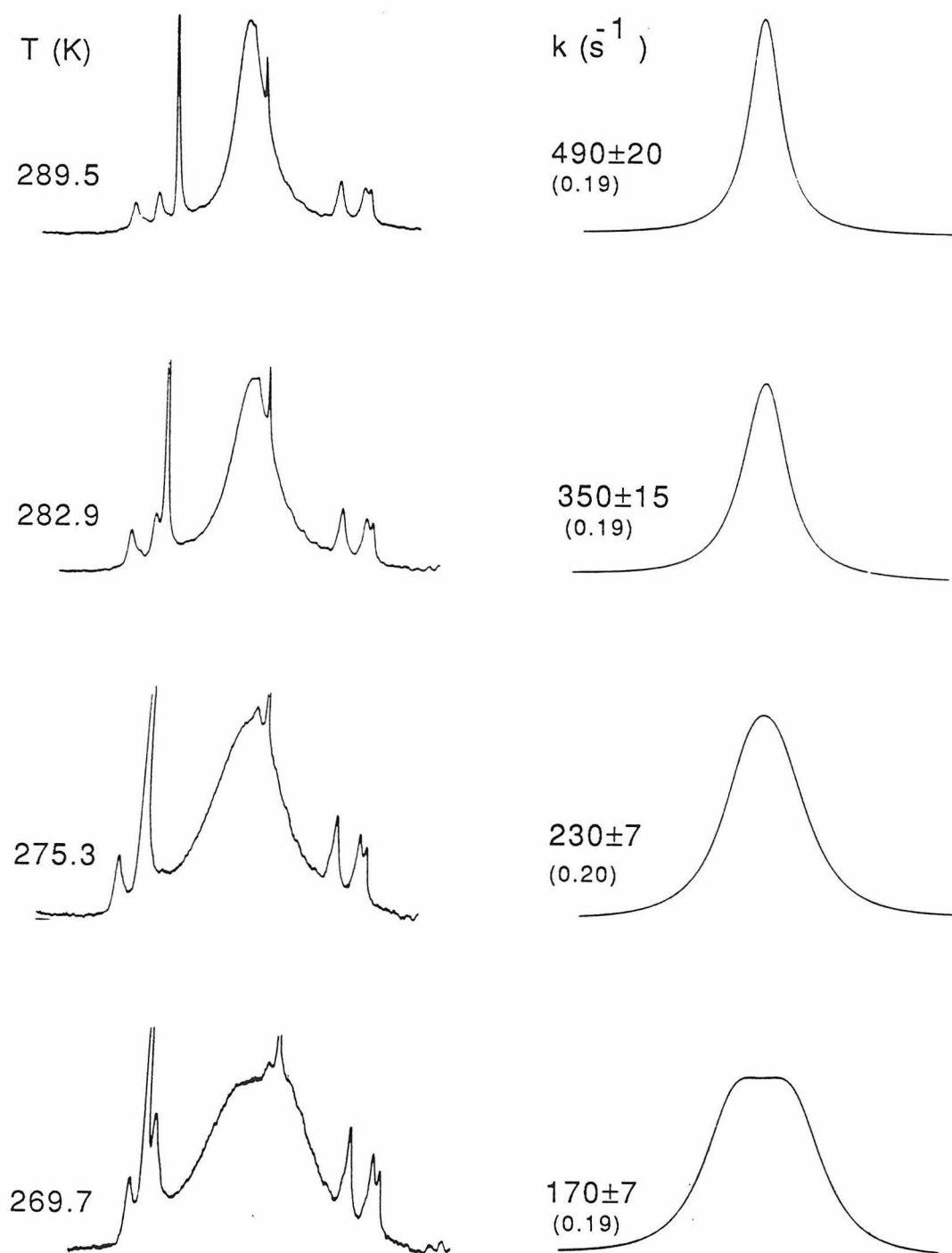


Figure 5.2. 400-MHz, variable temperature ^1H NMR spectra of the γ protons of **3** in CD_2Cl_2 . The values in parenthesis are T_{2eff} .

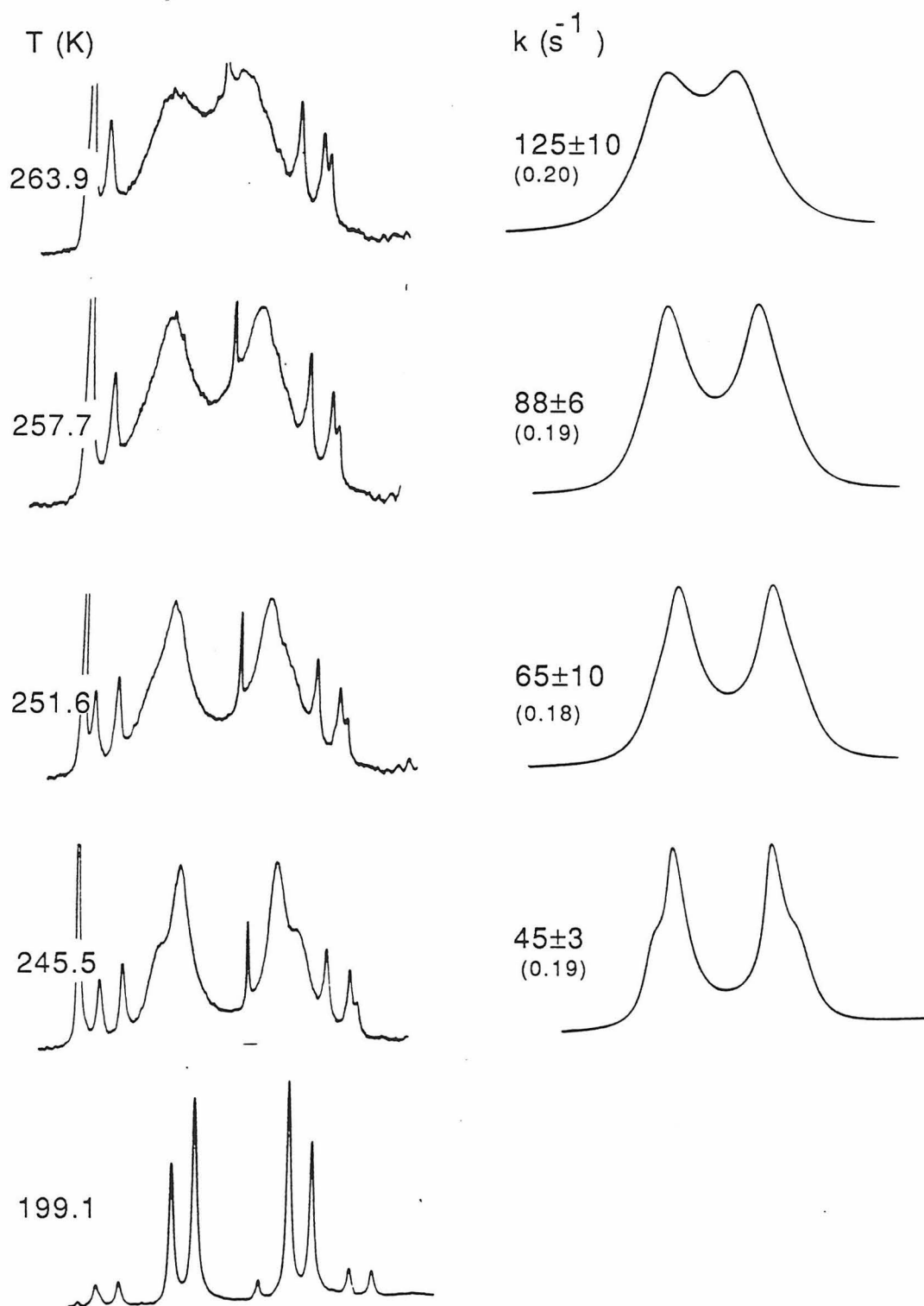


Figure 5.2 (continued).

Table 5.1. Enantiomerization Rates of **3**.^a

T (K) ^b	k (s ⁻¹)
245.5	45 ± 3
251.6	65 ± 10
257.5	88 ± 6
263.9	125 ± 10
269.7	170 ± 7
275.3	230 ± 7
282.9	350 ± 15
289.5	488 ± 20

^aCD₂Cl₂ ^b ± 1 K

Table 5.2. Activation Parameters for the Jump-Rope Reaction of **3** and **C15**.

	$\Delta G_{298}^{\ddagger a}$	$\Delta H^{\ddagger a}$	$\Delta S^{\ddagger b}$	ρ^c	$\sigma \Delta H^{\ddagger d}$	$\sigma \Delta S^{\ddagger d}$	pts. ^e	ΔT^f
3 ^g	13.6	7.20	-21.4	.9990	0.13	0.49	8	44
C15 ^h	13.4	7.56	-19.6	.9997	0.09	0.32	7	42

^a kcal/mol. ^b cal/mol·K. ^c Correlation coefficient. ^d Standard deviation.

^e Number of data points. ^f Temperature range. ^g 400-MHz CLS.

^h 500-MHz CLS.

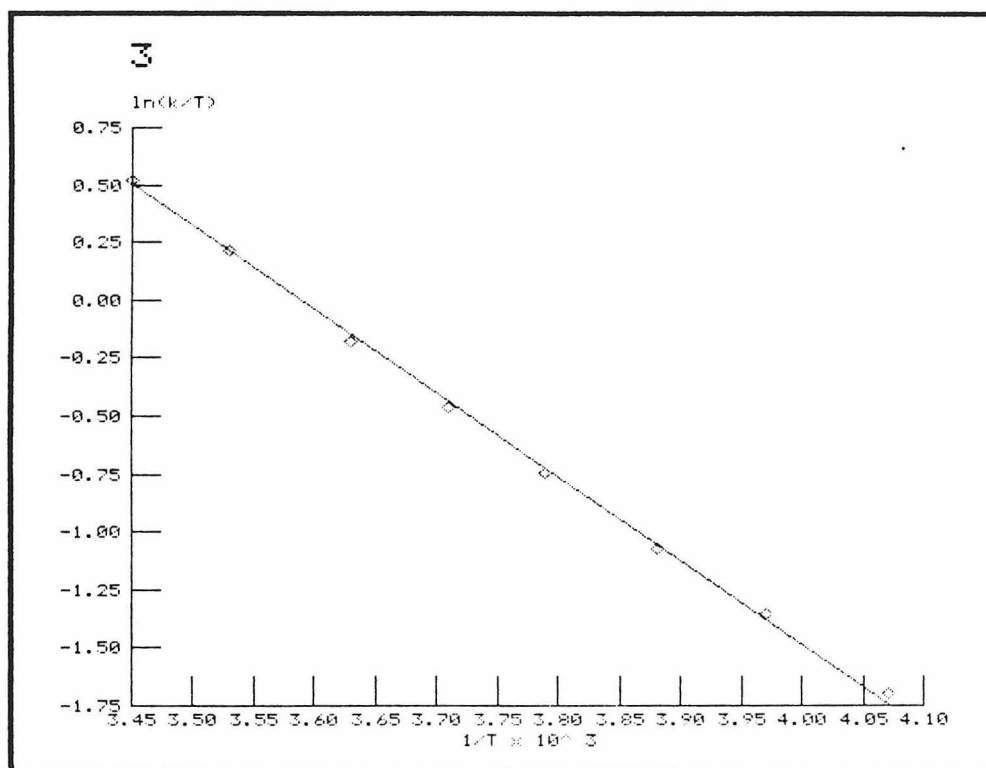


Figure 5.3. An Eyring plot for 3.

Table 5.3. Activation Parameters with Estimated Error Limits.

	$\Delta G_{298}^{\ddagger a}$	$\Delta H^{\ddagger a}$	$\Delta S^{\ddagger b}$
3	13.6 ± 0.2	7.2 ± 0.7	-21 ± 2
C15	13.4 ± 0.2	7.6 ± 0.7	-20 ± 2

^akcal/mol ^bcal/mol·K.

Discussion

As can be seen from Table 5.3, there is no change, within experimental error, in the activation parameters of the jump-rope reaction on going from **C15** to **3**. This implies that both the ground state and the transition state are perturbed to an equal extent by the gem-dimethyl substituents. However, MM calculations suggest changes might have been expected on going from **C15** to **3**. The two lowest energy conformations of **C15** are [83163] and [83712]. Neither of these conformations has a corner at the central carbon of the chain, the carbon bearing the gem-dimethyl substituents. However, two low energy conformations, [966] and [876], do have corners at the substituted carbon atom. In **3**, these two conformations should be stabilized with respect to [83163] and [83712]. As can be seen from Table 5.4, MM calculations on **3** indicate three conformations are very close in energy.

Table 5.4. Relative energies for various conformations of **3** and **C15**.^a

	3	C15
[83163]	0.1	0.0
[83712]	2.1	0.3
[966]	0.0	2.8
[876]	0.3	3.4

^akcal/mol.

Conclusion

Cyclophane **3** has been used to further investigate the effects of gem-dimethyl substituents on the jump-rope reaction kinetics. MM suggests that changes might be expected on going from **C15** to **3** due to the presence of additional very low-lying conformations in **3**. However, the DNMR study shows that no significant changes in the activation parameters for this process occur. These results, taken together with those of Chapter 4, indicate that substituent effects on the dynamic properties of macrocycles are complex and difficult to predict. Further studies will be required to gain a more detailed insight into the origin of substituent effects on the conformational properties of macrocycles.

EXPERIMENTAL SECTION

A. Methods:

Routine NMR spectra were recorded on a Varian EM-390 spectrometer. High-field NMR spectra were recorded on a JEOL GX-400 spectrometer. Chemical shifts are referenced to residual solvent peaks. The temperature controller on the probe was calibrated by using a coaxial tube of MeOH as an internal standard along with the standard Van Geet relationship.¹¹ Line shape analysis was performed using the program DNMR3.¹² The best fit was judged visually. The two outermost peaks of the aromatic triplet (δ 7.15) were used as an internal standard to determine T_{2eff} . Standard inert atmosphere techniques were applied for all reactions.

B. Materials:

DMF was distilled from CaO under vacuum and stored over a mixture of freshly regenerated 3 and 4 Å molecular sieves for at least one week before use. THF was distilled from benzophenone ketyl. Flash chromatography¹³ (diameter x length) was carried out with 230-400 mesh silica gel.

[2,2,4,4-²H₄]-Glutaric acid. Glutaric acid-d₄ was prepared as previously described⁷ except that the mixture was placed in a sealed thick-walled glass tube.

General Conversion of Diacid to Dibromide. Standard procedures were used. The diacids were reduced with BH₃·THF to the diol using the method of Brown.¹⁴ The diols were converted to the dibromides using an HBr/H₂SO₄ mixture according to the method of Kamm and Marvel.¹⁵

Grignard coupling of dibromides. The procedure used was an adaptation of the method of Freidman and Shani.¹⁶ Thus, 1,5-dibromo-3,3-dimethylpentane, **7** (2.7 g, 11 mmol), in 10 mL dry THF was added dropwise to 0.60 g Mg turnings in 5 mL THF with a slight evolution of heat. After the addition was complete, the mixture was heated to reflux for about 10 minutes and then transferred via canula to a dry addition funnel. The reagent so formed was then added dropwise with stirring to a mixture of 1,5-dibromo-2,2,4,4-tetradeuteropentane,⁷ **8** (5.97 g, 25.7 mmol), and small amounts (ca. 50 mg each) of oven-dried CuCl₂ and LiCl in 10 mL dry THF. After 20 h, 25 ml 0.5 N HCl was added, the THF layer was separated, and the aqueous layer extracted with CH₂Cl₂ (2 x 30 mL). The organic layers were combined, dried over MgSO₄, filtered, and the solvent was removed on a rotary evaporator at reduced pressure. Excess **8** was removed by Kügelröhr at 70 °C and 0.2 torr. The residue was subjected to flash chromatography (35 mm x 110 mm) using petroleum ether as the eluant. A 50 mL prerun and 50x6 mL fractions were collected, giving the desired product, **9** (1.157 g), in 27% yield in fractions 8-22 as a viscous oil after removal of the solvent. ¹H NMR (CDCl₃) δ 0.8 (s, 6H), 1.18-1.38 (m, 16H), 1.45 (quintet, 4H), 3.4 (t, 4H); ¹³C NMR (CDCl₃) δ 42.09, 34.18, 33.06, 32.80, 30.64, 29.03, 28.43, 27.49, and 24.25.

Preparation of 3. Dibromide **9** (0.266 g, 0.670 mmol) and dihydroxynaphthalene (0.107 g, 0.670 mmol) were combined in a dry 1 L round-bottomed flask. Dry DMF (700 mL) was added via canula and Cs₂CO₃ (0.9 g, 2.6 mmol) was quickly added. The mixture was heated to 50-60 °C for two days. The solvent was then removed on a rotary evaporator under reduced pressure, and the residue was taken up in CH₂Cl₂, washed with H₂O, dried

with MgSO_4 , and filtered. Flash chromatography (25 mm x 110 mm) was performed eluting with 1/5 benzene/petroleum ether. A 50 mL prerun and then 5 mL fractions were collected giving the desired product (0.061 g) in 23% yield in fractions 14-28 as a viscous oil after removal of the solvent. A small amount of impurity which could be seen in the 400-MHz ^1H NMR spectrum could not be removed by chromatography or distillation (0.050 torr, 200 °C). ^1H NMR (see text); ^{13}C NMR (CDCl_3) δ 154.04, 127.26, 124.61, 114.18, 106.44, 67.86, 42.09, 32.48, 30.13, 28.21, 27.73, 26.77, 25.54, and 23.16; exact mass calculated for $\text{C}_{27}\text{H}_{40}\text{O}_2$ 396.3028, found 396.3007; exact mass calculated for $\text{C}_{27}\text{H}_{32}\text{D}_8\text{O}_2$ 404.3530, found 404.3542.

REFERENCES

- (1) M. Dobler "Ionophores and Their Structure"; Wiley: New York, 1981.
- (2) For example: E.F. Gale, *et al.* "The Molecular Basis of Antibiotic Action", 2nd ed.; Wiley: London, 1981.
- (3) For an overview of the host-guest field, see: "Topics in Current Chemistry"; F. Vogtle, Ed.; Springer Verlag: Berlin, 1981 and 1982; Vol. 98 and 101.
- (4) B. Capon and S.P. McManus "Neighboring Group Participation"; Plenum Press: New York, 1976; Vol. 1, pp 59-70.
- (5) N.L. Allinger and U. Zalkow *J. Org. Chem.* **1960**, *25*, 701-704.
- (6) J. Dale *Acta. Chem. Scandi.* **1973**, *27*, 1149-1158.
- (7) M.H. Chang, B.B. Masek, and D.A. Dougherty *J. Am. Chem. Soc.* **1984**, *107*, 1124-1133.
- (8) For an excellent overview of the DNMR method, see: J. Sandström "Dynamic NMR Spectroscopy"; Academic Press: New York, 1982.
- (9) J.A. Irvin and T.I. Quickenden *J. Chem. Educ.* **1983**, *60*, 711-712.
- (10) U. Berg, S. Karlsson, and J. Sandström *Org. Magn. Reson.* **1977**, *10*, 117-121.
- (11) A.L. Van Geet *Anal. Chem.* **1970**, *42*, 679-680. *ibid* **1968**, *40*, 2227-2229.

- (12) D.A. Kleier and G. Binsch *Q.C.P.E.* **1979**, *11*, 165.
- (13) W.C. Still, M. Kahn, and A. Mitra, *J. Org. Chem.* **1977**, *42*, 3761-3764.
- (14) N.M. Yoon, C.S. Pak, H.C. Brown, S. Krishnamurthy,
and T.P. Stocky *J. Org. Chem.* **1973**, *38*, 2786-2792.
- (15) O. Kamm and C.S. Marvel "Organic Synthesis"; Wiley: New York, 1941;
Collect. Vol. I, pp 25-41.
- (16) L. Friedman and A. Shani *J. Am. Chem. Soc.* **1974**, *96*, 7101-7103.

Appendix A

The Structure Generating Program.

Before giving a listing of the source code, I will describe, in general, the structure of the program. A more detailed description of the structure generation and closure optimization processes will follow. Finally, the code will be presented.

The mainline starts by reading the x , y , and z intercepts of an ellipsoid which represents the space occupied by the naphthalene. The same values were always used for these parameters (3.358, 2.491, and 1.400 respectively). The naphthalene is assumed to sit in the xy plane. The C9-C10 bond is assumed to be coincident with the y axis with its midpoint at $x = y = 0$. Additionally, the closure and energy criterion are read. A parameter that allows a Van der Waals radius to be added to the x and y intercepts of the ellipsoid is also read, but in practice, a value of zero was used. Next, the chains are generated such that they stretch from the initial oxygen towards the target oxygen (vide infra). The subroutine CRUDE is then called to "fix" the closure distance and the two closure angles. Following this, a sequence of subroutines (XYZ, SETUPA, and SETUPB) is called to prepare for the energy evaluation by MM. They build connectivity tables, atom classification arrays, etc. The subroutine CE1 is then called. This routine, and all the routines called by it, are the energy evaluation routines and are taken directly from the program MODEL. Next, the subroutine CODE is called to classify the conformation generated. After all possible chains which meet the closure and energy criterion have been generated, the subroutine SORT is called to sort the structures according to the classes assigned. This way, similar conformations are output together. Finally, the dihedral angles of all the structures are written. A second

program, TRANS, reads this list, selects the conformations desired, and writes a file with coordinate and connectivity information which is ready to be read by BAKMOD, the MM program.

The chain building process occurs in the mainline, just after statement label 15. All the dihedral angles along the chain (i.e., α , β , γ , etc.) have been initialized to -60° (except α , which is initialized to -135°). Starting with the α angle, the α carbon is positioned. The position is checked to make sure that the carbon does not lie in the ellipsoid representing the naphthalene. Then, the distance to the terminal oxygen is calculated and checked to make sure that the remainder of the chain can span this distance. If both criteria are satisfied, the next atom is positioned, and so on, until a complete chain is built.

If one of the above criteria is not met, the dihedral angle is incremented by 120° (45° for α) and the atom is repositioned and rechecked. If all possibilities for the current angle have been tried without success, the preceding angle is incremented and the angles that follow it are returned to their initial values (-60°). This continues until all possibilities have been checked (when the α angle must be incremented, but is already $+135^\circ$). Structures so generated are each passed to the subroutine CRUDE for closure optimization.

Closure optimization occurs in the subroutine CRUDE. Starting with the α angle, 2° is added and subtracted to the dihedral angle. The positions of the last two atoms of the chain are recalculated for these two angles, and are used to evaluate closure energies. The angle which gives the lowest closure energy (including the starting angle) is retained. This process continues until all the dihedral angles have been considered. The energy change for the cycle

is checked, as is the total closure energy. If the optimization has converged, control passes back to the mainline. If not, another cycle is performed.

The code is given, starting with the mainline, on the following pages. The subroutines follow the mainline in alphabetical order. As previously mentioned, CE1 and the routines called by it were taken from MODEL and have not been modified. Therefore is not listed here.

C THIS PROGRAM IS DESIGNED TO FIND ALL POSSIBLE HYDROCARBON
C CHAINS OF LENGTH N WHICH STRETCH FROM ONE OXYGEN OF 1,5-DIOXANAPHTHALENE
C TO THE OTHER.
C

IMPLICIT REAL*4(A-H,O-Z)
DIMENSION CHI(2)
COMMON INP, IOUT, IPN, IPRINT, ENGY, ID(60), EC, EB, ESB, E14, EV, ET, EU
COMMON/Q/ X(4), Y(4), Z(4)
COMMON/CHAIN/ CHAIN(20,3)
COMMON/NOH/NOH
COMMON/CEPT/XINTER, YINTER, ZINTER, VDW
DIMENSION PSI(25), VECTOR(12000,20), ENRGY(12000,2), KODE(12000)
DIMENSION ROPE(20,3), XI(3), YI(3), ZI(3)
REAL CHECK(20)/0.0, 1.54, 2.51, 3.87, 5.00, 6.34, 7.5444,
1 8.8466, 10.0592, 11.3514, 12.5740, 13.8599, 15.0887,
1 16.3703, 17.6035, 18.8819, 20.1183, 21.3942,
1 22.6331, 23.9070/
REAL XF(3)/1.241, 1.241, 2.414/, YF(3)/2.781,
1 1.401, .705/, ZF(3)/0.0, 0.0, 0.0/
REAL I(20)
REAL INIT(20)/-135, -60, -60, -60, -60, -60, -60, -60, -60,
*-60, -60, -60, -60, -60, -60, -60, -60, -60, -60/
LOGICAL NOH/.TRUE./

C
C BYTE ID

KOK=0
PI=DATAN(1.0D0)*4.0D0
RADDEG=PI/180.0D0
DEGRAD=180.0D0/PI

C
C INPUT THE X,Y,Z INTERCEPTS FOR THE ELLIPSE THAT REPRESENTS THE
C EXCLUDED VOLUME OF THE OXYGENS. ALSO INPUT THE CLOSURE CRITERION,
C A VANDERWALLS PARAMETER AND THE ENERGY CRITERION ARE READ.
C VDW IS ADDED TO XINTER AND YINTER WHEN CHECKING TO SEE IF THE CHAIN
C HAS ENTERED THE NAPHTHALENE.
C
C

3 READ (5,3) XINTER, YINTER, ZINTER, CLOSURE1, VDW, ECRIT
FORMAT(6F10.5)

C
C THE CHECK ARRAY IS USED TO DETERMINE IF THE CHAIN IS WANDERING OFF INTO
C SPACE. CHECK IS INITIALIZED IN THE DATA STATEMENT ABOVE, SUCH THAT
C CHECK(I) IS THE MAXIMUM DISTANCE WHICH CAN BE SPANNED BY AN ALL TRANS
C CHAIN I CARBONS LONG.
C

2 DO 2 L=1,20
CHECK(L)=CHECK(L)+CLOSURE1

C
C THE INITIAL AND FINAL COORDINATE OF C2, C1 AND OXYGEN ARE RELATED BY
C A C2 AXIS.
C

4 DO 4 L=1,3
XI(L)=(-1.0)*XF(4-L)
YI(L)=(-1.0)*YF(4-L)
ZI(L)=0.0

C
C
C WRITE (60,*) ' 12 OMER NAPHTHALENEOPHANE'
C WRITE (60,*) ' REFINED CLOSURE CRITERION 2.5 A ',
C * ' CRUDE CLOSURE CRITERION ', CHECK(1), ' A '
C WRITE (60,*) ' ENERGY CUTOFF ', ECRIT
C WRITE (60,*) ' CARBONS NOT ALLOWED TO COME WITHIN ', VDW,
C \$ ' A OF AN ELLIPSE DEFINED BY'
C WRITE (60,*) ' (X^2)/(A^2) + (Y^2)/(B^2) + (Z^2)/(C^2)=1'

```
WRITE (60,*)' WHERE A= ',XINTER
WRITE (60,*)' B= ',YINTER
WRITE (60,*)' C= ',ZINTER
WRITE (60,4000)
C
C
C*****CHANGE*****
C THIS PART IS CHAIN LENGTH DEPENDENT
C
C N=12
C*****
C IUNIT=1
C
C INITIALIZE THE DIHEDRAL ANGLE VECTOR, I
C
C DO 5 L=1,N
5 I(L)=INIT(L)
C
C INITIALIZE THE CHAIN COORDINATE THE CHAIN IS BUILT UP FROM
C C2, C1 AND 0
C
C DO 10 L=1,3
CHAIN(L,1)=XI(L)
CHAIN(L,2)=YI(L)
10 CHAIN(L,3)=ZI(L)
C
C CONVERT TO RADIANS
C
C DO 15 L=1,N
15 PSI(L)=I(L)*RADDEG
C
C J IS THE CARBON COUNTER
C FIRST CARBON
C
C J=1
C
C ACC IS THE ANGLE IN RADIAN. RCC IS THE BOND DISTANCE TO BE
C USED IN PLACING THE NEXT ATOM.
C
C 25 ACC=1.9652
RCC=1.54
IF (J.NE.1) GOTO 30
ACC=2.042
RCC=1.43
30 CONTINUE
C
C PACK COORD OF LAST THREE ATOMS IN X, Y, AND Z MATRIX FOR USE BY COORD
C
C DO 40 L=1,3
X(L)=CHAIN(J+L-1,1)
Y(L)=CHAIN(J+L-1,2)
40 Z(L)=CHAIN(J+L-1,3)
C
C GENERATE NEXT ATOM
C
C CALL COORD(RCC,ACC,PSI(J),X(4),Y(4),Z(4))
IF (J.EQ.1.OR.J.EQ.N) GOTO 45
C
C CHECK TO SEE IF NEW ATOM IS IN THE NAPHTHALENE
C IF KOK IS 1, IT IS AND SO BAIL OUT
C
C CALL CNSTRN(X(4),Y(4),Z(4),KOK)
IF (KOK.EQ.1) GOTO 60
C
C CHECK TO SEE IF REMAINING CHAIN CAN REACH TERMINAL
```

```
C OXYGEN
C
45 CUT=(X(4)-XF(1))**2+(Y(4)-YF(1))**2+(Z(4)-ZF(1))**2
   CUT=SQRT(CUT)
   IF (CUT.GT.CHECK(N-J+1)) GOTO 60
C
C NEW ATOM PASSES TESTS, ADD TO CHAIN
C
   CHAIN(J+3,1)=X(4)
   CHAIN(J+3,2)=Y(4)
   CHAIN(J+3,3)=Z(4)
   GOTO 20
C
C ATOM FAILED TO PASS TESTS
C
C IF J.EQ 0 THEN ALL DONE
60 IF (J.LE.0) GOTO 1000
C
C CHECK TO SEE IF THIS IS THE LAST POSSIBILTY FOR CURRENT ANGLE
C
   IF (J.EQ.1.AND.(I(J).NE.135).OR.
      * ((J.NE.1).AND.(I(J).NE.180))) GOTO 80
C
C DECRIMENT ANGLE (GO BACK TO PREVIOUS ATOM) AND REINITALIZE DIHEDS
C FOR REMAINDER OF THE CHAIN.
C
   DO 70 L=J,N
70 I(L)=INIT(L)
   J=J-1
   GOTO 60
C
C INCREMENT ANGLE VALUE
C
80 INC=120
   IF (J.EQ.1) INC=45
   I(J)=I(J)+INC
   DO 90 L=1,N
90 PSI(L)=I(L)*RADDEG
   GOTO 25
C
C NEXT ATOM AND ANGLE
C
20 J=J+1
   IF (J.LE.N) GOTO 25
C
C PASS CHAIN TO CLOSURE OPTIMIZER
C
   CALL CRUDE(CUT,N,PSI,ROPE)
   E1=CUT
C
C GET SET UP TO DO ENERGY EVALUATION
C
   CALL XYZ(N,ROPE)
   IF (IUNIT.GT.1) GOTO 91
   CALL SETUPA(N,IUNIT)
C
C CE1 STARTS THE ENERGY EVALUTION
C
91 CALL CE1(IUNIT)
C
C CHECK ENERGY
C
   IF (ENGY.GT.ECRIT) GOTO 99
C
C CLASSIFY NEW CONFORMATION
```

```
C      CALL CODE(PHI,N,KODE(IUNIT))
C
C      STORE NEW CONFORMATION
C
C      DO 95 L=1,N+3
95     VECTOR(IUNIT,L)=PHI(L)
        ENRGY(IUNIT,1)=E1
        ENRGY(IUNIT,2)=ENGY
C
C      INCREMENT CONFORMATION COUNTER
C
C      IUNIT=IUNIT+1
C
C      J=N
99     GOTO 60
C
C      ALL DONE!
C
C      1000 IF (IUNIT.EQ.1) THEN
        WRITE(60,6001)
6001   FORMAT(1X,'NO VECTORS FOUND?')
        GOTO 130
        ELSE
        END IF
C
C      SORT THE CONFORMATIONS ACCORDING TO CLASS
C
C      CALL SORT(VECTOR,ENRGY,KODE,IUNIT-1,N)
C
C      OUTPUT THE RESULTS!
C
C      KOUT=N+3
        KOUT2=KOUT/2
        IF (KOUT.NE.KOUT2*2) KOUT2=KOUT2+1
        WRITE(60,*) 'THERE WERE ',IUNIT-1,' STRUCTURES'
        DO 100 L=1,IUNIT-1
        IF (L.NE.1) GOTO 109
        WRITE(60,3010) ABS(KODE(L))
        GOTO 110
109    IF (ABS(KODE(L)).EQ.ABS(KODE(L-1))) GOTO 110
        WRITE(60,3010) ABS(KODE(L))
110    WRITE(60,3000) L,ENRGY(L,1),ENRGY(L,2)
        IF (KODE(L).LT.0) GOTO 112
        WRITE(60,3020) (VECTOR(L,J)*DEGRAD,J=1,KOUT2),ENRGY(L,2)
        WRITE(60,3030) (VECTOR(L,KOUT+1-J)*DEGRAD,J=1,KOUT2)
        GOTO 100
112    WRITE(60,3020) (VECTOR(L,KOUT+1-J)*DEGRAD,J=1,KOUT2),ENRGY(L,2)
        WRITE(60,3040) (VECTOR(L,J)*DEGRAD,J=1,KOUT2)
100    CONTINUE
3000   FORMAT(1X,'GUESS # ',I4,' CLOSURE ENERGY =',F8.3,
* ' TOTAL NOH ENERGY =',F12.4)
3010   FORMAT(/,1X,I10/)
3020   FORMAT(1X,8F10.1,10X,'ENERGY = ',F12.4)
3030   FORMAT(1X,8F10.1/)
3040   FORMAT(1X,8F10.1,10X,'INVERTED VECTOR'/)
4000   FORMAT(/,6X,'ALPHA',5X,'BETA',6X,'GAMMA',5X,'DELTA',5X,
* 'EPSILON',3X,'ZETA',6X,'ETA',7X,'THETA',5X,'IOTA',6X,
* 'KAPPA',5X,'LAMDA'/)
130    STOP
        END
```

THESE THREE ROUTINES ARE MODIFICATIONS OF AN ANGLE ROUTINE
TAKEN FROM THE PROGRAM BIGSTRN3: R.B. NACHBAR, JR.

```
C
C FUNCTION ANGLE CALCULATES THE VALENCE ANGLES
C COORDS OF POINT 1 ARE IN A(1), B(1), C(1) ETC.
C
  FUNCTION ANGLE(A,B,C)
  IMPLICIT REAL*4(A-H,O-Z)
  DIMENSION A(4),B(4),C(4)
  D1=SQRT((A(3)-A(2))**2+(B(3)-B(2))**2+(C(3)-C(2))**2)
  D2=SQRT((A(4)-A(3))**2+(B(4)-B(3))**2+(C(4)-C(3))**2)
  D3=SQRT((A(4)-A(2))**2+(B(4)-B(2))**2+(C(4)-C(2))**2)
  A1=(D1**2+D2**2-D3**2)/(2*D1*D2)
  IF (A1.LT.-1.0D0.AND.((A1+1.0D0)**2.LT..0001)) A1=-1.0D0
  IF (A1.GT.1.0D0.AND.((A1-1.0D0)**2.LT..0001)) A1=1.0D0
  ANGLE=ACOS(A1)
  RETURN
  END

C
C CALCULATES ANGLES ALSO, BUT COORDS USED ARE
C POINT 1: A,B,C
C POINT 2: X(3), Y(3), Z(3)
C POINT 3 X(2) ETC.
C
  FUNCTION ANGLE2(A,B,C)
  IMPLICIT REAL*4(A-H,O-Z)
  COMMON/Q/ X(4),Y(4),Z(4)
  D1=SQRT((X(3)-X(2))**2+(Y(3)-Y(2))**2+(Z(3)-Z(2))**2)
  D2=SQRT((X(3)-A)**2+(Y(3)-B)**2+(Z(3)-C)**2)
  D3=SQRT((X(2)-A)**2+(Y(2)-B)**2+(Z(2)-C)**2)
  A1=(D1**2+D2**2-D3**2)/(2*D1*D2)
  IF (A1.LT.-1.0D0.AND.((A1+1.0D0)**2.LT..0001)) A1=-1.0D0
  IF (A1.GT.1.0D0.AND.((A1-1.0D0)**2.LT..0001)) A1=1.0D0
  ANGLE2=ACOS(A1)
  RETURN
  END

C
C CALCULATES THE A,B,C ANGLE
C
  FUNCTION ANGLE1(A,B,C)
  IMPLICIT REAL*4(A-H,O-Z)
  DIMENSION A(3),B(3),C(3)
  D1=SQRT((A(1)-B(1))**2+(A(2)-B(2))**2+(A(3)-B(3))**2)
  D2=SQRT((C(1)-B(1))**2+(C(2)-B(2))**2+(C(3)-B(3))**2)
  D3=SQRT((A(1)-C(1))**2+(A(2)-C(2))**2+(A(3)-C(3))**2)
  A1=(D1**2+D2**2-D3**2)/(2*D1*D2)
  IF (A1.LT.-1.0D0.AND.((A1+1.0D0)**2.LT..0001)) A1=-1.0D0
  IF (A1.GT.1.0D0.AND.((A1-1.0D0)**2.LT..0001)) A1=1.0D0
  ANGLE1=ACOS(A1)
  RETURN
  END
```

```
FUNCTION ARCOS(X)
Y=X
IF(Y .GT. 1.00) Y =1.00
IF(Y .LT. -1.00) Y =-1.00
ARCOS=ACOS(Y)
RETURN
END
```

```
C
C THIS SUBROUTINE CHECKS TO SEE IF AN ATOM (X,Y,Z) HAS ENTERED
C THE EXCLUDED VOLUME OF THE NAPHTHALENE, DESCRIBED AS AN ELLIPSOID
C IF SO, IT RETURNS A VALUE OF KOK=1, OF NOT KOK=0.
C
```

```
      SUBROUTINE CNSTRN(X,Y,Z,KOK)
      IMPLICIT REAL*4(A-H,O-Z)
      COMMON/CEPT/XINTER,YINTER,ZINTER,VDW
      KOK=0
      A=XINTER+VDW
      B=YINTER+VDW
      C=ZINTER
      CRIT=(X**2)/(A**2)+(Y**2)/(B**2)+(Z**2)/(C**2)
      IF (CRIT.LT.1) KOK=1
      IF (Z.LT.-1.7) KOK=1
      IF (X.LT.XINTER.AND.Y.LT.YINTER.AND.Z.LT.(-1.4)) KOK=1
      RETURN
      END
```

```
C
C THIS SUBROUTINE IS USED FOR TRANSITION STATES
C IT THE EXCLUDED VOLUME IS AN INFINITELY TALL BOX
C DIMENSION X=2 TO -2, Y= 1.2 TO -1.2
C
```

```
      SUBROUTINE CNSTRN(X,Y,Z,KOK)
      IMPLICIT REAL*4(A-H,O-Z)
      COMMON/CEPT/XINTER,YINTER,ZINTER,VDW
      KOK=0
      A=XINTER+VDW
      B=YINTER+VDW
      C=ZINTER
      CRIT=(X**2)/(A**2)+(Y**2)/(B**2)+(Z**2)/(C**2)
      IF (CRIT.LT.1) KOK=1
      IF (ABS(Z).GT.2.0) KOK=1
      IF (ABS(X).LT.2.0.AND.ABS(Y).LT.1.2) KOK=1
      RETURN
      END
```

```
C
C THIS SUBROUTINE ASSIGNS AN INTEGER WITH N-5 DIGITS TO EACH CONFORMATION
C A DIGIT OF 3 IMPLIES AN ANTI ANGLE
C A DIGIT OF 2 IMPLIES A GAUCHE PLUS
C A DIGIT OF 1 IMPLIES A GAUCHE MINUS
C
      SUBROUTINE CODE(PHI,N,KODE)
      IMPLICIT REAL*4(A-H,O-Z)
      DIMENSION PHI(N+3)
      PI=DATAN(1.0D0)*4.0D0
      RADDEG=PI/180.0D0
      KROD=0
C
C THE FIRST AND LAST FOUR DIHEDRAL ANGLES ARE NOT CLASSIFIED
C
      DO 10 I=5,N-1
C
C GAUCHE MINUS GOTO 1
C
      IF ( (PHI(I).LT.0) .AND. (PHI(I).GT.-120.*RADDEG) )
        * GOTO 1
C
C GAUCHE PLUS GOTO 2
      IF ( (PHI(I).GE.0) .AND. (PHI(I).LE.120.*RADDEG) )
        * GOTO 2
C
C HERE IF ANTI
C THE DIGIT 3 IS ENTERED INTO THE N-I-1TH DECIMAL PLACE
C
      KODE=KODE+3*10**(N-I-1)
      GOTO 10
C
C IF GAUCHE MINUS
C THE DIGIT 1 IS ENTERED INTO THE N-I-1TH DECIMAL PLACE
C
      KODE=KODE+10**(N-I-1)
      GOTO 10
C
C IF GAUCHE PLUS
C THE DIGIT 2 IS ENTERED INTO THE N-I-1TH DECIMAL PLACE
C
      KODE=KODE+2*10**(N-I-1)
10 CONTINUE
C
C INVERT THE CODE
C
      IREM=KODE
      DO 20 I=5,N-1
      IDIG=IREM/(10**(N-I-1))
      IREM=IREM-(IDIG*10**(N-I-1))
20 KROD=KROD+IDIG*(10**(I-5))
C
C USE WHICHEVER IS LEAST, KODE OR KROD
C IF ANGLE VECTOR IS INVERTED, KODE IS NEGATIVE
C
      IF (KROD.LT.KODE) KODE=KROD*(-1)
      RETURN
      END
```

```

C
C THIS SUBROUTINE WAS TAKEN FROM THE PROGRAM SCOORD
C WRITTEN BY J.D ANDOSE
C IT ATTACHES AN ATOM(4, COORDS Q,R,S) TO 3 WITH A BOND LENGTH RCD
C A VALENCE ANGLE 4-3-2 OF THBCD
C AND A DIHEDRAL ANGLE (4-3-2-1) OF PHABCD
C
      SUBROUTINE COORD(RCD,THBCD,PHABCD,Q,R,S)
      IMPLICIT REAL*4(A-H,O-Z)
      COMMON/Q/ X(4),Y(4),Z(4)
C
C   DEFINE A UNIT VECTOR <UV1> WITH COMPONENTS UX1,UY1, AND UZ1
C   COLINEAR WITH AND HAVING THE SAME DIRECTION AS <BC>
C
      PI=DATAN(1.0D0)*4.0D0
      A=X(3)-X(2)
      B=Y(3)-Y(2)
      C=Z(3)-Z(2)
      D1=SQRT(A**2+B**2+C**2)
      UX1=A/D1
      UY1=B/D1
      UZ1=C/D1
C
C   DEFINE A SECOND UNIT VECTOR <UV2> WITH COMPONENTS UX2,UY2, AND UZ2
C   AND HAVING THE SAME DIRECTION AS THE CROSS PRODUCT <BC> X <BA>
C
      D=X(1)-X(2)
      E=Y(1)-Y(2)
      F=Z(1)-Z(2)
      X2=B*F-C*E
      Y2=C*D-A*F
      Z2=A*E-B*D
      D2=SQRT(X2**2+Y2**2+Z2**2)
      UX2=X2/D2
      UY2=Y2/D2
      UZ2=Z2/D2
C
C   DEFINE A THIRD UNIT VECTOR <UV3> WITH COMPONENTS UX3,UY3, AND UZ3
C   DEFINED AS THE CROSS PRODUCT:      <UV3> = <UV2> X <UV1>
C
      UX3=UY2*UZ1-UZ2*UY1
      UY3=UZ2*UX1-UX2*UZ1
      UZ3=UX2*UY1-UY2*UX1
C
C   IF RCD AND THBCD ARE HELD FIXED AND PHABCD IS ALLOWED TO VARY
C   OVER TWO PI RADIANs THEN POINT 4 (INDEXED AS ND) WILL DESCRIBE
C   A CIRCLE IN SPACE WITH RADIUS GIVEN BELOW. THE CENTER OF THIS CIR
C   CLE IS DENOTED AS POINT E. THE VECTOR <CD> IS THEN FOUND AS THE
C   VECTOR SUM OF <CE> + <ED>
C
      RADIUS=RCD*SIN(PI-THBCD)
      COSA=COS(PI-THBCD)
100  SINPHI=SIN(PHABCD)
      COSPHI=COS(PHABCD)
C
      CDX=RCD*COSA*UX1 + RADIUS*(UX2*SINPHI + UX3*COSPHI)
      CDY=RCD*COSA*UY1 + RADIUS*(UY2*SINPHI + UY3*COSPHI)
      CDZ=RCD*COSA*UZ1 + RADIUS*(UZ2*SINPHI + UZ3*COSPHI)
C
C   THE COORDINATES OF POINT 4 ARE
C
      Q = X(3) + CDX
      R = Y(3) + CDY
      S = Z(3) + CDZ
C
C
100  RETURN
      END

```

```

C
C THIS SUBROUTINE OPTIMIZES THE FINAL CLOSURE BY CHANGING
C THE DIHEDRAL ANGLES ALONG THE CHAIN A FEW DEGREES AND RETAINING
C CHANGES THAT RESULT IN AN IMPROVEMENT OF THE MM CLOSURE ENERGY.
C
      SUBROUTINE CRUDE(C,N,OPSI,CHAIN)
      IMPLICIT REAL*4(A-H,O-Z)
      COMMON/Q/ X(4),Y(4),Z(4)
      COMMON/CEPT/XINTER,YINTER,ZINTER,VDW
      COMMON/CHAIN/ CH(20,3)
      DIMENSION OPSI(25),ORSI(25),CHAIN(20,3),DSI(25),Q(3,3),
      *CHAINEW(20,3),DBETA(3),CUT(3)
      REAL XF(3)/1.241,1.241,2.414/,YF(3)/2.781,
      * 1.401,.705/,ZF(3)/0.0,0.0,0.0/

C
C
C      KOK=0
      ANERGY=10000000

C
C      MODE = 0, OPTIMIZE CLOSURE ON BOND LENGTH ONLY
C
      MODE=0
      PI=DATAN(1.0D0)*4.0D0
      DEGRAD=180.0D0/PI
      RADDEG=PI/180.0D0

C
C      PUT THE ORIGINAL CHAINS COORDS (ARRAY CH) INTO ARRAY CHAIN
C
      DO 2 J=1,N+3
      DO 1 L=1,3
1      CHAIN(J,L)=CH(J,L)
2      CONTINUE

C
C      ZERO THE DEVIATION VECTOR DSI
C
      DO 5 J=1,N
5      DSI(J)=0.0D0
      ORSI(J)=OPSI(J)

C
C      LOOP OVER ALL ANGLES
C
8      DO 100 J=1,N

C
C      LOAD THE COORDS OF THE THREE BASE ATOMS (A, B, C) INTO THE X MATRIX
C      LOAD THE COORDS OF THE LAST ATOM INTO Q(2, )
C
      DO 10 K=1,3
10     X(K)=CHAIN(J+K-1,1)
      Y(K)=CHAIN(J+K-1,2)
      Z(K)=CHAIN(J+K-1,3)
      Q(2,K)=CHAIN(N+3,K)
      X(4)=CHAIN(N+3,1)
      Y(4)=CHAIN(N+3,2)
      Z(4)=CHAIN(N+3,3)

C
C      IF (MODE.LE.0) MODE=0
C
C      EVALUTE THE INITIAL CLOSURE ENERGY
C
      CUT(2)=ENERGY(X,Y,Z,MODE,CHAIN(N+2,1),CHAIN(N+2,2)
      *,CHAIN(N+2,3))

C
C      CHECK TO SEE THAT THE ATOMS AREN'T COLINEAR

```

```

C
  ALPHA=ANGLE(X,Y,Z)
  LINE=ABS(PI-ALPHA)
  IF(LINE.LT.0.01) GOTO 90
C
C  FIND THE DIHEDAL ANGLE (A, B, C, LAST)
C
  BETA=DIHED(X,Y,Z)
C
C  FIND THE DISTANCE (C-LAST)
C
  RCD=SQRT( (X(4)-X(3))**2 + (Y(4)-Y(3))**2 + (Z(4)-Z(3))**2)
  IF (MODE.EQ.1.AND.J.NE.N) THEN
C
C  FIND THE ANGLE (B,C,NEXTLAST)
C
  ALPHA2=ANGLE2(CHAIN(N+2,1),CHAIN(N+2,2),CHAIN(N+2,3))
  LINE=ABS(PI-ALPHA2)
  IF(LINE.LT.0.01) GOTO 90
C
C  FIND THE DIHEDRAL ANGLE (A,B,C,NEXTLAST) AND DISTANCE (C-NEXTLAST)
C
  BETA2=DIHED2(CHAIN(N+2,1),CHAIN(N+2,2),CHAIN(N+2,3))
  RCD2=SQRT( (CHAIN(N+2,1)-X(3))**2 +
  * (CHAIN(N+2,2)-Y(3))**2 +
  * (CHAIN(N+2,3)-Z(3))**2)
  ELSE
  END IF
C
C  DBETA IS PLUS OR MINUS 2 DEGREES
C
  DO 15 L=1,3
15  DBETA(L)=(L-2)*2.0*RADDEG
C
C  FIND THE COORDINATES OF LAST WITH NEW DIHEDRAL ANGLES
C
  DO 20 K=1,3,2
  CALL COORD(RCD,ALPHA,BETA+DBETA(K),X(4),Y(4),Z(4))
  IF (MODE.EQ.1.AND.J.NE.N) THEN
C
C  FIND THE COORDINATES OF NEXTLAST WITH NEW DIHEDRAL ANGLES
C
  CALL COORD(RCD2,ALPHA2,BETA2+DBETA(K),A,B,C)
  ELSE
  A=CHAIN(N+2,1)
  B=CHAIN(N+2,2)
  C=CHAIN(N+2,3)
  END IF
  IF (MODE.LE.0) MODE=-K
C
C  EVALUTE CLOSURE ENERGETICS WITH THE NEW COORDS FOR LAST AND NEXTLAST
C
20  CUT(K)=ENERGY(X,Y,Z,MODE,A,B,C)
C
C  FIND OUT WHICH ANGLE HAS THE BEST CLOSURE ENERGETICS
C
  DO 40 K=1,2
  DO 35 L=K+1,3
  IF (CUT(K).LT.CUT(L)) GOTO 35
  DUMMY=CUT(K)
  CUT(K)=CUT(L)
  CUT(L)=DUMMY
  DUMMY=DBETA(K)
  DBETA(K)=DBETA(L)
  DBETA(L)=DUMMY

```

```

35  CONTINUE
40  CONTINUE
C
C  UPDATE THE DIHEDRAL ANGLE VECTOR
C
      INDEX=1
C
C  CHECK TO SEE THAT NO ANGLE CHANGES BY OVER 60 DEGREES
C
45  IF (INDEX.GT.3.OR.DBETA(INDEX).EQ.0) GOTO 90
      OMEGA=DSI(J)+DBETA(INDEX)
      IF (OMEGA.LT.(60*PI/180)) GOTO 50
      INDEX=INDEX+1
      GOTO 45
50  CONTINUE
C
C  FILL IN THE REST OF THE CHAIN AT THE NEW COORDS
C  CHECK TO MAKE SURE CHAIN DOESN'T GO IN NAPHTHALENE
C
      OPSI(J)=ORSI(J)+OMEGA
      DO 70 K=J,N
      ACC=1.9652
      RCC=1.54
      IF(K.NE.1) GOTO 60
      RCC=1.43
      ACC=2.0420
60  CALL COORD(RCC,ACC,OPSI(K),X(4),Y(4),Z(4))
C
C
      IF (K.EQ.1.OR.K.EQ.N) GOTO 57
      CALL CNSTRN(X(4),Y(4),Z(4),KOK)
      IF (KOK.EQ.1) THEN
      INDEX=INDEX+1
      DO 55 L=1,3
      X(L)=CHAIN(J+L-1,1)
      Y(L)=CHAIN(J+L-1,2)
55  Z(L)=CHAIN(J+L-1,3)
      GOTO 45
      ELSE
      END IF
57  CHAINEW(K+3,1)=X(4)
      CHAINEW(K+3,2)=Y(4)
      CHAINEW(K+3,3)=Z(4)
      DO 65 L=1,3
      X(L)=X(L+1)
      Y(L)=Y(L+1)
65  Z(L)=Z(L+1)
70  CONTINUE
C
C  NO CARBONS ENTERED NAPHTHALENE, UPDATE CHAIN ARRAY
C
      DO 80 K=J,N
      DO 75 L=1,3
75  CHAIN(K+3,L)=CHAINEW(K+3,L)
80  CONTINUE
C
C  UPDATE DSI
C
      DSI(J)=OMEGA
      GOTO 100
C
C  RESTORE DIHEDRAL ANGLE TO ORIGINAL VALUE
C
90  OPSI(J)=ORSI(J)+DSI(J)
100 CONTINUE

```

```
C
C CHECK TO SEE IF OPTIMIZATION CONVERGED
C
  IF (MODE.EQ.1.AND.CUT(INDEX).LT.1.5) GOTO 150
  IF (MODE.EQ.1.AND.(ABS(ANERGY-CUT(INDEX)).LT.1.5)) GOTO 150
  IF (MODE.EQ.1) ANERGY=CUT(INDEX)
  DCUT=ABS(ACUT-CUT(INDEX))
  ACUT=CUT(INDEX)
C
C CHECK TO SEE IF WE WILL SWITCH TO MODE 1
C CLOSURE ENERGY DEPENDENT ON BOND LENGTH AND ANGLES
C
  IF (MODE.LE.0.AND.DCUT.LT.0.0001) MODE=1
  GOTO 8
C
C ALL DONE
C UPDATE ALL ARRAYS AND RETURN
C
150 DO 180 J=1,N
180 OPSI(J)=ORSI(J)+DSI(J)
  DO 180 K=1,3
  X(4)=XF(K)
  Y(4)=YF(K)
  Z(4)=ZF(K)
  OPSI(N+K)=DIHED(X,Y,Z)
  DO 170 J=1,3
  X(J)=X(J+1)
  Y(J)=Y(J+1)
  Z(J)=Z(J+1)
170 CONTINUE
180 C=CUT(INDEX)
  RETURN
  END
```

THESE ROUTINES ARE MODIFICATIONS OF ROUTINES TAKEN FROM
THE PROGRAM BIGSTRN3: R.B. NACHBAR, JR.

```

C
C CALCULATES THE DIHEDRAL ANGLE OF ATOMS STORED IN X,Y,Z ARRAY
C
      FUNCTION DIHED(X,Y,Z)
      IMPLICIT REAL*4(A-H,O-Z)
      DIMENSION E(4,3,4),X(4),Y(4),Z(4),A(3),B(3),C(3)
      DO 20 I=1,3
      E(1,I,I+1)=X(I+1)-X(I)
      E(2,I,I+1)=Y(I+1)-Y(I)
      E(3,I,I+1)=Z(I+1)-Z(I)
      E(4,I,I+1)=SQRT(E(1,I,I+1)**2+E(2,I,I+1)**2+E(3,I,I+1)**2)
10      DO 10 J=1,3
10      E(J,I,I+1)=E(J,I,I+1)/E(4,I,I+1)
20      CONTINUE
      A(1)=E(2,1,2)*E(3,2,3)-E(2,2,3)*E(3,1,2)
      A(2)=E(3,1,2)*E(1,2,3)-E(3,2,3)*E(1,1,2)
      A(3)=E(1,1,2)*E(2,2,3)-E(1,2,3)*E(2,1,2)
      B(1)=E(2,2,3)*E(3,3,4)-E(2,3,4)*E(3,2,3)
      B(2)=E(3,2,3)*E(1,3,4)-E(3,3,4)*E(1,2,3)
      B(3)=E(1,2,3)*E(2,3,4)-E(1,3,4)*E(2,2,3)
      C(1)=A(2)*B(3)-B(2)*A(3)
      C(2)=A(3)*B(1)-B(3)*A(1)
      C(3)=A(1)*B(2)-B(1)*A(2)
C
      D1=C(1)*E(1,2,3)+C(2)*E(2,2,3)+C(3)*E(3,2,3)
      D2=A(1)*B(1)+A(2)*B(2)+A(3)*B(3)
      DIHED=ATAN2(D1,D2)
      RETURN
      END
C
C CALCULATES THE DIHEDRAL ANGLE FOR THE POINTS STORED
C IN X(I), I=1,2,3 AND POINT 4, PASSED AS Q,R,S
C
      FUNCTION DIHED2(Q,R,S)
      IMPLICIT REAL*4(A-H,O-Z)
      COMMON/Q/ X(4),Y(4),Z(4)
      DIMENSION E(4,3,4),A(3),B(3),C(3),XI(4),YI(4),ZI(4)
      DO 5 L=1,3
      XI(L)=X(L)
      YI(L)=Y(L)
5      ZI(L)=Z(L)
      XI(4)=Q
      YI(4)=R
      ZI(4)=S
      DO 20 I=1,3
      E(1,I,I+1)=XI(I+1)-XI(I)
      E(2,I,I+1)=YI(I+1)-YI(I)
      E(3,I,I+1)=ZI(I+1)-ZI(I)
      E(4,I,I+1)=SQRT(E(1,I,I+1)**2+E(2,I,I+1)**2+E(3,I,I+1)**2)
10      DO 10 J=1,3
10      E(J,I,I+1)=E(J,I,I+1)/E(4,I,I+1)
20      CONTINUE
      A(1)=E(2,1,2)*E(3,2,3)-E(2,2,3)*E(3,1,2)
      A(2)=E(3,1,2)*E(1,2,3)-E(3,2,3)*E(1,1,2)
      A(3)=E(1,1,2)*E(2,2,3)-E(1,2,3)*E(2,1,2)
      B(1)=E(2,2,3)*E(3,3,4)-E(2,3,4)*E(3,2,3)
      B(2)=E(3,2,3)*E(1,3,4)-E(3,3,4)*E(1,2,3)
      B(3)=E(1,2,3)*E(2,3,4)-E(1,3,4)*E(2,2,3)
      C(1)=A(2)*B(3)-B(2)*A(3)
      C(2)=A(3)*B(1)-B(3)*A(1)
      C(3)=A(1)*B(2)-B(1)*A(2)
C
      D1=C(1)*E(1,2,3)+C(2)*E(2,2,3)+C(3)*E(3,2,3)
      D2=A(1)*B(1)+A(2)*B(2)+A(3)*B(3)
      DIHED2=ATAN2(D1,D2)
      RETURN
      END

```

```
C
C THIS SUBROUTINE EVALUATES THE ENERGY OF THE CLOSURE
C IF MODE = 0, ONLY BOND STRETCHING IS CONSIDERED.
C IF MODE = 1, THE FULL NOH MM TREATMENT OF THE CLOSURE IS USED.
C
  FUNCTION ENERGY(X,Y,Z,MODE,A,B,C)
  IMPLICIT REAL*4(A-H,O-Z)
  DIMENSION X(4),Y(4),Z(4),QLAST(3),QLM1(3)
  REAL F(3)/1.149142,2.778801,0.0/
  REAL FM1(3)/1.219355,1.400713,0.0/
  REAL IOTA
C
  ENERGY=SQRT((X(4)-F(1))**2 + (Y(4)-F(2))**2 + (Z(4)-F(3))**2)
  IF (ENERGY.GT.2.5.AND.MODE.LE.0) GOTO 100
  IF (ENERGY.LT.2.5.AND.MODE.LT.0) GOTO 100
  MODE=1
  D=ENERGY
  QLAST(1)=X(4)
  QLAST(2)=Y(4)
  QLAST(3)=Z(4)
  QLM1(1)=A
  QLM1(2)=B
  QLM1(3)=C
  THETA=ANGLE1(QLAST,F,FM1)
  IOTA =ANGLE1(QLM1,QLAST,F)
C
  ENERGY=385.815 * (D-1.43)**2 +50.385 * (IOTA-1.9652)**2
  $      +55.425*(THETA-2.042)**2
C
100  RETURN
     END
```

```
C
C THIS SUBROUTINE SETS UP THE CONNECTIVITY TABLES
C FOR USE BY CE1
C
SUBROUTINE SETUPA(N,IUNIT)
IMPLICIT REAL*4(A-H,O-Z)
COMMON/ATOMS/ M,X(100),Y(100),Z(100),ITYPE(100),
1 NAME(30),WT(30),JJ(100),JBOND(100,4)
REAL LIGAND(10)/10*0/
DIMENSION IBOND(100,4)

C
C
C
LIGAND(1)=N+10
LIGAND(5)=2
LIGAND(6)=N+5
LIGAND(10)=N+9
DO 10 J=1,10
JI=J+N+4
LL=JI-1
MM=JI+1
IF (J.GE.8) MM=J-7
IF (J.EQ.10) LL=1
IF (J.GT.8) JI=J-8
KK=LL
IF (JI.NE.2*(JI/2)) KK=MM
IBOND(JI,1)=LL
JBOND(JI,1)=LL
IBOND(JI,2)=KK
JBOND(JI,2)=MM
IBOND(JI,3)=MM
JBOND(JI,3)=LIGAND(J)
IBOND(JI,4)=LIGAND(J)
JJ(JI)=2
IF (LIGAND(J).NE.0) JJ(JI)=3
10 CONTINUE
C
DO 15 J=1,N
IBOND(3+J,1)=2+J
JBOND(3+J,1)=2+J
IBOND(3+J,2)=4+J
JBOND(3+J,2)=4+J
IBOND(3+J,3)=0
JBOND(3+J,3)=0
IBOND(3+J,4)=0
JBOND(3+J,4)=0
JJ(3+J)=2
15 CONTINUE
C
IBOND(3,1)=2
JBOND(3,1)=2
IBOND(3,2)=4
JBOND(3,2)=4
IBOND(3,3)=0
JBOND(3,3)=0
IBOND(3,4)=0
JBOND(3,4)=0
JJ(3)=2
IBOND(4+N,1)=3+N
JBOND(4+N,1)=3+N
IBOND(4+N,2)=5+N
JBOND(4+N,2)=5+N
IBOND(4+N,3)=0
JBOND(4+N,3)=0
```

```
      IBOND(4+N,4)=0
      JBOND(4+N,4)=0
      JJ(4+N)=2
C
      DO 40 J=1,N+12
      DO 25 K=1,3
      DO 20 KK=K+1,4
      IF (IBOND(J,K).EQ.0.OR.IBOND(J,KK).EQ.0) GOTO 20
      IF (IBOND(J,K).LE.IBOND(J,KK)) GOTO 20
      ISCRTCH=IBOND(J,K)
      IBOND(J,K)=IBOND(J,KK)
      IBOND(J,KK)=ISCRTCH
20     CONTINUE
25     CONTINUE
C
      DO 35 L=1,3
      DO 30 LL=L+1,4
      IF (JBOND(J,L).EQ.0.OR.JBOND(J,LL).EQ.0) GOTO 30
      IF (JBOND(J,L).LE.JBOND(J,LL)) GOTO 30
      ISCRTCH=JBOND(J,L)
      JBOND(J,L)=JBOND(J,LL)
      JBOND(J,LL)=ISCRTCH
30     CONTINUE
35     CONTINUE
40     CONTINUE
C
C
      CALL SETUPB(IBOND,N+12)
      RETURN
      END
```

```
C
C FINISHES SETTING UP FOR CE1
C
  SUBROUTINE SETUPB(ICON,N)
  IMPLICIT REAL*4(A-H,O-Z)
  COMMON/BNDS/IBND1(100),IBND2(100)
  COMMON/CONTB/ IATMS(200),IBNDS(100),IXYZ(100)
  COMMON/ATOMS/ M,X(100),Y(100),Z(100),JTYPE(100)
  DIMENSION ICON(100,4),IBNDO(100),JBND(100,4),
  *JNBNS(100)
  REAL ITYPE(82)/6,6,8,12*6,8,8*6,58*0/

C
C
C
C
  ICHG=0
  NBNS=0
  DO 50 K=1,N
  DO 40 KK=1,4
  LA=K
  LB=ICON(K,KK)
  IF(LB.EQ.0) GOTO 50
  IF(LB.GT.LA) GOTO 20
  L=LA
  LA=LB
  LB=L
20  CALL CHECK(NBNS,LA,LB,LC)
  IF(LC.NE.0) GOTO 30
  NBNS=NBNS+1
  IBND1(NBNS)=LA
  IBND2(NBNS)=LB
  IBNDO(NBNS)=1
  GOTO 40
30  IBNDO(LC)=IBNDO(LC)+1
40  CONTINUE
50  CONTINUE
  DO 60 K=1,NBNS
  IBNDO(K)=IBNDO(K)/2
  DO 100 K=1,N
  NB=0
  DO 70 KK=1,NBNS
  IF(IBND1(KK).EQ.K.OR.IBND2(KK).EQ.K) THEN
  NB=NB+1
  JBND(K,NB)=KK
  ELSE
  END IF
70  CONTINUE
  JNBNS(K)=NB
  IF (ITYPE(K).EQ.1) JTYPE(K)=5
  IF (ITYPE(K).EQ.0) JTYPE(K)=20
  IF (ITYPE(K).EQ.6) GOTO 80
  IF (ITYPE(K).EQ.8) GOTO 90
  GOTO 100
80  JTYPE(K)=1
  DO 86 LK=1,JNBNS(K)
  IF(IBNDO(JBND(K,LK)).EQ.1) GOTO 86
  IF(IBNDO(JBND(K,LK)).EQ.3) THEN
  JTYPE(K)=4
  GOTO 100
  ELSE
  END IF
82  JTYPE(K)=2
  DO 83 KK=1,3
  MN=JBND(K,KK)
  IF (IBNDO(MN).NE.2) GOTO 83
```

```
      IF (ITYPE (IBND1 (MN)) .EQ. 8 .OR. ITYPE (IBND2 (MN)) .EQ. 8) JTYPE (K) = 3
83     CONTINUE
      GOTO 100
86     CONTINUE
      GOTO 100
90     JTYPE (K) = 6
      IF (JNBDS (K) .EQ. 3) JTYPE (K) = 7
100    CONTINUE
      DO 110 K = 1, N
      IWORD1 = 0
      IWORD2 = 0
      CALL IPTBYT (JTYPE (K), IWORD1, 1, 6)
      CALL IPTBYT (ICHG, IWORD1, 7, 2)
      CALL IPTBYT (JNBDS (K), IWORD1, 9, 3)
      DO 102 KK = 1, 3
      KL = 5 + 7 * KK
      CALL IPTBYT (JBND (K, KK), IWORD1, KL, 7)
102    CONTINUE
      CALL IPTBYT (JBND (K, 4), IWORD2, 1, 7)
      IATMS ( (2 * K) - 1) = IWORD1
110    IATMS (2 * K) = IWORD2
      DO 120 K = 1, NBDS
      IWORD1 = 0
      CALL IPTBYT (IBND0 (K), IWORD1, 1, 2)
      CALL IPTBYT (IBND1 (K), IWORD1, 5, 7)
      CALL IPTBYT (IBND2 (K), IWORD1, 12, 7)
120    IBDS (K) = IWORD1
      C
      C
      CALL XYZIXYZ
      C
      RETURN
      END
```

C
 C THIS SUBROUTINE SORTS THE CONFORMATIONS ACCORDING TO CODE
 C

```

SUBROUTINE SORT(V,E,KODE,M,N)
IMPLICIT REAL*4(A-H,O-Z)
DIMENSION V(12000,20),E(12000,2),KODE(M)
DO 100 I=1,M-1
DO 90 J=I+1,M
IF (ABS(KODE(I)).LE.ABS(KODE(J))) GOTO 90
DO 20 K=1,N+3
AUX=V(I,K)
V(I,K)=V(J,K)
20 V(J,K)=AUX
AUX=E(I,1)
E(I,1)=E(J,1)
E(J,1)=AUX
AUX=E(I,2)
E(I,2)=E(J,2)
E(J,2)=AUX
AUX=KODE(I)
KODE(I)=KODE(J)
KODE(J)=AUX
90 CONTINUE
100 CONTINUE
RETURN
END
  
```

C

C
 C THIS SUBROUTINE FILLS THE X,Y, AND Z MATRICES OF COMMON BLOCK
 C /ATOMS/ WITH THE COORDINATES OF THE NAPH, OXYGENS, AND CHAIN
 C FOR USE BY CE1, THE ENERGY EVALUATION ROUTINES
 C

```

SUBROUTINE XYZ(N,ROPE)
IMPLICIT REAL*4(A-H,O-Z)
COMMON/ATOMS/M,X(100),Y(100),Z(100)
DIMENSION ROPE(20,3)
REAL CAR(10,3)/1.241,2.414,2.414,1.241,0.0,0.0,-1.241,
1 -2.414,-2.414,-1.241,1.401,.705,-.705,-1.401,-.709,
2 0.709,1.401,.705,-.705,-1.401,10*0.0/
REAL OXYGEN(2,3)/1.241,-1.241,2.781,-2.781,0.0,0.0/
  
```

C

```

M=N+12
DO 10 J=1,10
JJ=J+N+4
IF (J.GT.8) JJ=J-8
X(JJ)=CAR(J,1)
Y(JJ)=CAR(J,2)
10 Z(JJ)=CAR(J,3)
C
  
```

```

DO 15 J=4,N+3
X(J)=ROPE(J,1)
Y(J)=ROPE(J,2)
Z(J)=ROPE(J,3)
15 CONTINUE
C
  
```

15

C

C

```

DO 20 J=1,2
IF (J.EQ.1) JO=4+N
IF (J.EQ.2) JO=3
X(JO)=OXYGEN(J,1)
Y(JO)=OXYGEN(J,2)
Z(JO)=OXYGEN(J,3)
20 CONTINUE
C
  
```

20

C

```

RETURN
END
  
```

Appendix B

The X-ray Coordinates and Gaussian Parameters for C16.

Table B1. Atom Coordinates and U_{eq} 's ($\times 10^4$).

Atom	x	y	z	U_{eq}
O	1807(4)	2176(5)	-1055(2)	858(14)
C(1)	1410(7)	2583(9)	-605(2)	685(24)
C(2)	392(8)	3603(9)	-497(3)	763(27)
C(3)	52(8)	3910(8)	-24(3)	826(27)
C(4)	736(9)	3163(8)	336(3)	771(25)
C(9)	1809(7)	2137(7)	240(2)	610(22)
α	942(7)	2736(8)	-1432(3)	934(23)
β	1336(8)	1881(13)	-1866(3)	1177(31)
γ	1122(10)	250(13)	-1812(3)	1207(32)
δ	-443(14)	-199(14)	-1741(3)	1602(39)
ϵ	-684(14)	-1752(18)	-1577(5)	2125(60)
ζ	-264(14)	-2008(12)	-1060(5)	1888(61)
η	-1117(11)	-1184(10)	-694(4)	1591(44)
θ	-727(10)	-1581(9)	-181(4)	1602(48)

Table B2. Anisotropic Gaussian Parameters, U_{ij} 's ($\times 10^4$).

Atom	U_{11}	U_{22}	U_{33}	U_{12}	U_{13}	U_{23}
O	735(33)	1144(39)	696(26)	125(28)	-83(30)	190(33)
C(1)	477(55)	745(60)	834(55)	-22(41)	-64(47)	138(53)
C(2)	709(62)	757(70)	822(69)	64(50)	-113(52)	214(57)
C(3)	808(67)	575(58)	1095(66)	210(49)	-29(62)	-106(63)
C(4)	910(67)	639(57)	764(56)	29(49)	-72(55)	-15(52)
C(9)	498(50)	410(47)	923(50)	-19(36)	-56(47)	-11(48)
α	761(52)	1218(66)	824(48)	129(47)	114(47)	260(52)
β	845(60)	1713(93)	974(64)	378(68)	10(49)	489(70)
γ	1031(71)	1832(100)	758(54)	339(84)	-108(59)	-253(64)
δ	1767(114)	1927(112)	1112(62)	398(115)	-386(74)	-769(80)
ϵ	1342(98)	1993(145)	3039(186)	147(100)	-200(101)	-1662(160)
ζ	1731(122)	659(70)	3275(194)	-136(72)	-199(122)	-177(109)
η	1161(78)	868(77)	2744(130)	-13(66)	-442(95)	-203(86)
θ	1173(88)	882(71)	2752(178)	9(65)	-139(88)	588(88)

Table B3. Hydrogen Atom Coordinates ($\times 10^4$) and B's.

Atom	x	y	z	B
H(2)	60(51)	4148(45)	-721(14)	3.5(15)
H(3)	-551(41)	4536(41)	55(13)	1.7(14)
H(4)	365(55)	3374(57)	627(14)	5.4(17)
H(α)	1159	3800	-1484	6.0
H(α)	-124	2611	-1359	6.0
H(β)	2391	2069	-1942	6.0
H(β)	711	2230	-2137	6.0
H(γ)	1699	-87	-1531	6.0
H(γ)	1498	-242	-2107	6.0
H(δ)	-963	-74	-2054	6.0
H(δ)	-884	472	-1500	6.0
H(ϵ)	-107	-2431	-1783	6.0
H(ϵ)	-1760	-1992	-1611	6.0
H(ζ)	795	-1716	-1029	6.0
H(ζ)	-363	-3078	-995	6.0
H(η)	-2181	-1402	-746	6.0
H(η)	-935	-115	-741	6.0
H(θ)	339	-1385	-129	6.0
H(θ)	-930	-2649	-130	6.0

The Structure Factor Amplitudes for C16.

The following pages consist of twelve columns, made up of three groups of four columns each. For each group, the four columns are:

1	$10 \cdot F_o$	$10 \cdot F_c/k$	$10 \cdot [(F_o)^2 - (F_c/k)^2] / \sigma_{F_o}^2$
---	----------------	------------------	---

C26H38O2

				26	28	25	2	4	155	154	2
	0	0	1					5	-19	14	-13
4	388	376	37		2	0	1	6	154	151	9
8	647	642	10	0	95	92	13	7	280	285	-18
12	191	199	-32	1	31	34	-6	8	135	140	-20
16	146	141	14	2	968	978	-13	9	172	178	-23
20	105	101	9	3	736	742	-11	10	374	353	59
24	200	203	-9	4	357	357	0	11	94	83	31
				5	77	76	6	12	176	178	-6
	1	0	1	6	329	340	-40	13	201	200	3
				7	173	169	22	14	86	85	2
0	9	0	3	8	240	240	-3	15	15	5	3
1	769	781	-22	9	30	7	29	16	87	85	6
2	185	180	33	10	34	40	-13	17	22	25	-2
3	65	65	-2	11	195	201	-31	18	-15	9	-5
4	207	202	29	12	314	306	30	19	85	94	-21
5	269	272	-15	13	467	471	-13	20	46	39	8
6	838	833	8	14	41	36	10	21	76	67	16
7	69	68	3	15	-18	6	-10	22	36	45	-9
8	45	52	-23	16	172	167	22	23	74	68	9
9	26	24	3	17	22	26	-5	24	50	43	8
10	163	167	-25	18	45	21	38	25	68	60	11
11	13	3	5	19	76	90	-48				
12	247	228	82	20	36	52	-28	3	0	1	
13	489	506	-46	21	102	105	-9	0	13	0	3
14	252	246	22	22	131	137	-20	1	339	346	-27
15	39	29	20	23	195	190	17	2	55	44	34
16	12	20	-7	24	145	151	-22	3	45	21	52
17	18	27	-11	25	45	49	-6	4	245	250	-21
18	14	32	-22	26	12	6	2	5	299	294	19
19	30	32	-3					6	232	233	-10
20	49	44	11	2	1	1		7	60	62	-8
21	101	106	-13					8	104	105	-7
22	45	39	10	0	1894	1893	0	9	93	86	28
23	121	114	20	1	1098	1081	19	10	305	294	42
24	77	87	-25	2	916	906	14	11	244	237	25
25	81	90	-24	3	353	351	7	12	161	163	-12
26	9	27	-13	4	154	152	7	13	108	110	-7
				5	200	207	-37	14	125	125	2
	1	1	1	6	260	258	8	15	24	23	1
0	929	929	0	7	111	114	-16	16	56	49	17
1	239	231	33	8	213	219	-40	17	-22	8	-13
2	839	811	41	9	276	279	-12	18	55	48	14
3	51	50	1	10	179	168	56	19	-13	7	-5
4	676	648	50	11	146	153	-37	20	-18	11	-9
5	366	362	11	12	37	20	27	21	18	30	-11
6	150	156	-26	13	188	185	12	22	140	150	-33
7	110	106	15	14	118	107	51	23	137	142	-17
8	573	571	3	15	153	149	20	24	54	64	-19
9	-17	31	-31	16	30	24	9	25	35	20	15
10	59	53	16	17	19	10	6				
11	327	350	-75	18	28	15	13	3	1	1	
12	245	244	3	19	57	55	4				
13	83	91	-23	20	32	31	0	0	291	299	-28
14	245	234	37	21	77	70	17	1	264	266	-8
15	-9	13	-5	22	120	117	7	2	52	57	-16
16	-18	6	-7	23	51	49	3	3	114	116	-10
17	15	17	-1	24	115	111	11	4	74	76	-8
18	-29	6	-16	25	72	80	-18	5	38	34	9
19	10	16	-2	26	25	19	4	6	188	187	4
20	163	164	-3					7	114	122	-42
21	14	17	-1	2	2	1		8	148	149	-2
22	69	66	4	0	132	122	33	9	261	261	-1
23	53	47	6	1	1110	1088	24	10	291	287	15
24	69	62	10	2	68	78	-29	11	192	188	19
25	57	70	-20	3	327	323	12	12	171	168	14
								13	174	180	-24

C26H38O2

2	156	145	41	18	-39	9	-27	15	24	11	4
3	72	71	2	19	28	15	9	16	20	18	0
4	193	184	37	20	14	20	-3				
5	96	86	33	21	46	29	19		6	0	1
6	52	52	0								
7	28	4	17		5	3	1	0	105	96	24
8	117	117	0					1	8	23	-9
9	83	80	6	0	57	66	-19	2	44	21	29
10	332	309	71	1	65	59	14	3	204	210	-25
11	49	45	7	2	50	37	22	4	40	49	-14
12	48	49	-1	3	73	79	-17	5	32	16	15
13	110	98	34	4	115	111	11	6	36	15	21
14	146	129	53	5	68	68	1	7	85	88	-8
15	41	41	0	6	55	44	20	8	18	20	-1
16	-37	4	-23	7	89	79	25	9	130	140	-35
17	52	26	34	8	48	44	7	10	40	0	28
18	114	110	13	9	80	76	10	11	-5	15	-4
19	23	1	9	10	-12	23	-13	12	16	32	-12
20	36	34	3	11	39	35	5	13	51	65	-25
21	-9	11	-3	12	75	75	0	14	55	45	16
22	-22	28	-20	13	121	129	-23	15	88	85	5
				14	15	19	-1	16	-20	11	-9
	5	1	1	15	107	111	-10	17	34	11	17
				16	96	110	-36	18	44	35	11
0	92	84	22	17	72	69	6	19	37	36	0
1	285	290	-20	18	33	40	-7				
2	244	254	-39	19	44	28	18		6	1	1
3	155	165	-43	20	66	54	20				
4	85	76	25					0	127	127	0
5	69	71	-7		5	4	1	1	132	138	-19
6	160	156	15					2	65	50	29
7	84	91	-21	0	90	76	33	3	119	123	-14
8	153	147	22	1	214	219	-17	4	55	37	29
9	97	109	-41	2	105	100	12	5	95	101	-16
10	64	61	8	3	52	70	-37	6	39	27	13
11	129	136	-23	4	65	65	0	7	99	95	12
12	34	10	21	5	72	53	37	8	112	103	25
13	64	70	-12	6	76	77	-1	9	18	19	0
14	16	16	0	7	90	94	-10	10	69	62	15
15	39	46	-9	8	91	90	1	11	41	52	-16
16	72	67	8	9	85	93	-20	12	55	63	-14
17	65	60	8	10	86	95	-25	13	71	62	16
18	11	12	0	11	24	33	-8	14	120	113	19
19	32	33	-1	12	68	62	12	15	90	80	22
20	19	7	5	13	45	52	-11	16	69	80	-23
21	44	33	13	14	51	54	-5	17	13	10	0
22	24	25	0	15	59	61	-3	18	26	34	-7
				16	38	46	-10	19	-26	16	-15
	5	2	1	17	56	72	-28				
				18	9	6	0		6	2	1
0	94	91	6								
1	54	53	2		5	5	1	0	-27	2	-13
2	84	78	19					1	53	35	29
3	110	115	-16	0	266	279	-29	2	105	92	36
4	128	127	3	1	120	106	22	3	45	45	0
5	139	141	-5	2	173	172	2	4	21	25	-3
6	91	82	27	3	39	14	12	5	34	10	19
7	40	43	-3	4	29	53	-17	6	46	51	-8
8	65	67	-5	5	85	75	13	7	5	34	-19
9	129	134	-17	6	42	37	4	8	34	22	11
10	108	109	-3	7	136	132	6	9	37	56	-30
11	76	75	2	8	123	127	-5	10	120	112	23
12	142	137	17	9	127	127	0	11	49	39	14
13	89	90	-3	10	82	74	10	12	68	66	3
14	150	155	-17	11	21	3	4	13	56	62	-10
15	100	111	-32	12	23	11	3	14	70	67	6
16	83	78	11	13	34	19	7	15	70	72	-4
17	31	28	2	14	20	31	-4	16	68	74	-11

C26H38O2

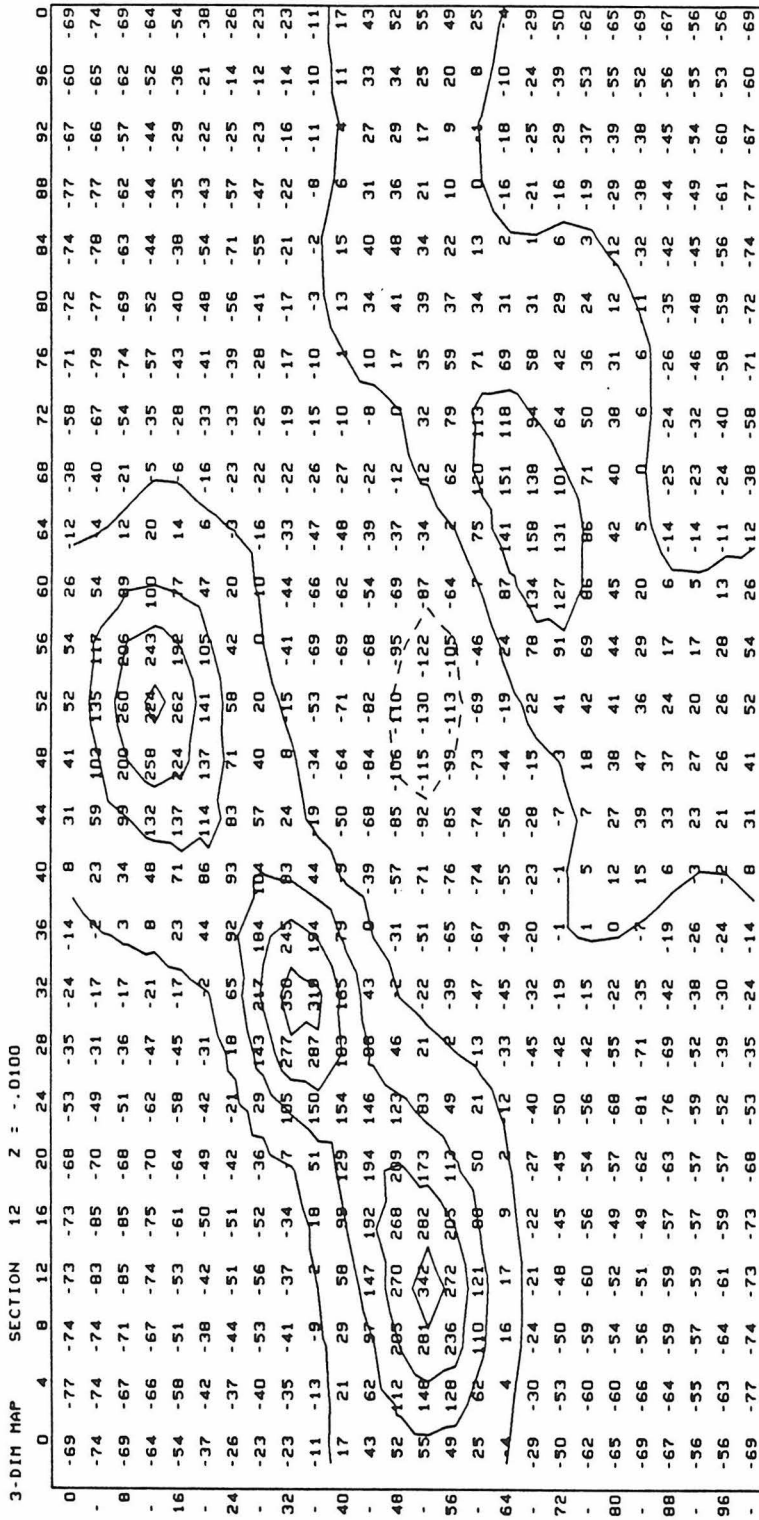
17	37	43	-7					6	102	87	39
18	24	8	7	7	0	1		7	115	116	-3
	6	3	1	0	-27	0		8	109	114	-13
				1	33	17	-8	9	34	46	-14
0	31	43	-15	2	43	41	14	10	72	76	-9
1	50	56	-11	3	188	192	-15	11	77	70	14
2	51	44	11	4	58	51	10	12	49	59	-14
3	65	59	11	5	108	102	18	13	37	27	10
4	35	2	22	6	29	4	13		7	4	1
5	68	82	-32	7	89	86	8				
6	52	46	9	8	69	66	6	0	18	26	-5
7	88	87	2	9	-15	13	-6	1	33	27	5
8	114	107	18	10	30	8	14	2	41	37	5
9	85	77	18	11	27	11	10	3	38	32	7
10	39	41	-1	12	16	8	3	4	63	56	12
11	30	36	-6	13	50	50	0	5	40	44	-5
12	43	37	7	14	75	72	7	6	68	70	-2
13	-29	22	-22	15	46	29	17	7	73	72	1
14	32	38	-6	16	75	68	12	8	53	58	-7
15	44	53	-11					9	69	77	-17
16	46	60	-21	7	1	1		10	34	29	5
17	11	22	-5								
	6	4	1	0	39	37	3	7	5	1	
				1	69	56	24				
0	62	46	24	2	51	55	-8	0	48	56	-10
1	75	63	27	3	36	48	-16	1	14	14	0
2	60	67	-14	4	99	94	13	2	53	46	8
3	55	57	-2	5	33	35	-2	3	-4	24	-7
4	67	82	-32	6	47	32	18	4	26	33	-5
5	85	78	16	7	-15	8	-4	5	55	63	-10
6	40	40	0	8	79	81	-4				
7	115	117	-6	9	61	60	2	8	0	1	
8	101	102	-1	10	55	48	11				
9	96	101	-13	11	19	23	-2	0	30	7	13
10	51	62	-18	12	-21	9	-9	1	-26	10	-13
11	43	34	10	13	54	37	26	2	27	15	8
12	37	24	12	14	109	111	-7	3	23	6	8
13	77	56	42	15	24	44	-20	4	27	22	4
14	-13	30	-18	16	47	67	-11	5	19	16	1
15	26	36	-9					6	16	8	3
	6	5	1	7	2	1		7	37	37	0
				8				8	74	89	-34
0	48	47	0	0	23	20	1	9	54	51	4
1	78	76	2	1	64	76	-26	10	-35	0	-19
2	62	61	-2	2	41	25	18	11	18	18	0
3	82	86	-8	3	38	52	-20				
4	11	45	-22	4	25	15	6	8	1	1	
5	53	44	10	5	54	47	11				
6	79	93	-26	6	78	94	-36	0	24	2	9
7	78	77	0	7	46	20	27	1	18	14	1
8	93	89	7	8	72	82	-21	2	13	19	-2
9	26	55	-29	9	133	144	-32	3	-18	38	-29
10	-25	18	-12	10	45	44	2	4	63	52	20
11	38	41	-2	11	62	34	42	5	23	24	0
12	18	19	0	12	21	20	0	6	38	8	23
	6	6	1	13	33	20	10	7	61	56	8
				14	24	26	-1	8	67	73	-11
0	124	118	9	15	69	71	-2	9	28	48	-23
1	36	47	-8					10	43	52	-13
2	70	93	-29	7	3	1					
3	25	30	-2								
4	58	61	-3								
5	69	78	-10								
6	33	28	2								
				0	22	29	-5	8	2	1	
				1	47	45	2	0	60	57	3
				2	36	32	5	1	-10	14	-5
				3	42	37	6	2	47	42	5
				4	68	60	15	3	55	73	-35
				5	-9	13	-4	4	52	57	-8

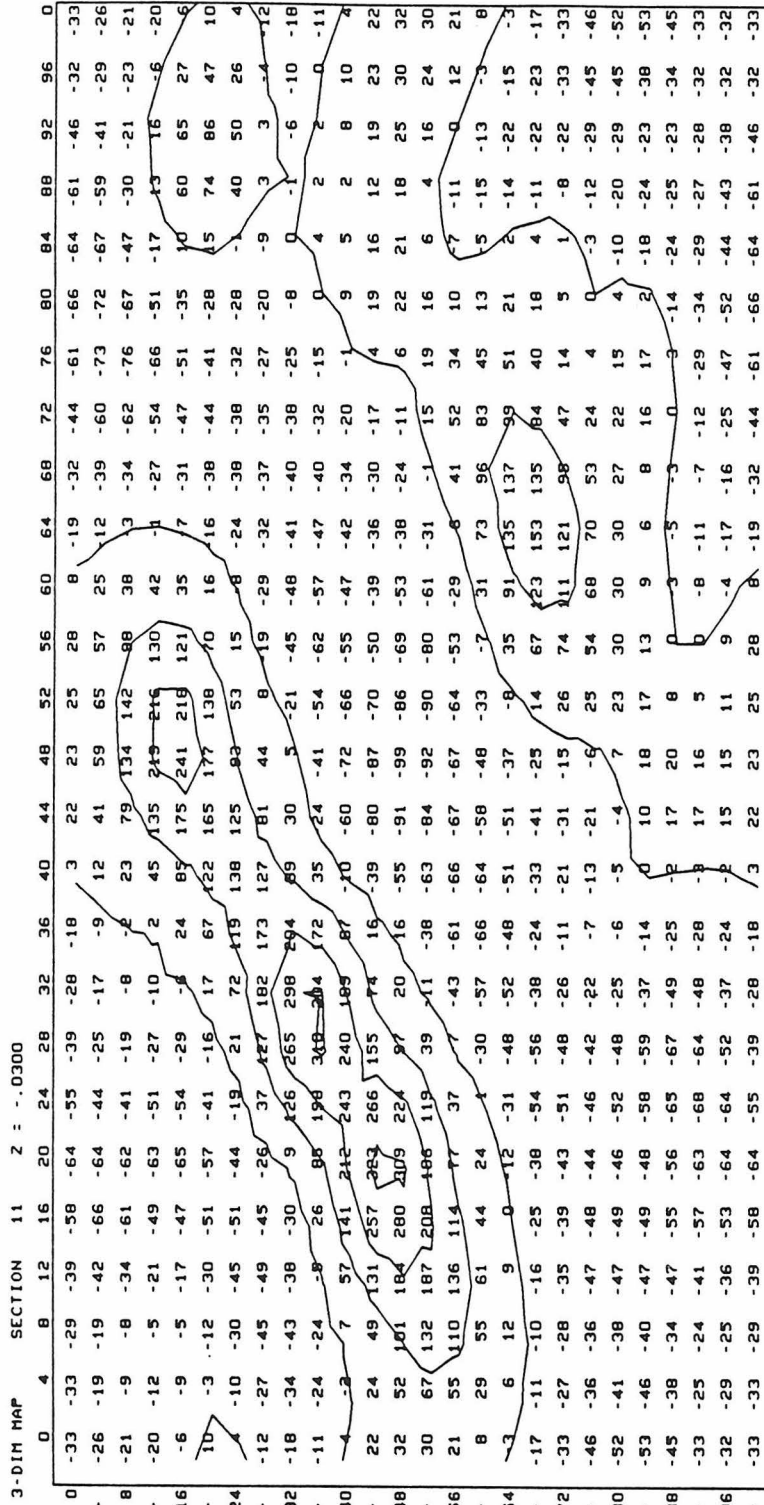
C26H38O2

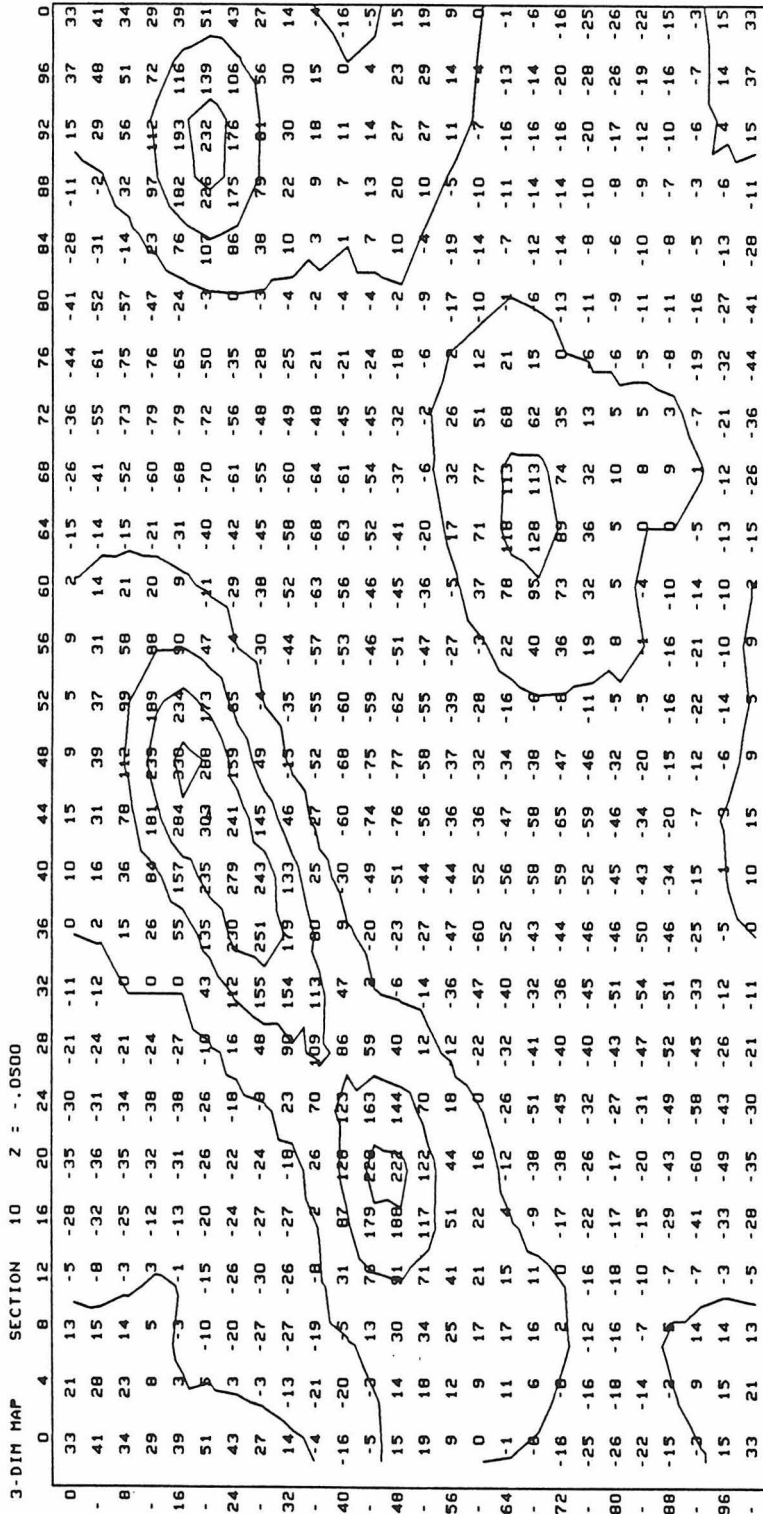
5	17	22	-3					2	41	35	8
6	96	94	2	8	3	1		3	42	47	-6
7	35	29	5					4	52	35	23
8	93	89	7	0	-26	17	-14	5	56	61	-7
9	90	92	-4	1	20	33	-10	6	45	66	-22

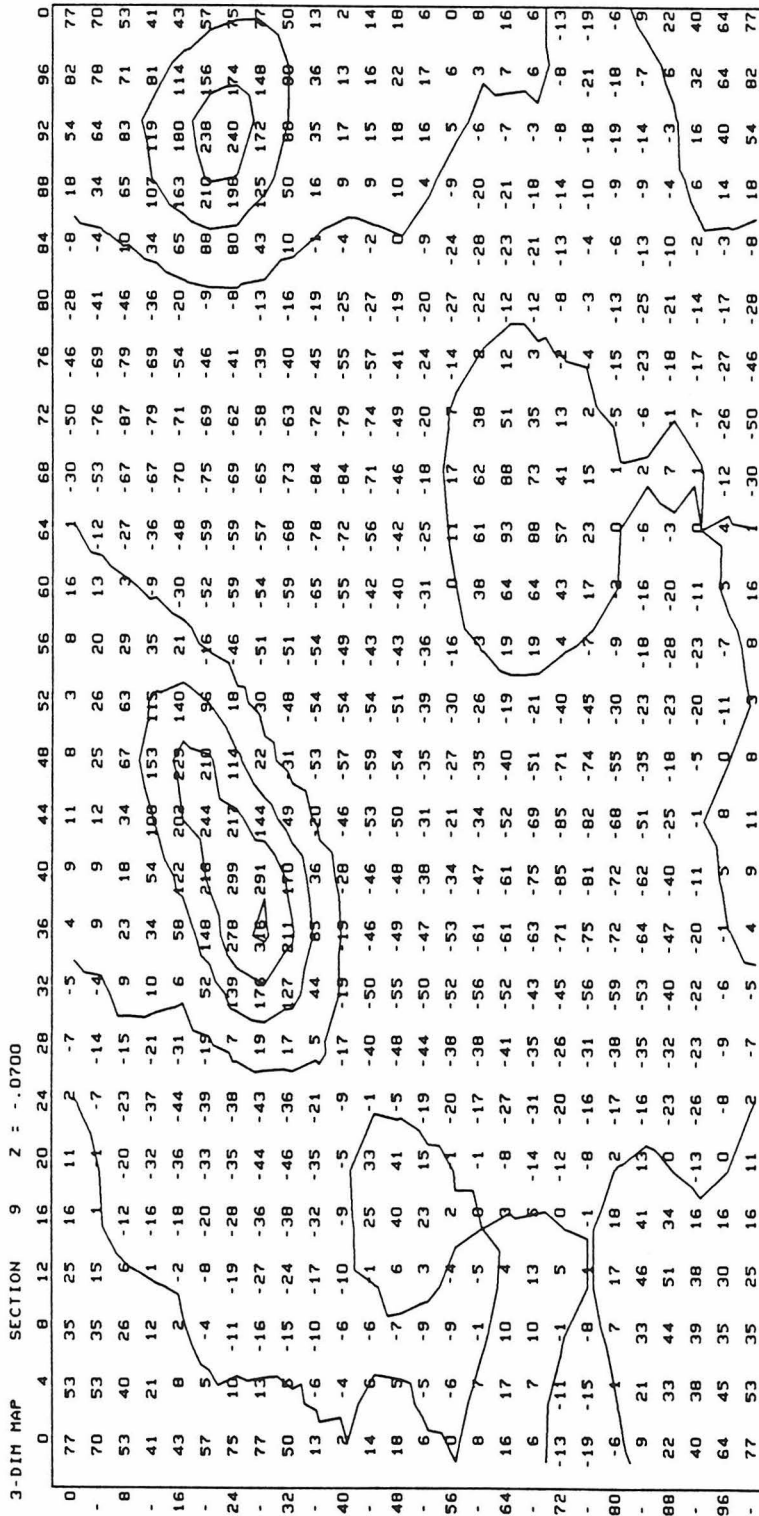
The Fourier Map for C14

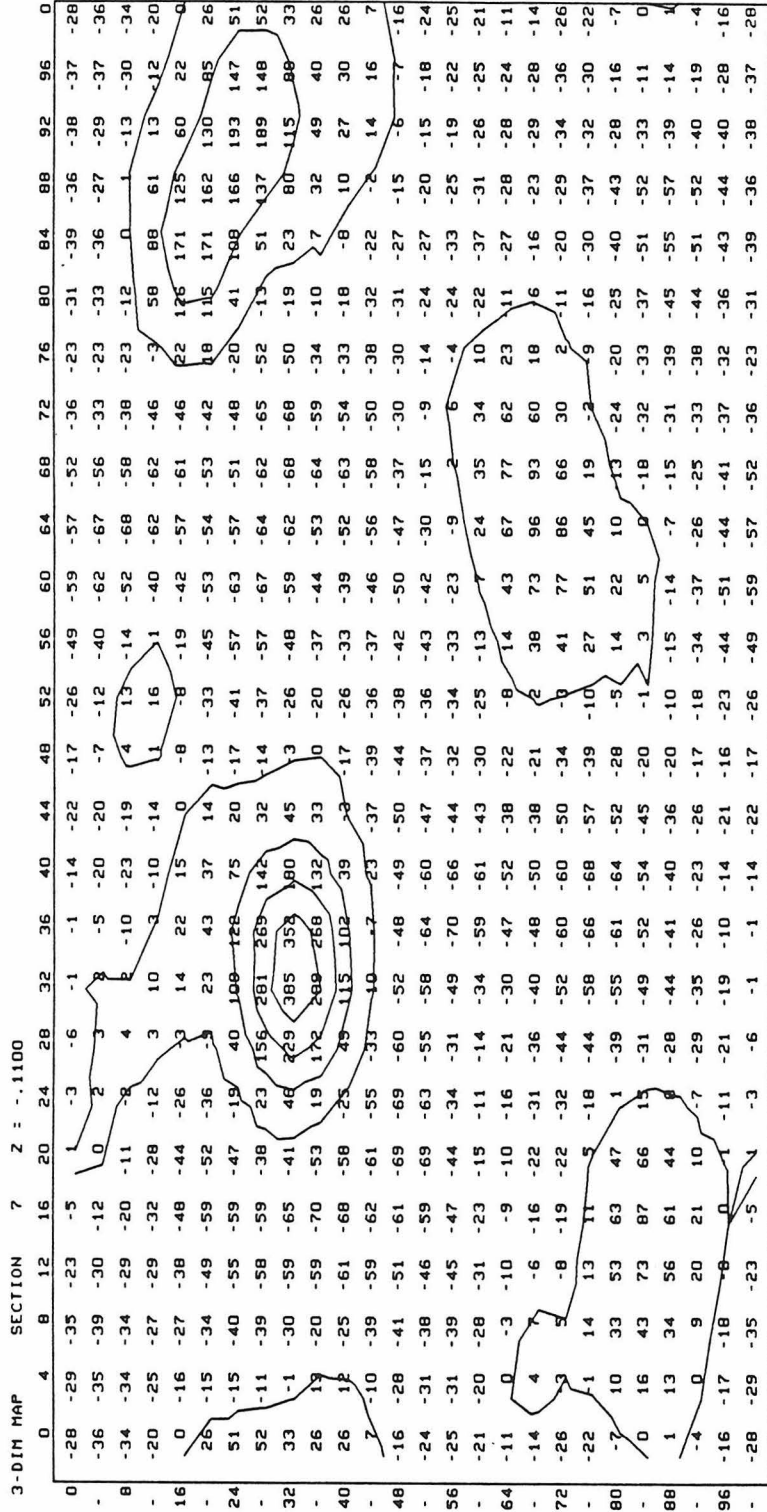
The structure was phased on the naphthalene and the oxygens, which were placed in positions (found by MULTAN) similar to those found for C16. Each slice is parallel to the xy plane. The axes are in fractional coordinates, with y running from 0.0 to 1.0 (right to left) as you read the map, and x running from 0.0 to 1.0 (top to bottom) as you read the map. The scale of the points is $10 \times e^{-}/\text{\AA}^3$.

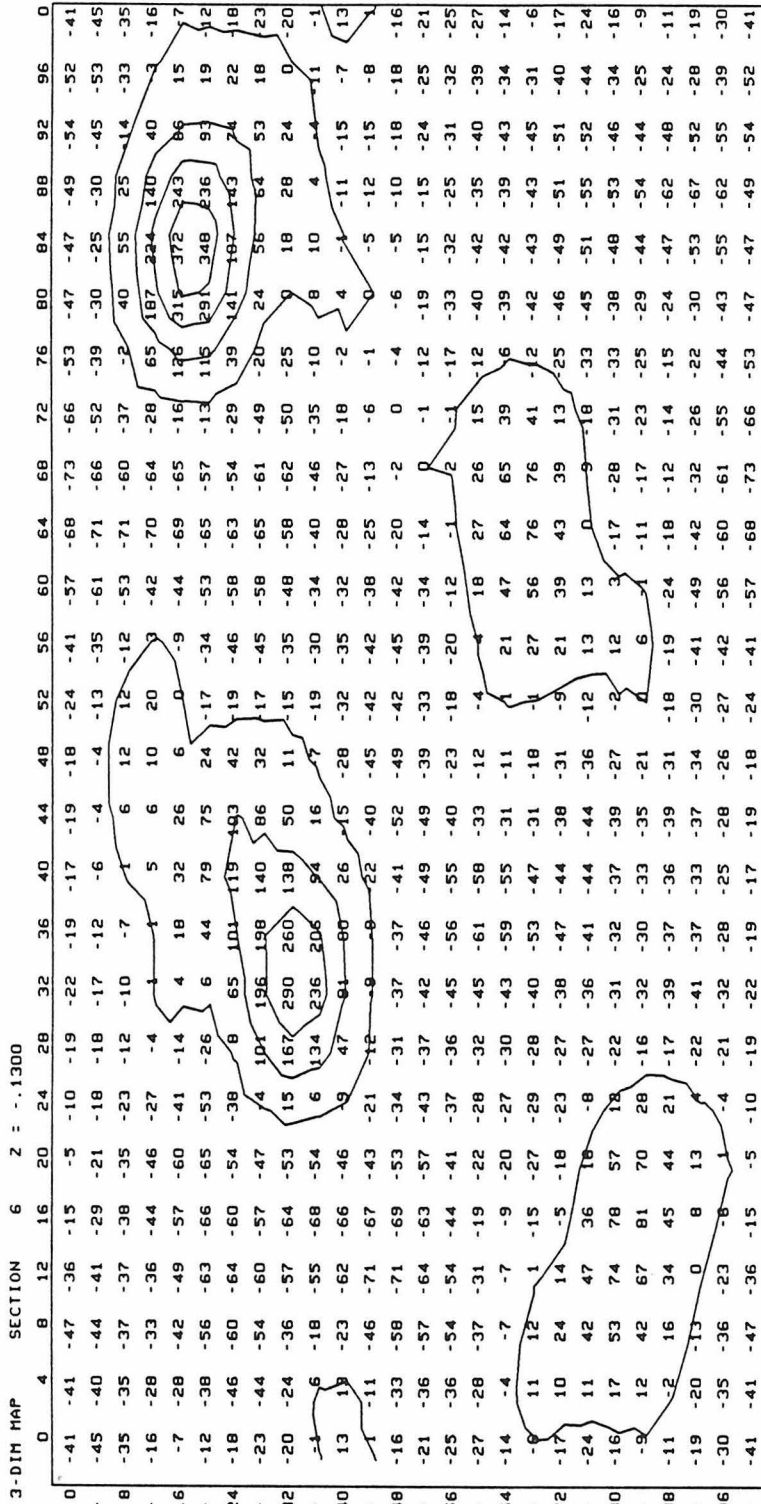


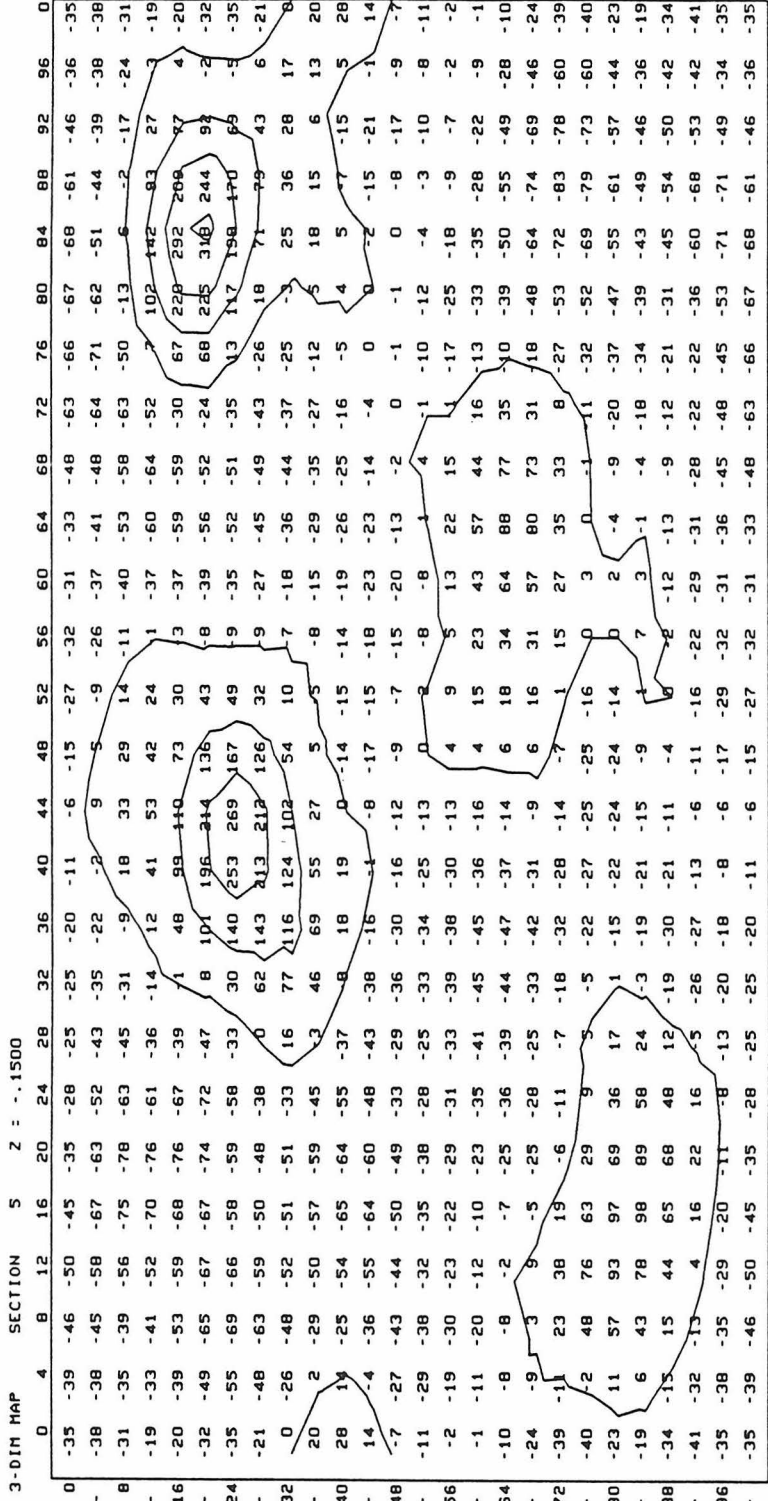


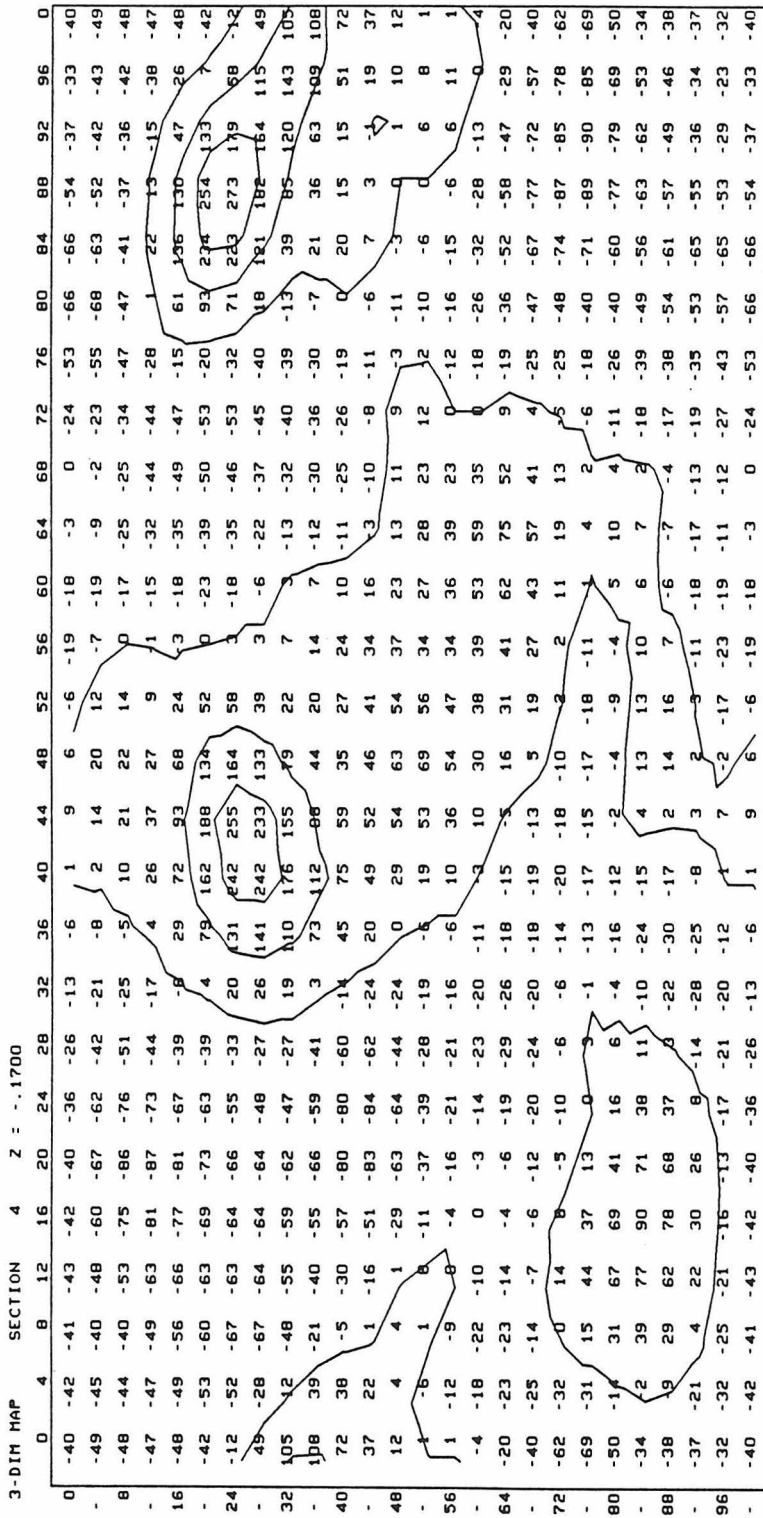


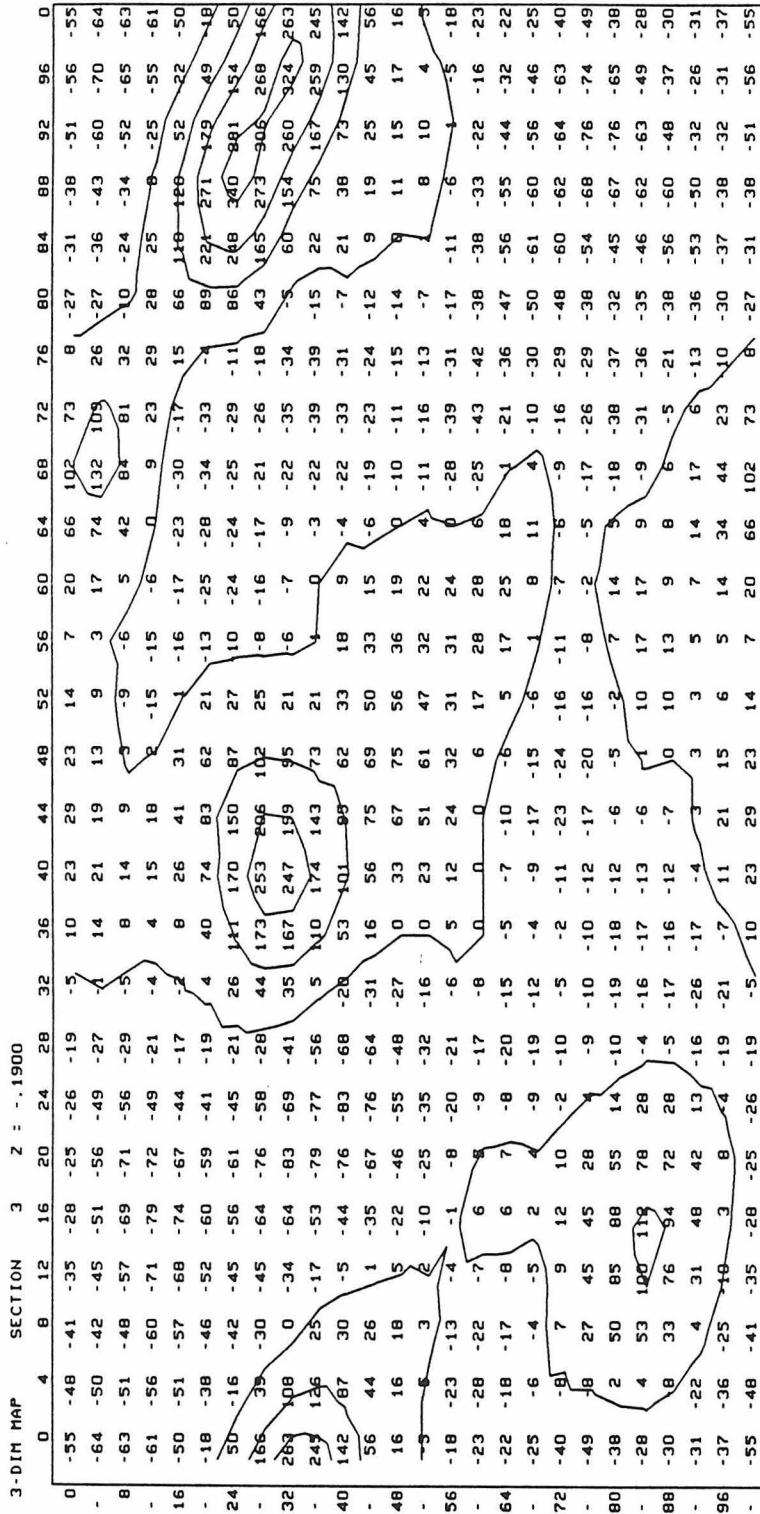


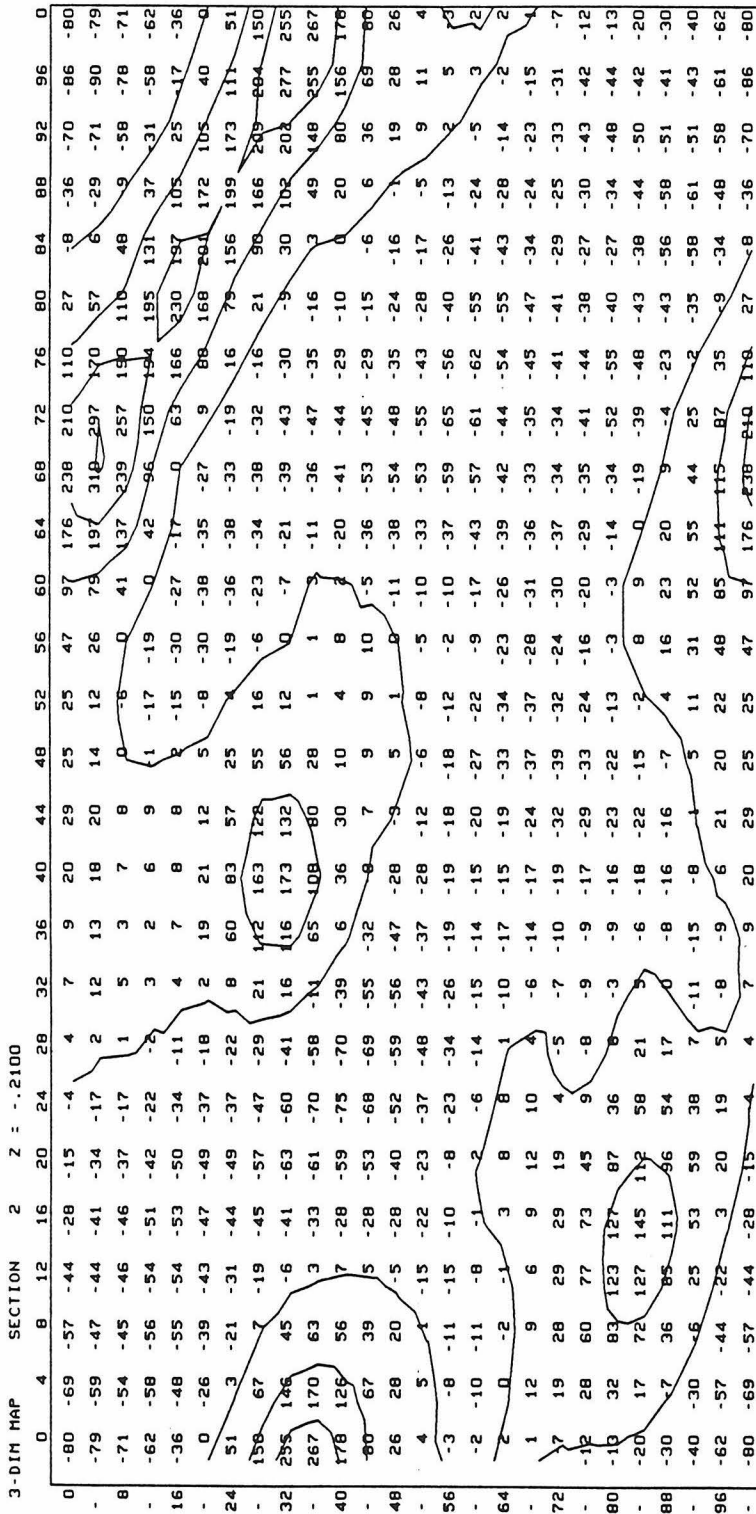


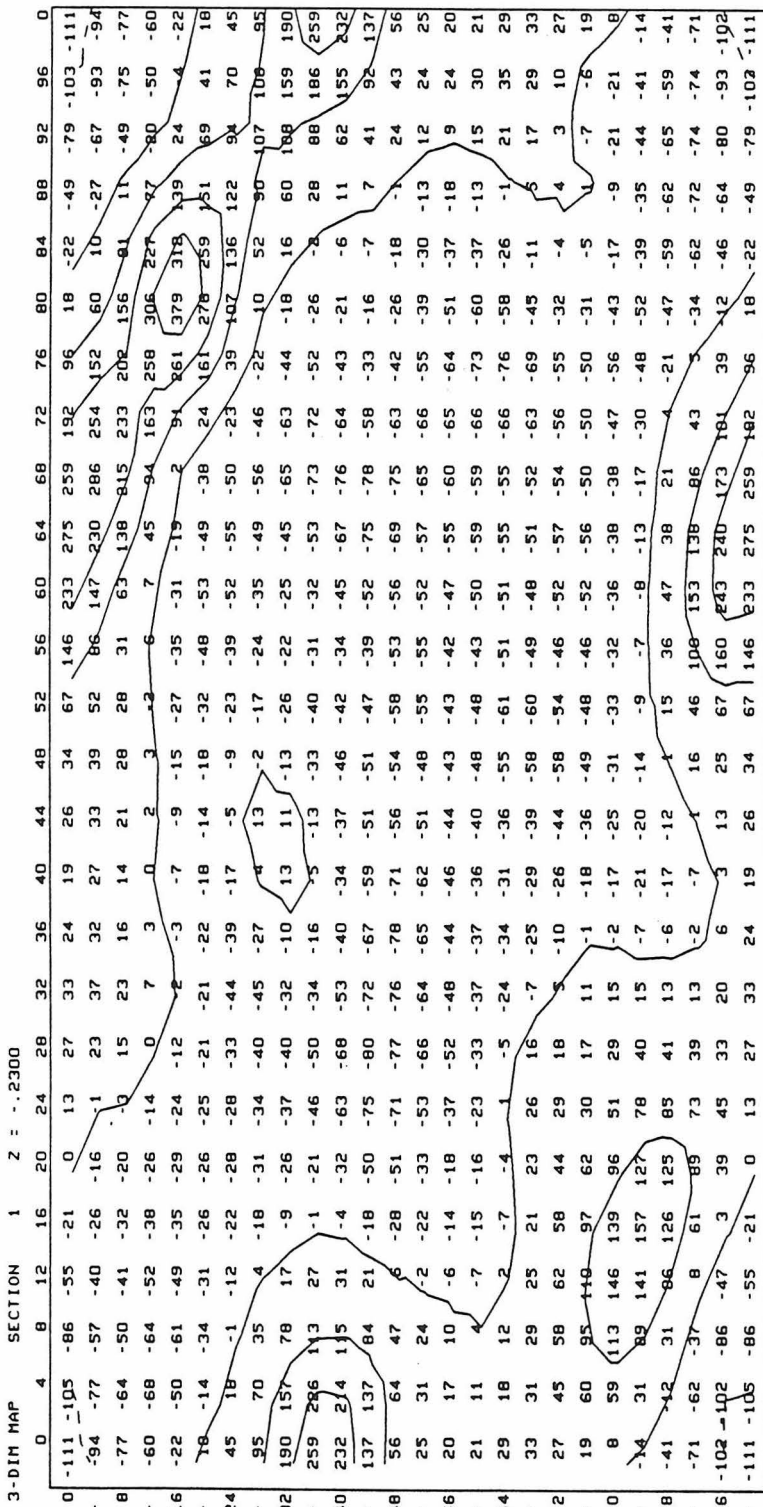


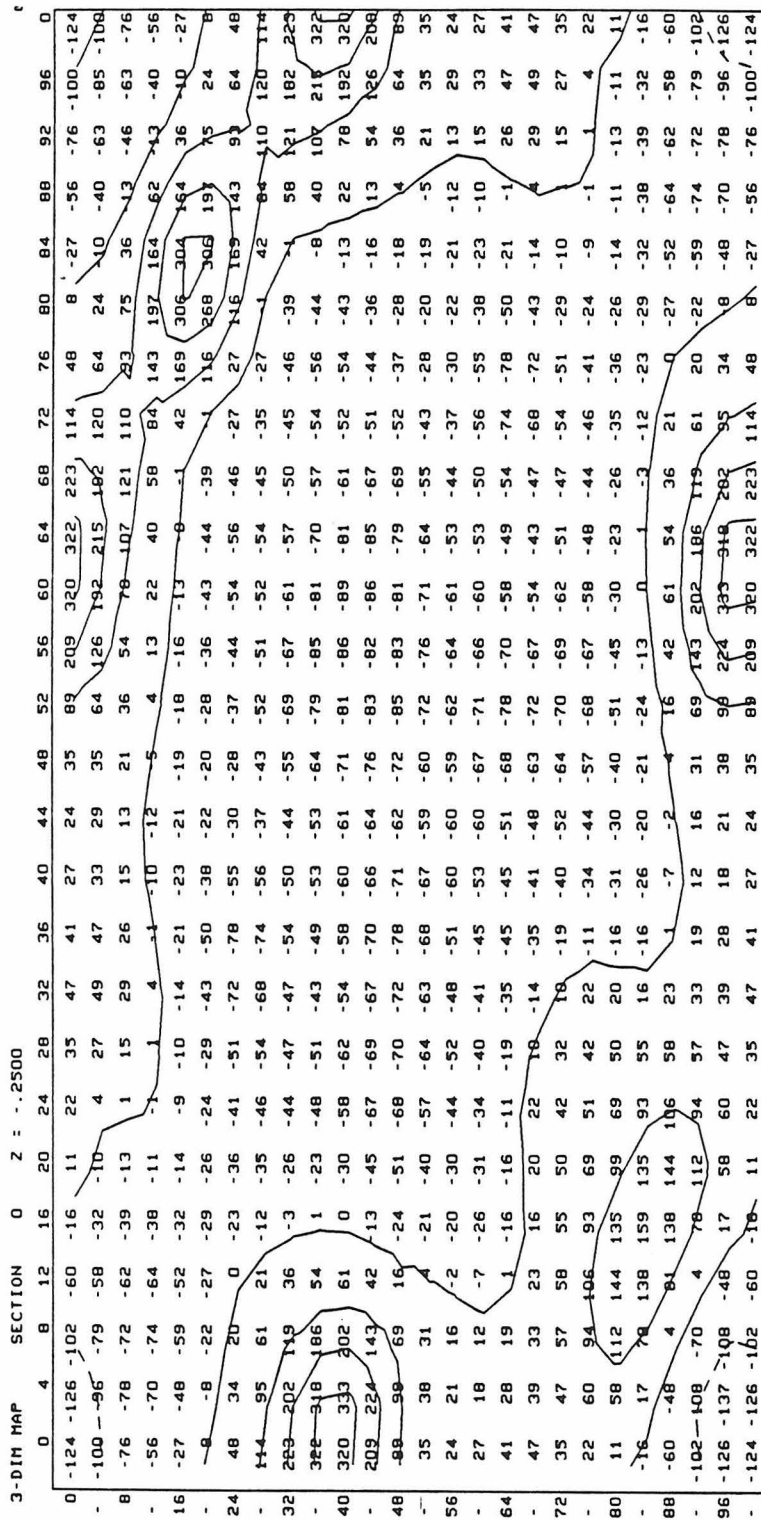






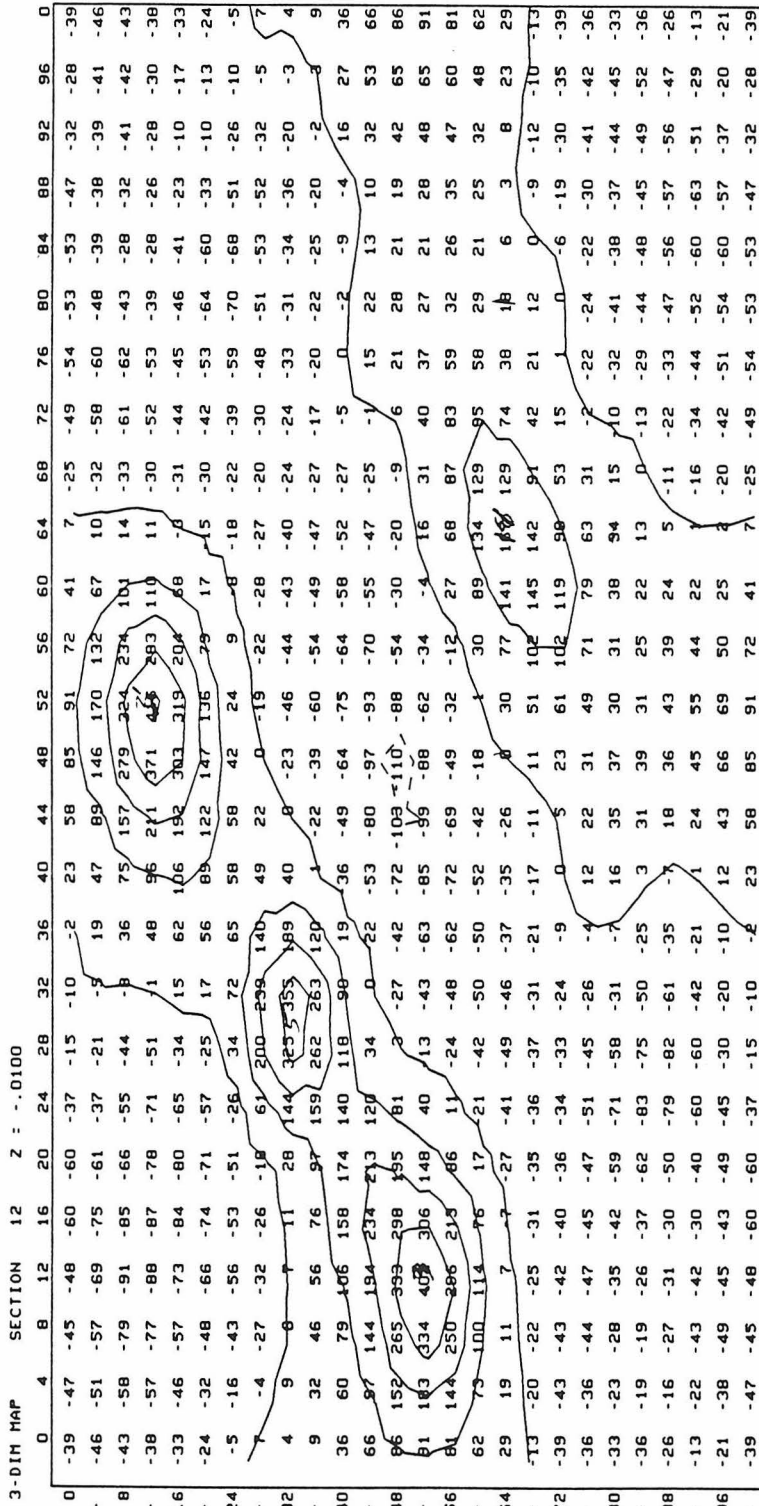


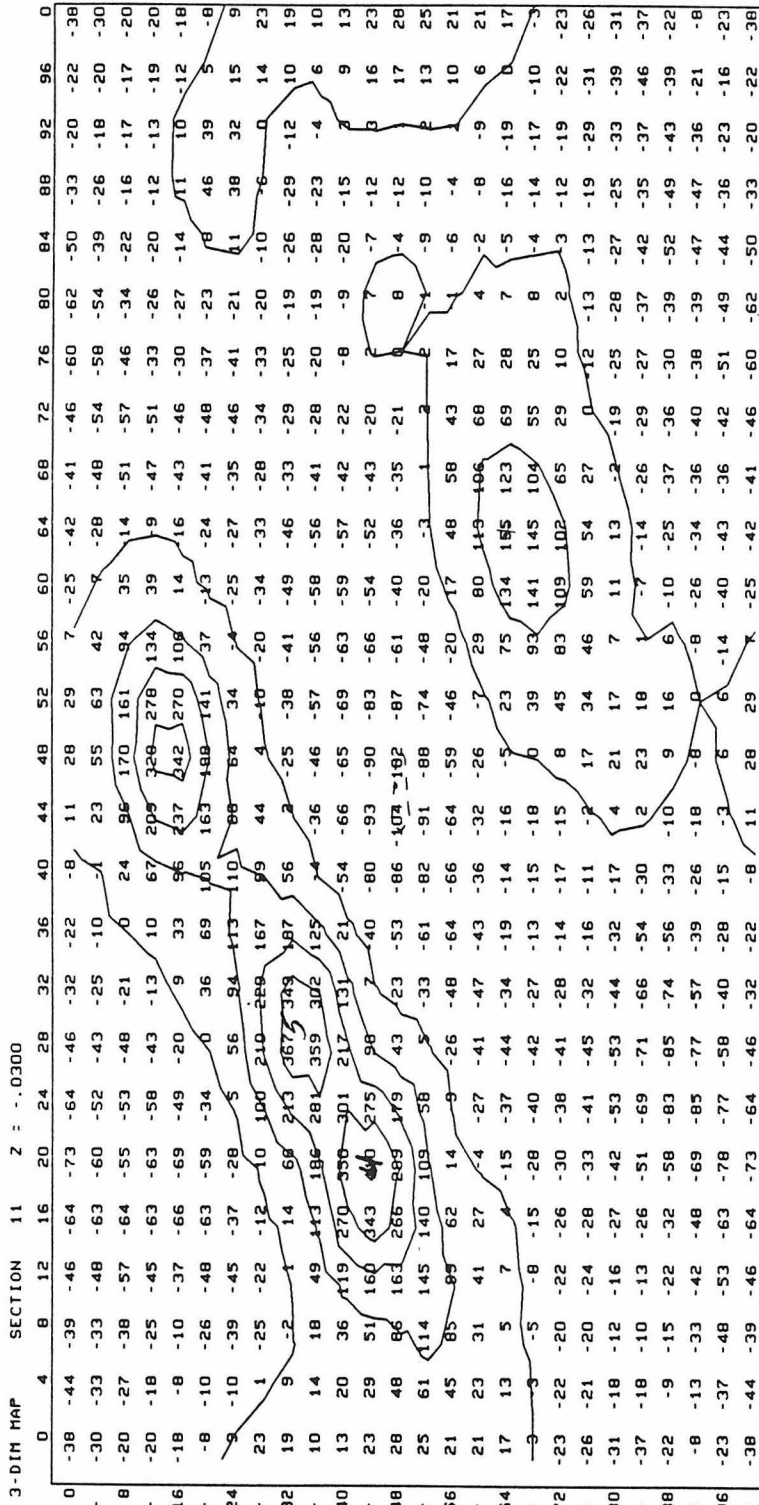


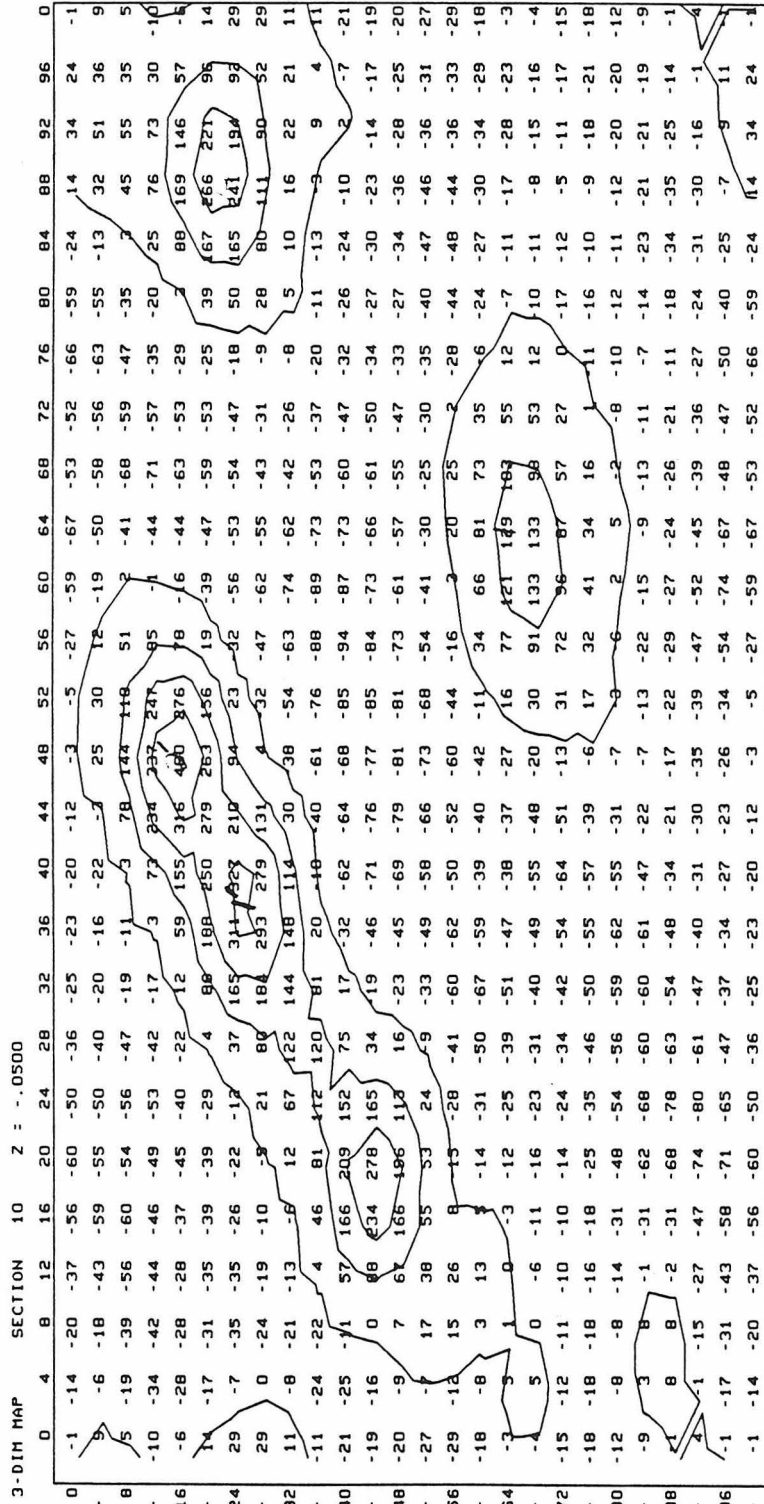


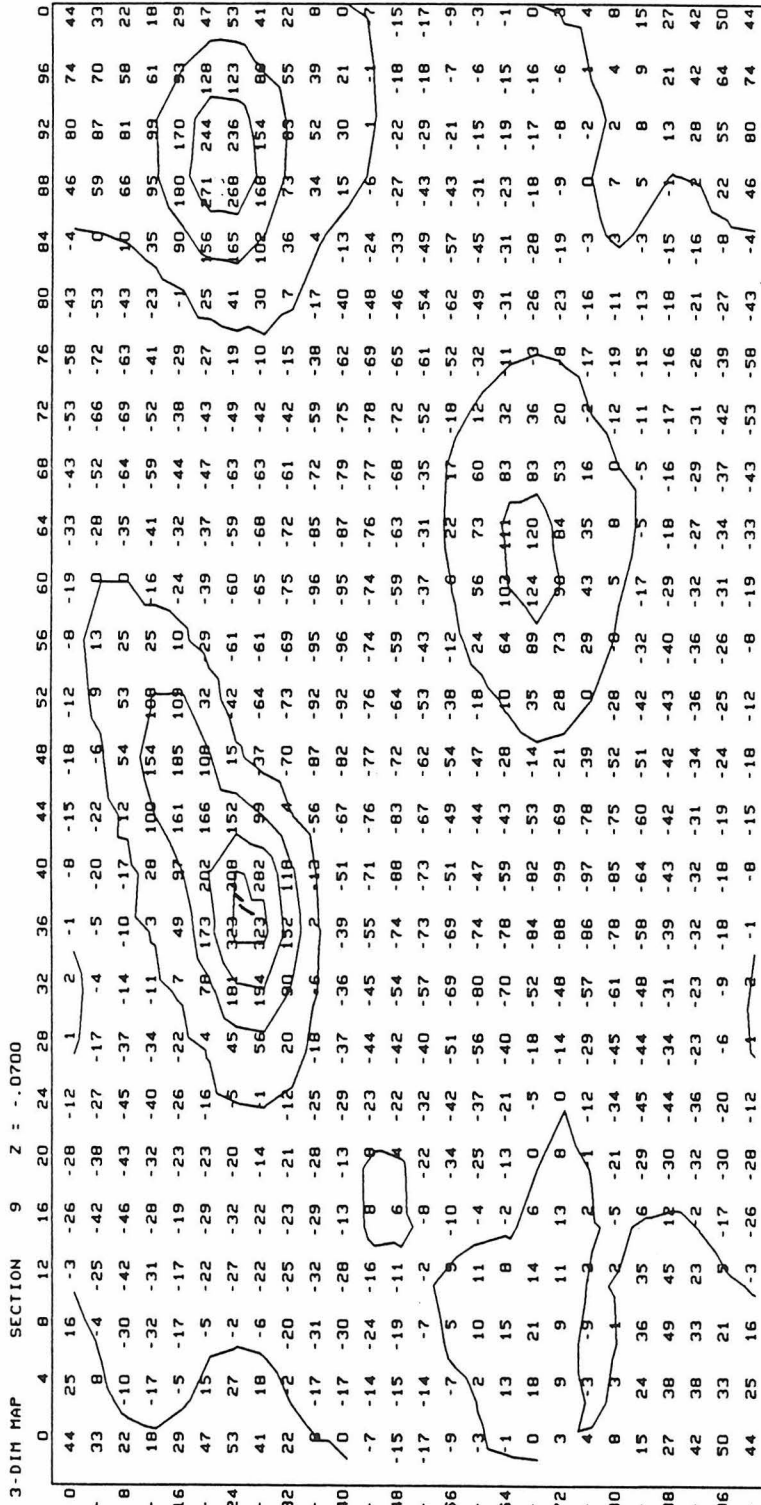
The Fourier Map for C15

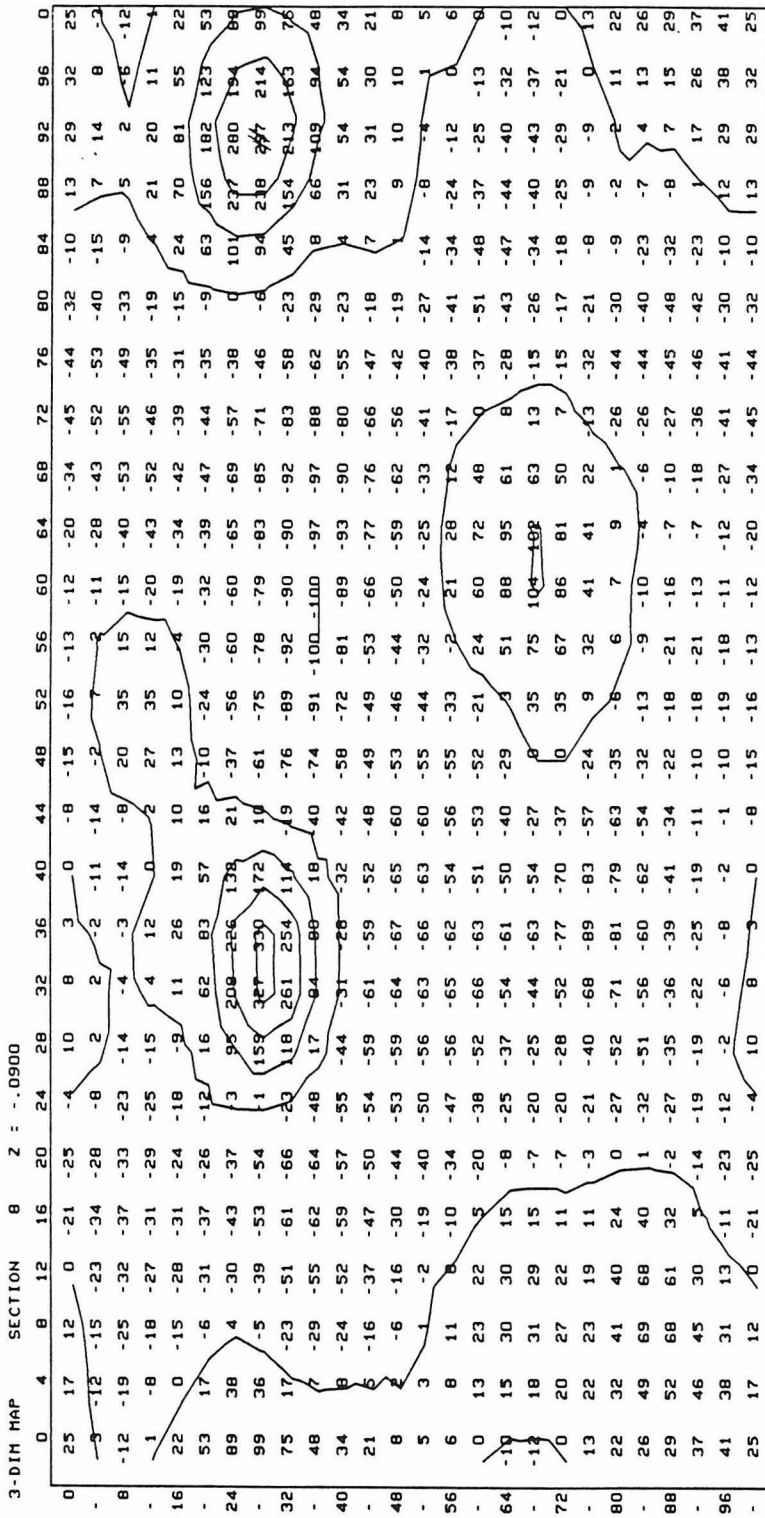
The structure was phased on the naphthalene and the oxygens, which were placed in positions (found by MULTAN) similar to those found for C16. Each slice is parallel to the xy plane. The axes are in fractional coordinates, with y running from 0.0 to 1.0 (right to left) as you read the map, and x running from 0.0 to 1.0 (top to bottom) as you read the map. The scale of the points is $10 \times e^-/\text{\AA}^3$.

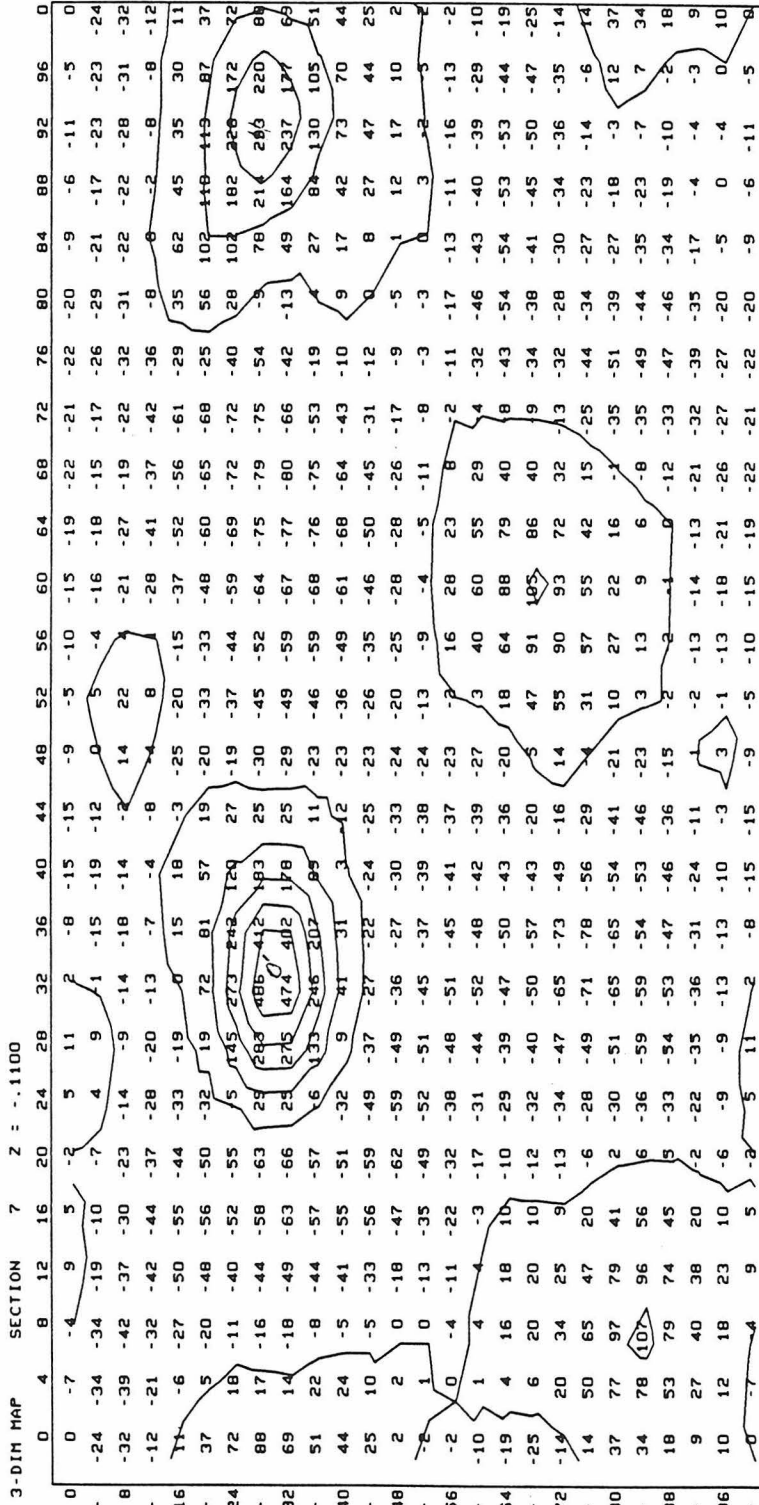


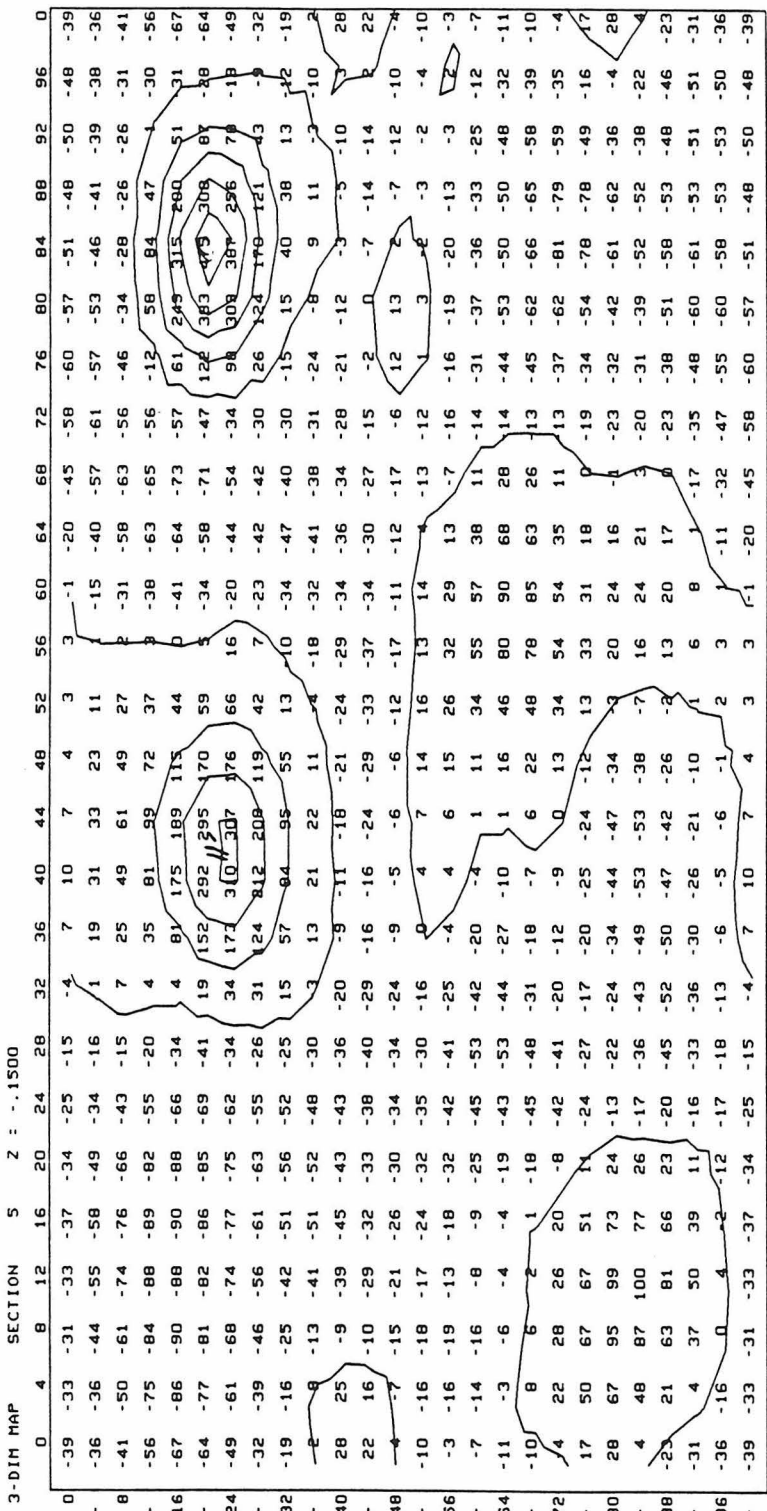




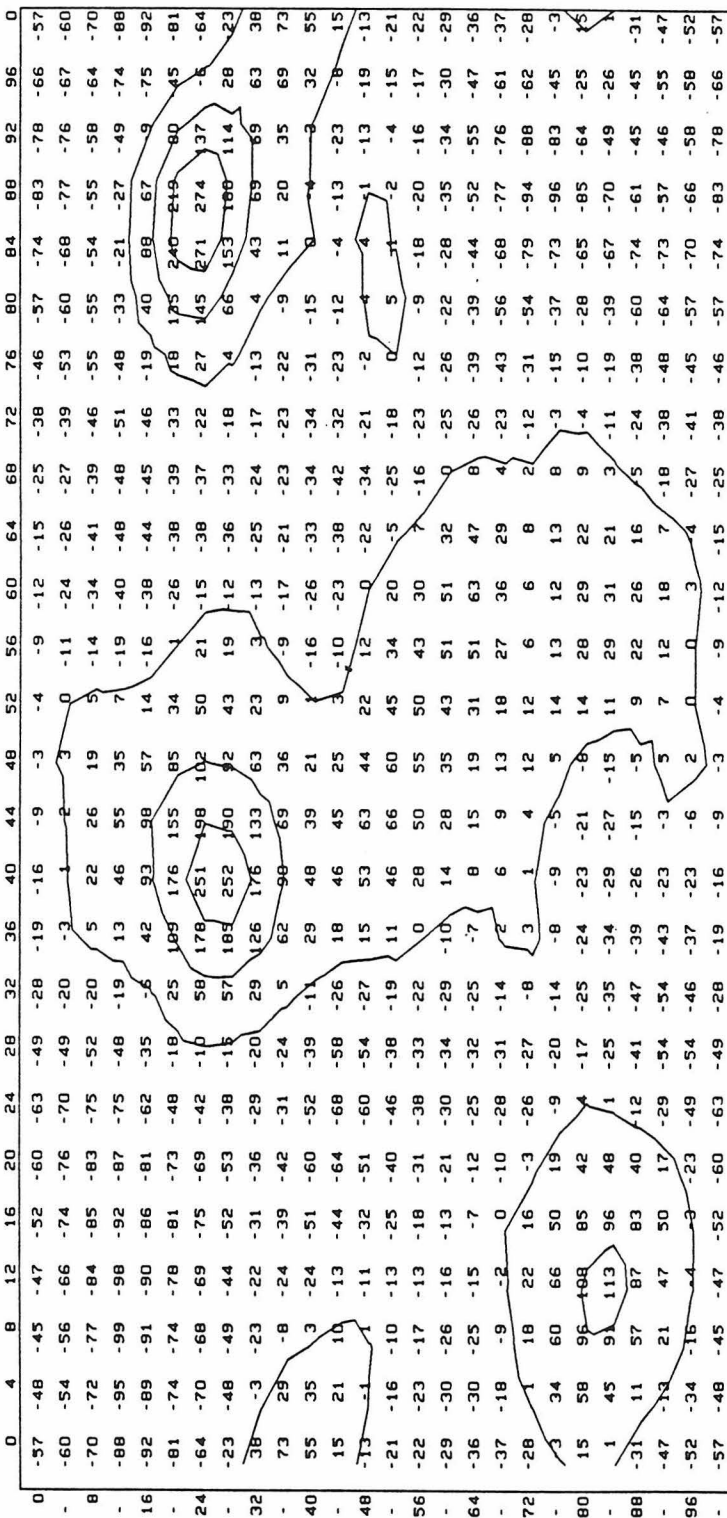


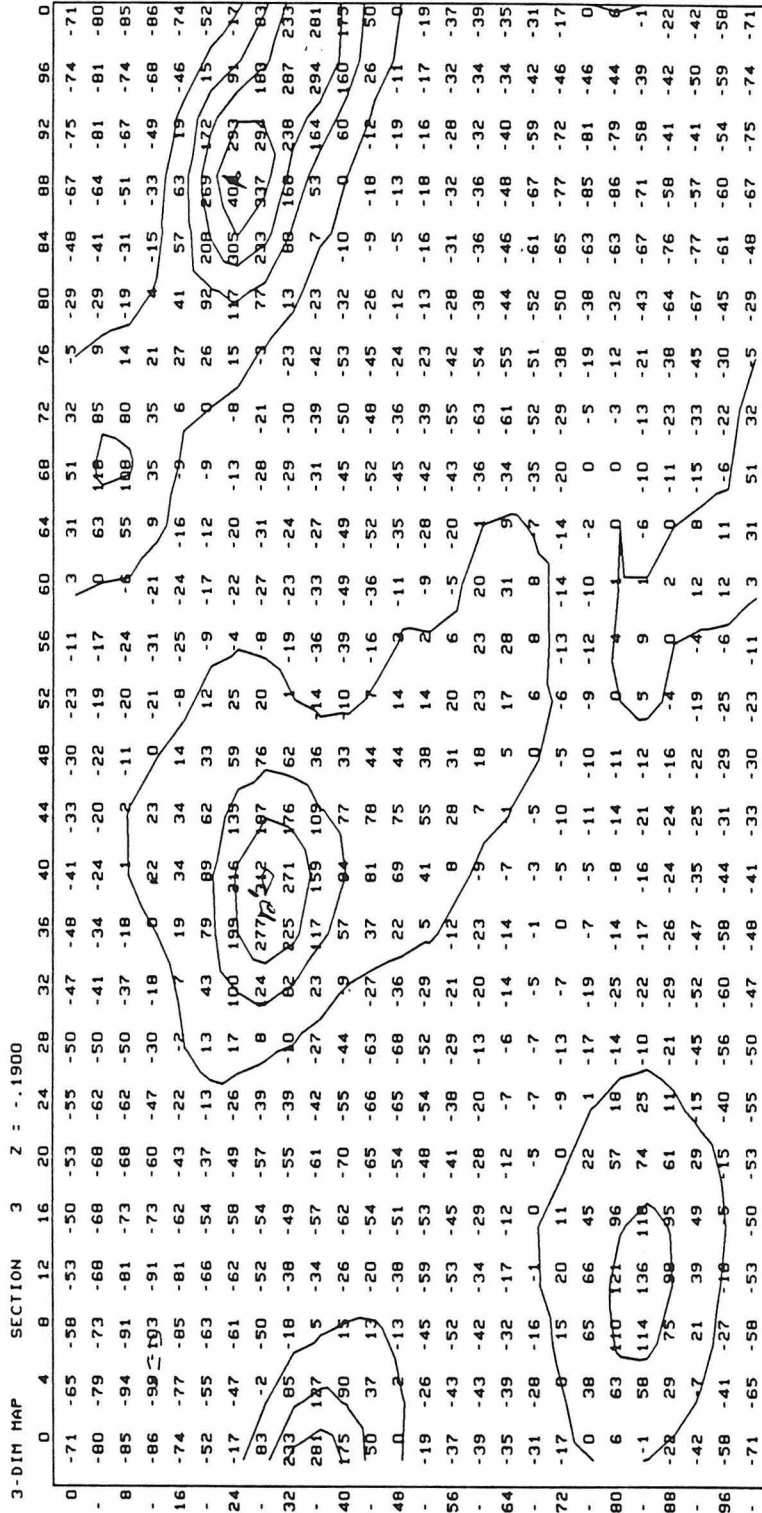


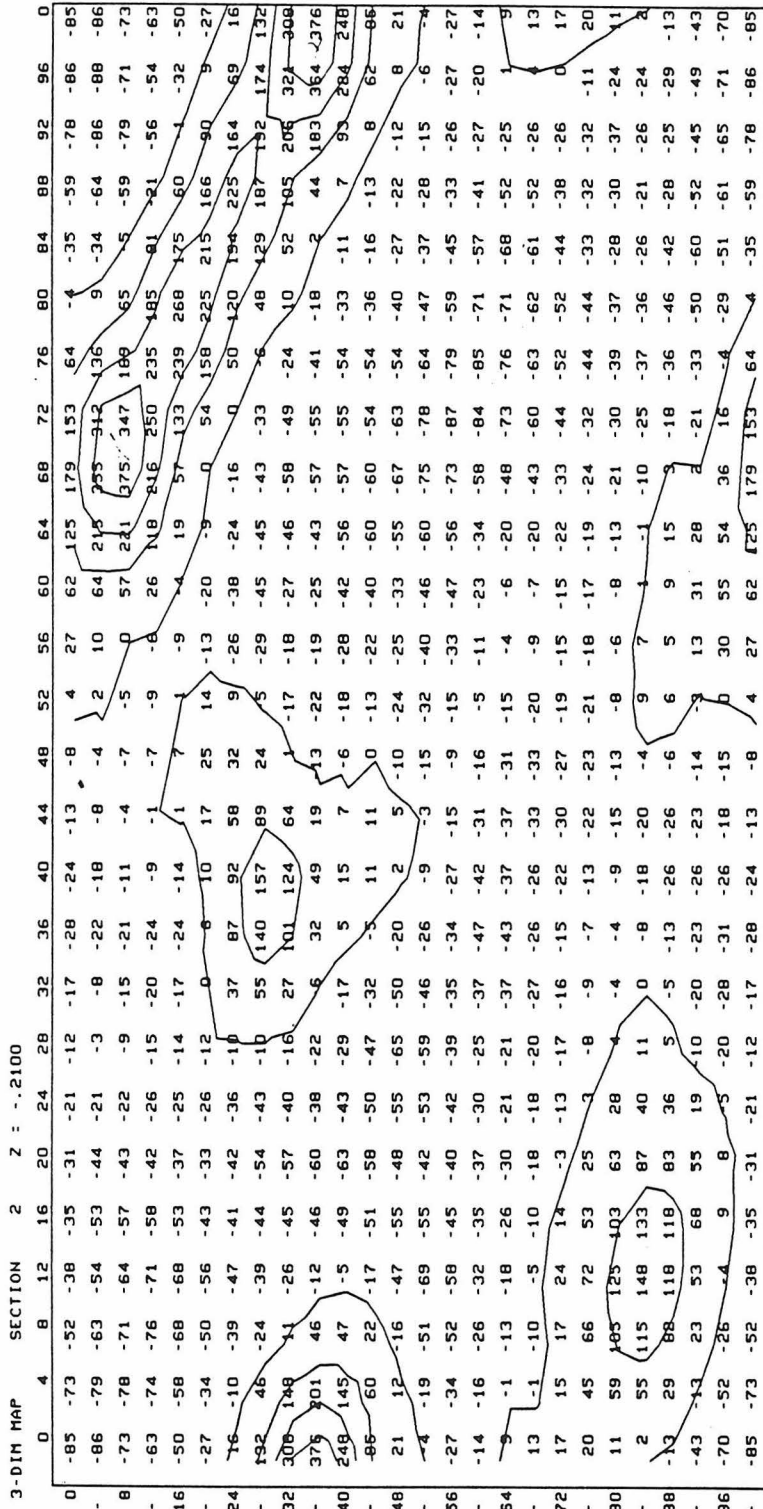


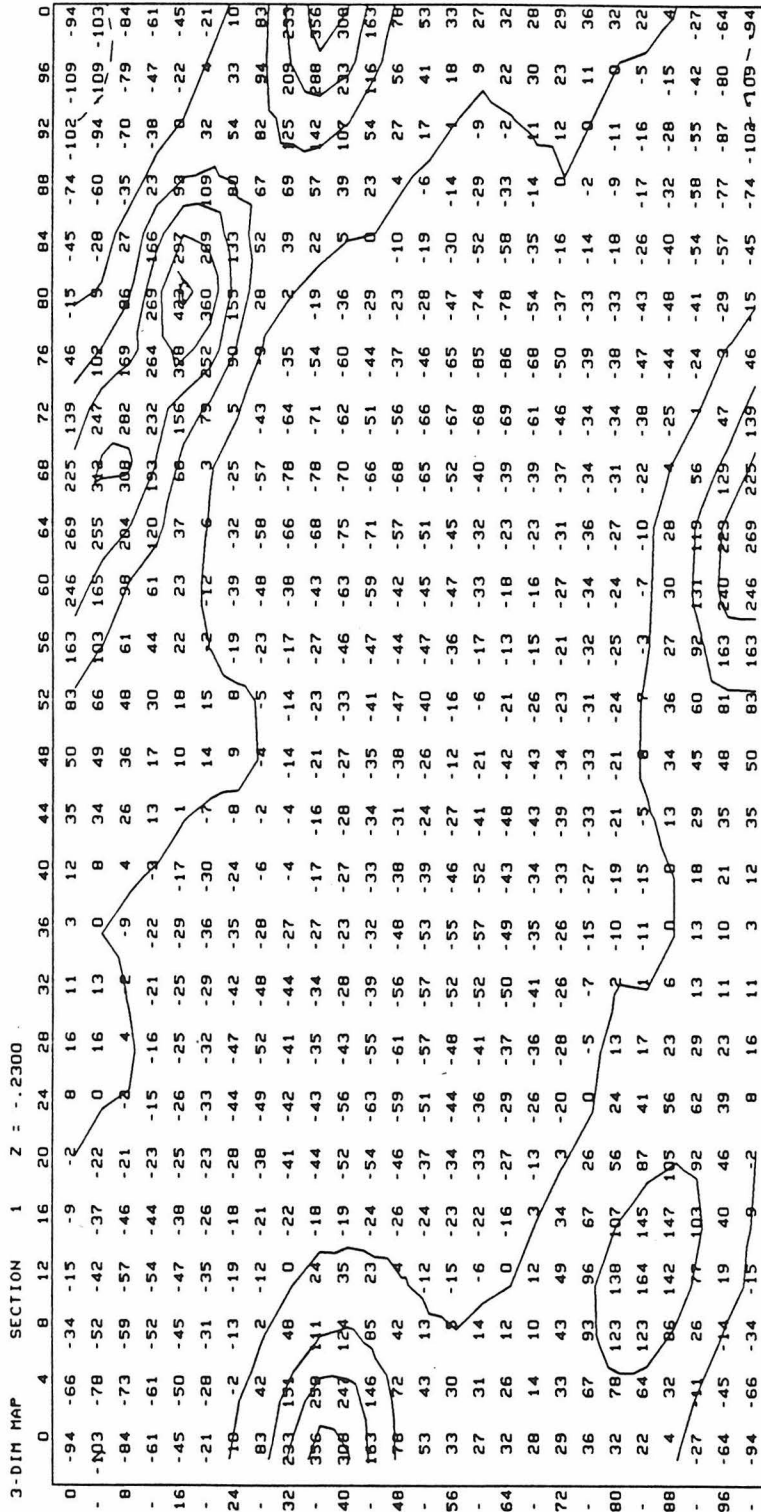


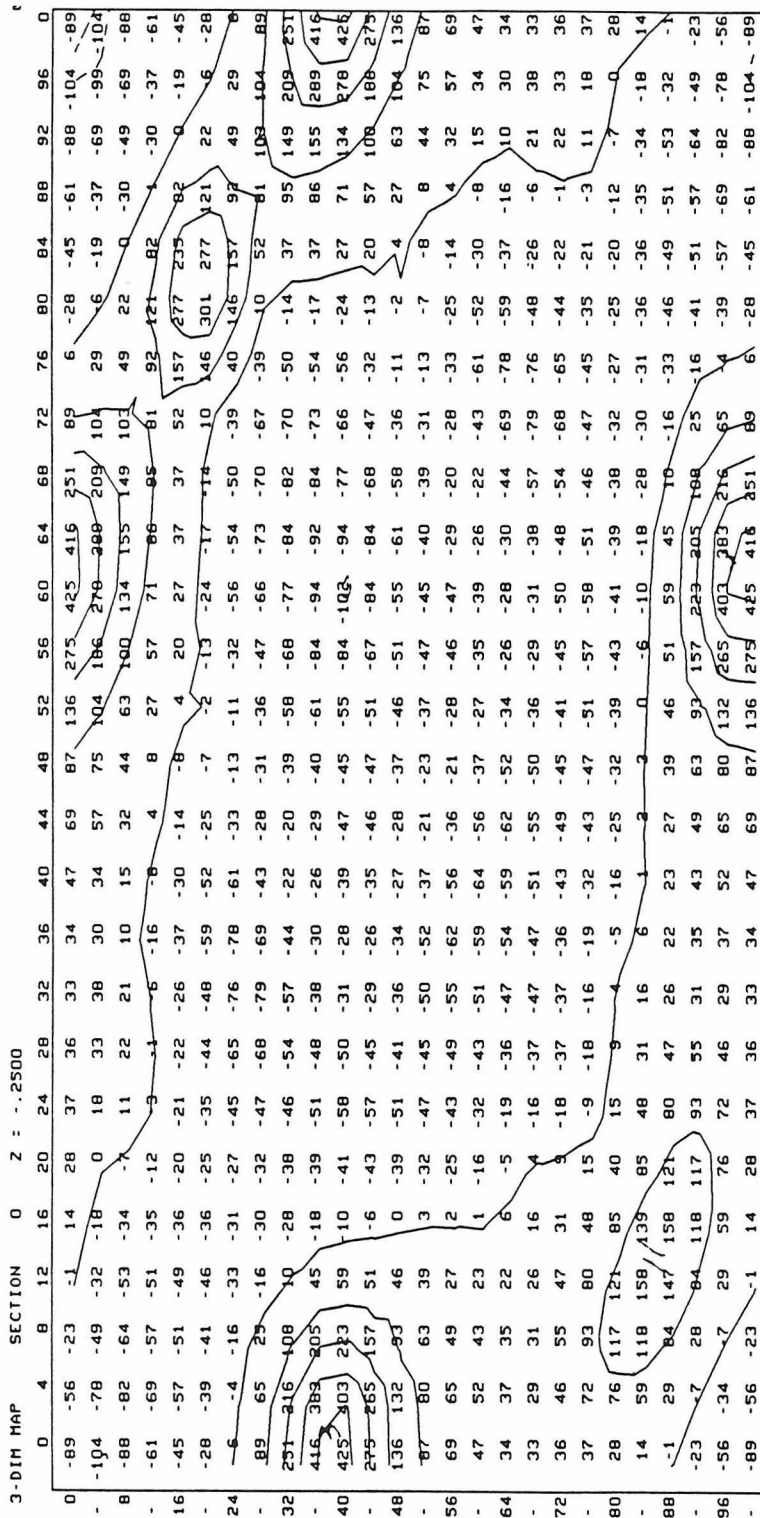
3-DIM MAP SECTION 4 Z : -.1700



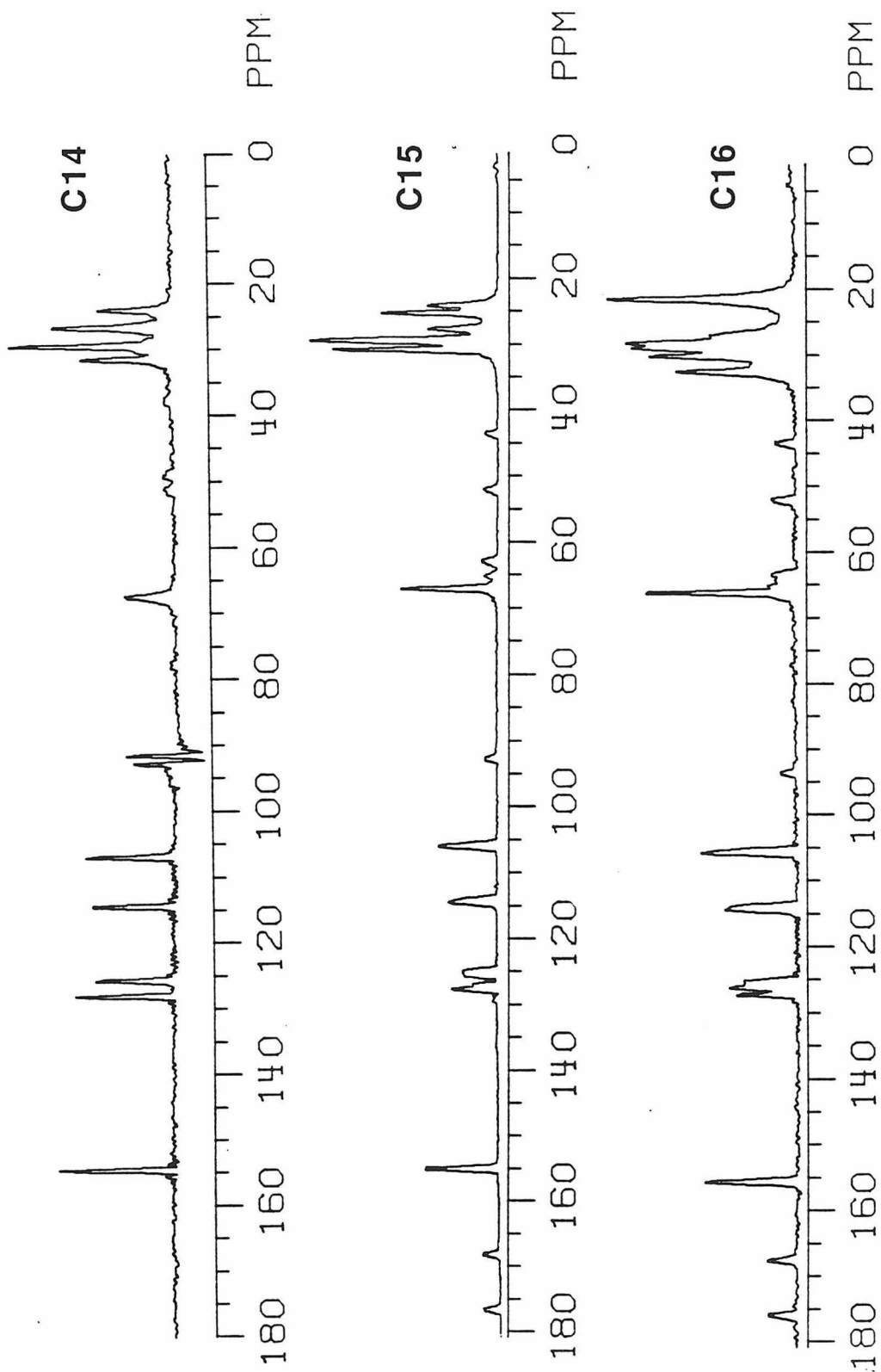








Appendix C



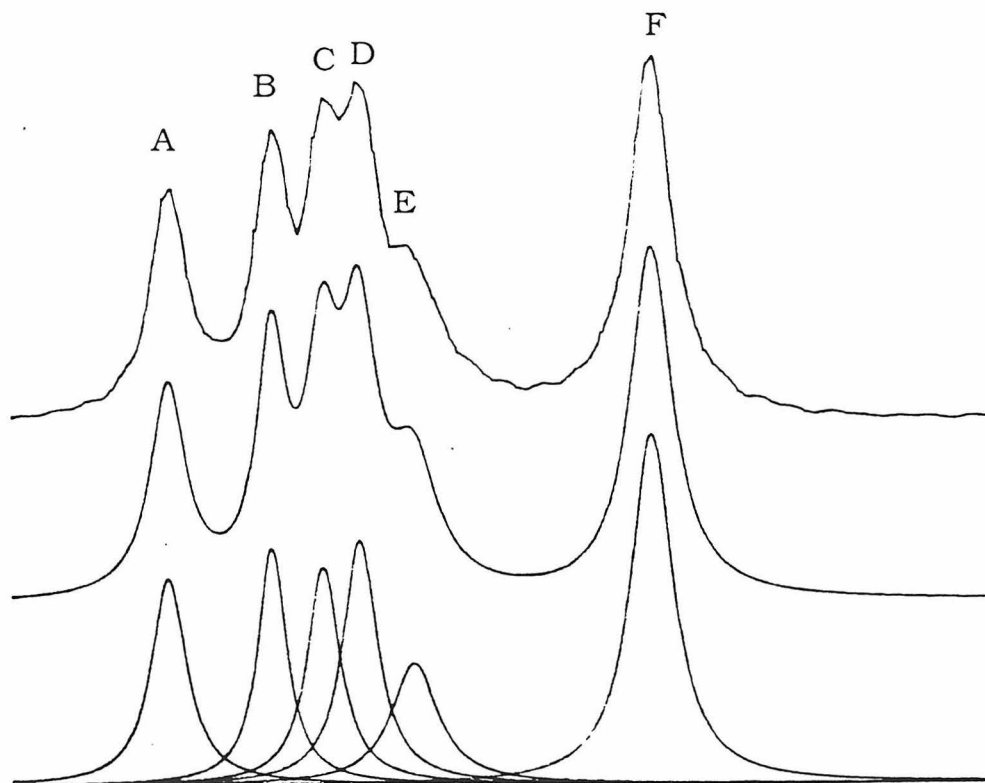
The solid state CP-MAS ^{13}C NMR spectra of **C14**, **C15**, and **C16**.

The deconvolution of the aliphatic region of the
solid state CP-MAS ^{13}C NMR.

C16

Peak	Area	% Area	Ratio
A	677	14.4	1
B	647	13.8	1
C	675	14.4	1
D	786	16.8	1
E	536	11.4	1
F	1371	29.2	2

Top: experimental.
Middle : simulation.
Bottom: individual simulation peaks.

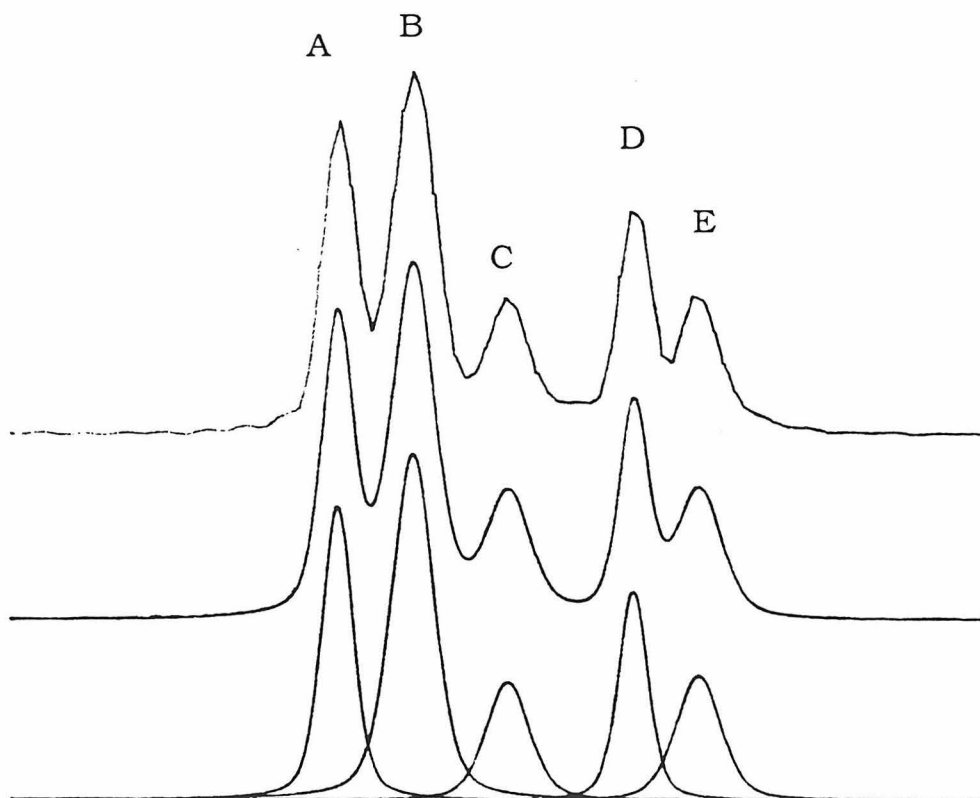


The deconvolution of the aliphatic region of the
solid state CP-MAS ^{13}C NMR.

C15

Peak	Area	% Area	Ratio
A	821	22.2	3
B	1322	35.8	4
C	474	12.8	2
D	559	15.1	2
E	515	14.0	2

Top: experimental.
Middle : simulation.
Bottom: individual simulation peaks.

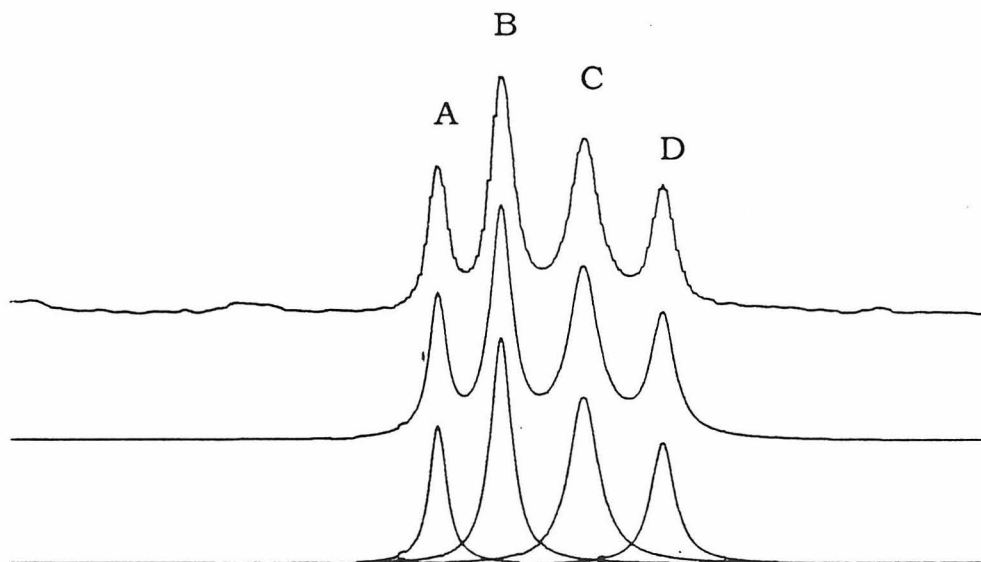


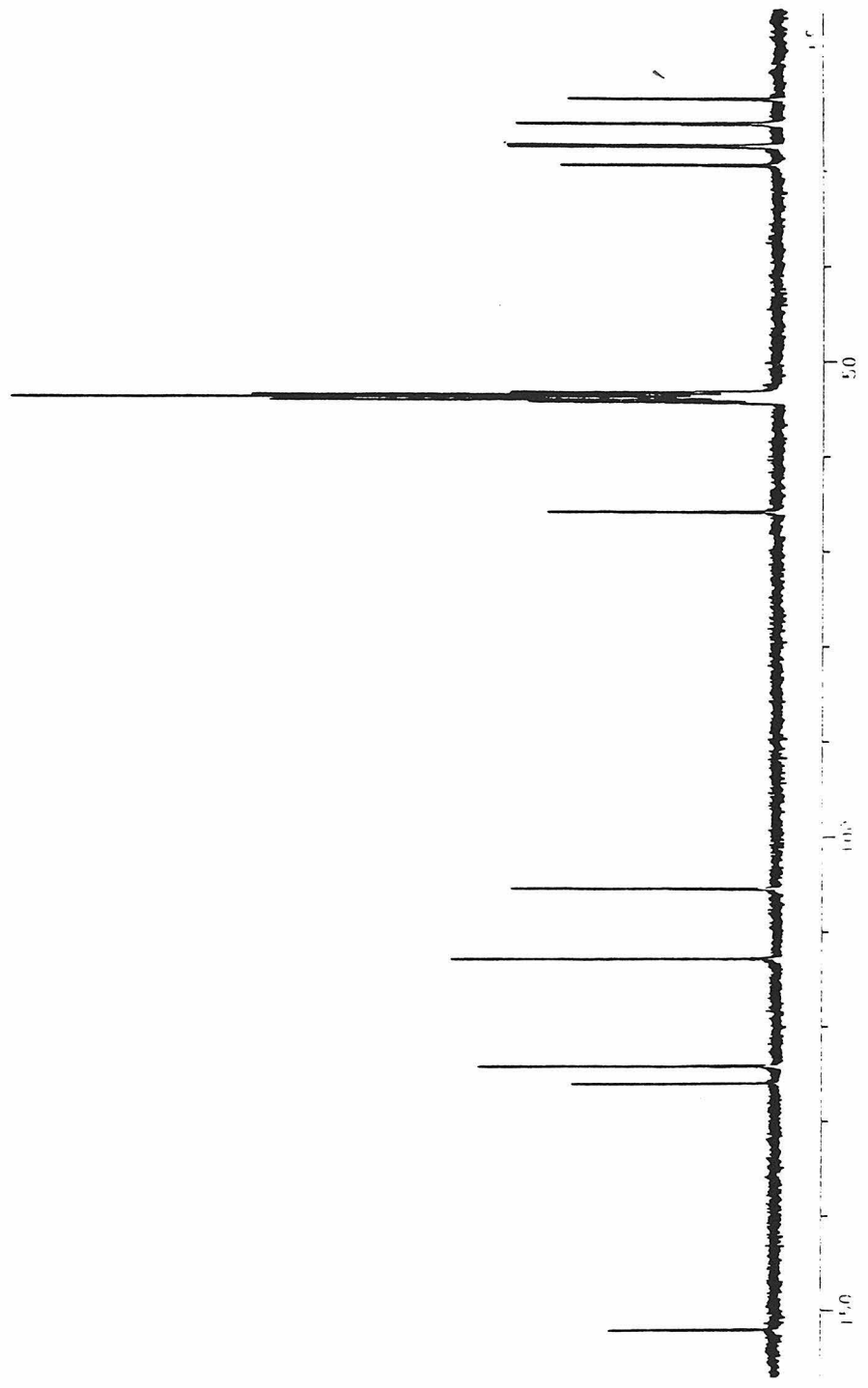
The deconvolution of the aliphatic region of the
solid state CP-MAS ^{13}C NMR.

C14

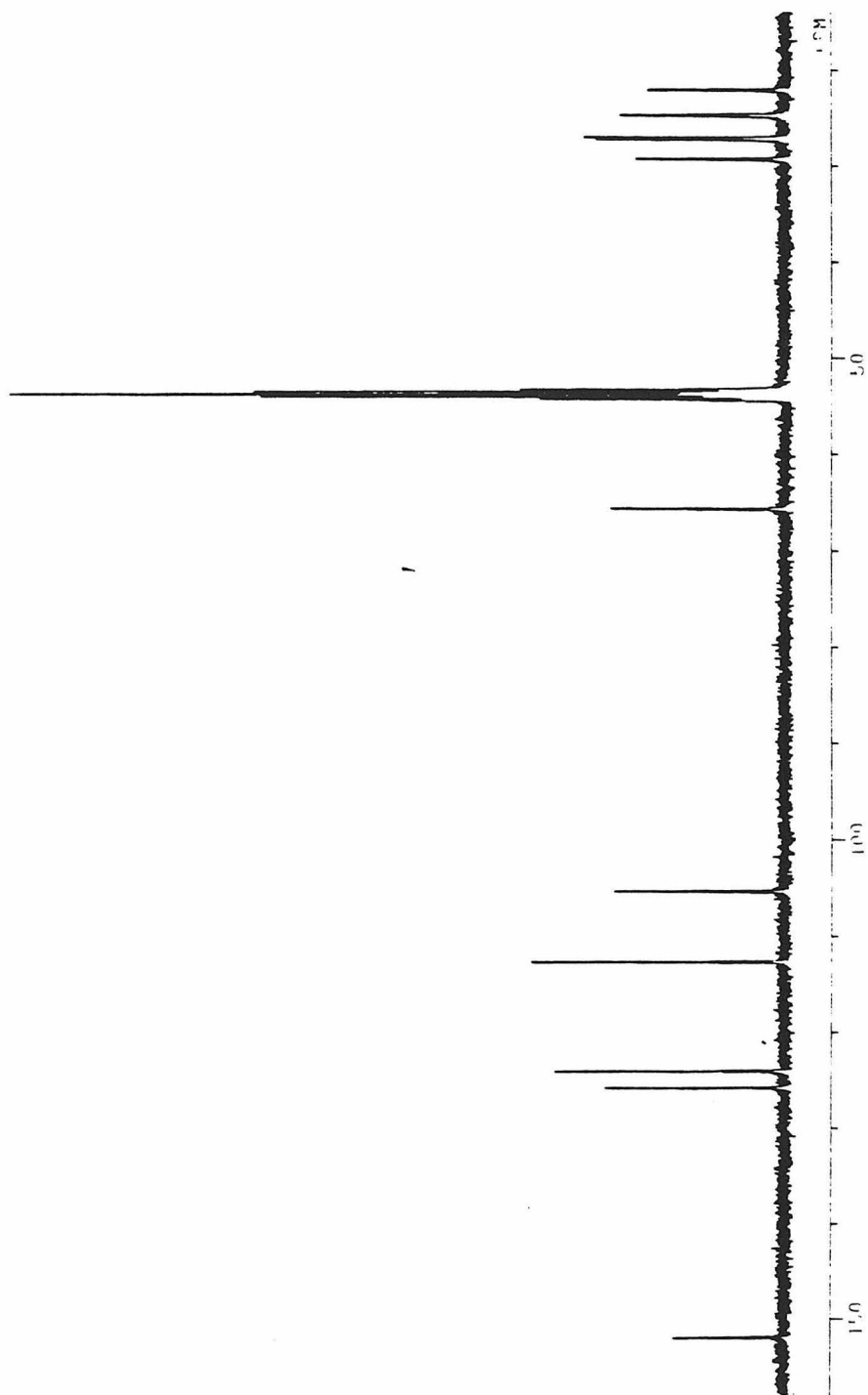
Peak	Area	% Area	Ratio
A	301	15.6	1
B	623	33.3	2
C	631	32.8	2
D	371	19.3	1

Top: experimental.
Middle : simulation.
Bottom: individual simulation peaks.

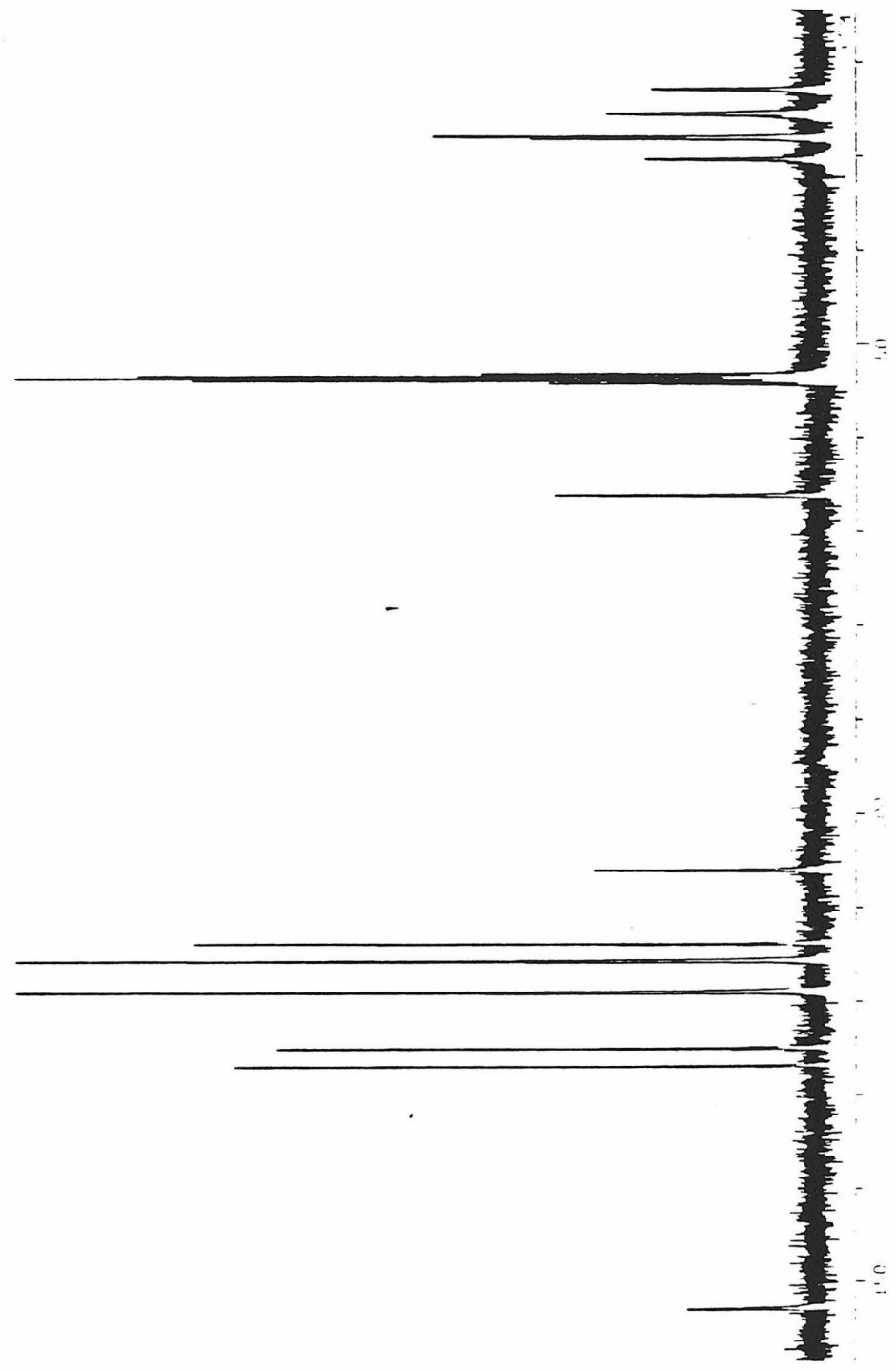




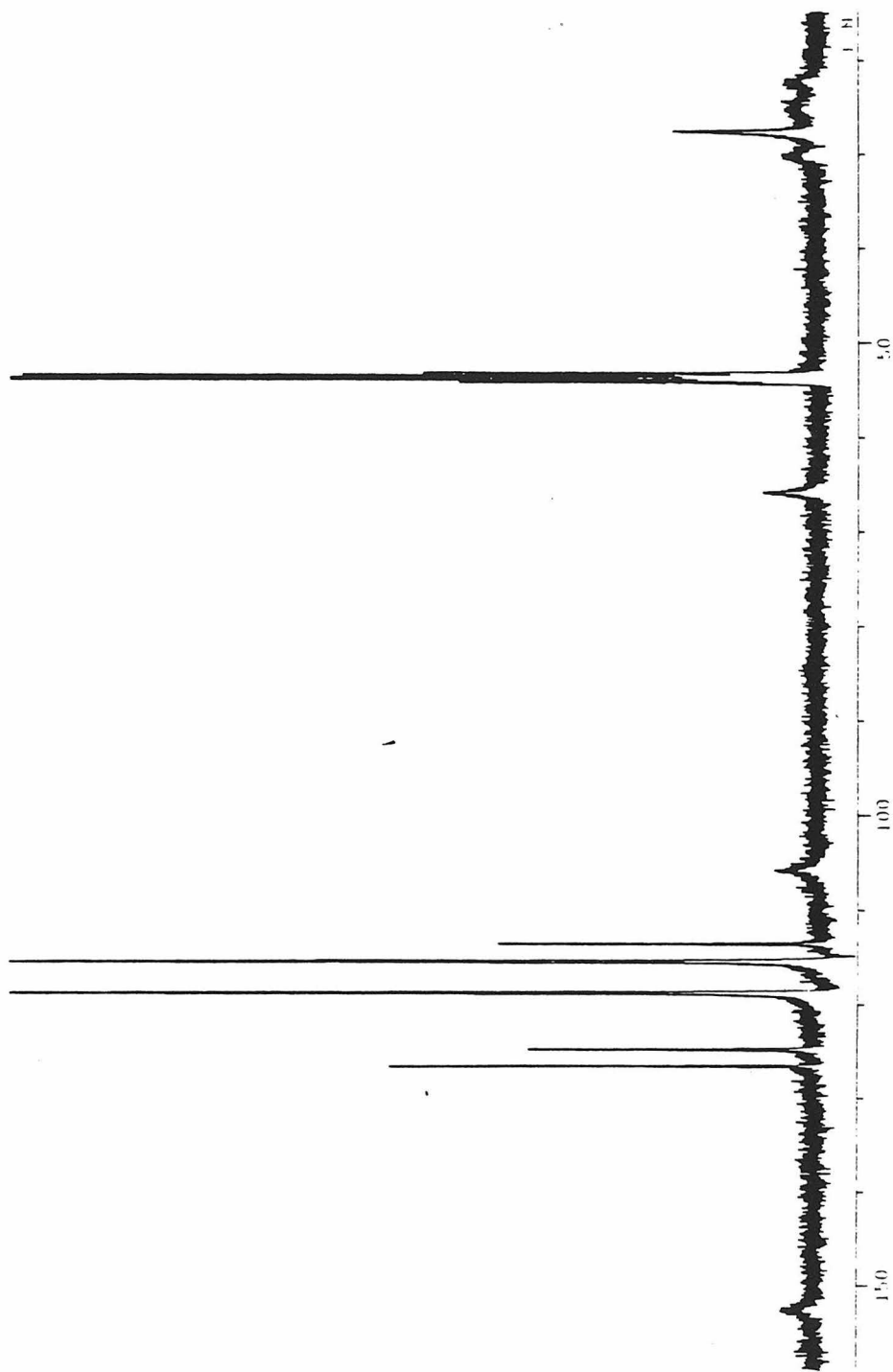
The ^1H -decoupled ^{13}C NMR spectrum of C14 at 193 K in CD_2Cl_2 .



The ^1H -decoupled ^{13}C NMR spectrum of C14 at 183 K in CD_2Cl_2 .



The ^1H -decoupled ^{13}C NMR spectrum of C14 at 168 K in $1/3 \text{CD}_2\text{Cl}_2/\text{CFC1}_3$.



The ^1H -decoupled ^{13}C NMR spectrum of C14 at 153 K in $1/3 \text{ CD}_2\text{Cl}_2 / \text{CFCl}_3$.